REPUBLIQUE ALGERIENNE DEMOCRATIQUE ET POPULAIRE

MINISTERE DE L'ENSEIGNEMENT SUPERIEUR ET DE LA RECHERCHE SCIENTIFIQUE

UNIVERSITE MOHAMED BOUDIAF - M'SILA

FACULTE DE SCIENCES ET TECHNOLOGIE

DEPARTEMENT DE GENIE ELECTRIQUE

N° : ……..

DOMAINE : SCIENCES ET TECHNOLOGIE

FILIERE : ELECTROTECHNIQUE

OPTION : COMMMANDE ELECTRIQUE

Mémoire présenté pour l'obtention

du diplôme de Master Académique

Préparé par : Somia Neguez

Manal Touirat

Intitulé

Power Management of Hybrid Fuel Cell System

Soutenu devant le jury composé de :

Mr. Ali Chebabhi	Université Mohamed Boudiaf - M'sila	Président
Mr. Said Barkat	Université Mohamed Boudiaf - M'sila	Encadreur
Mr. Abdelhafid Benyounes	Université Mohamed Boudiaf - M'sila	Co-Encadreur
Mr. Faycel Ouagni	Université Mohamed Boudiaf - M'sila	Examinateur

Année universitaire : 2022 / 2023

Acknowledgements

Despite the efforts, which have been undertaken to hold this work, it would not have been possible without the support and help of many Individuals. Therefore, we would like first of all to thank our supervisor Dr. Said Barkat and co-supervisor Dr. Abdelhafid Benyounes, for their guidance, fruitful comments, and constant supervision as well as for providing us with the necessary information regarding the research topic content, the research methodology, and the way a dissertation is written. Their constant guidance and willingness to share their knowledge and experience made us understand our research deeply and helped us to complete this academic task on time.

We would like to express our gratitude towards the members of the board of examiners for their acceptance to assess this work. Their fruitful comment and feedback will help us to reflect on our work and provide the best version of it.

We are sincerely grateful to Drs. Mohamed Bedboudi, Lyamani Laissaoui, Hiba Azzeddine, and Karima Laadjel for their support and assistance, which have favorably impacted our lives.

We also want to express our gratitude and affection to our parents and friends, who have willingly helped us with all their knowledge and emotions to make this work a reality.

Dedication

To my parents

Madani and Sabah Touirat

To My brothers and sister

Younes, Aissa, and Maria

To my darling family

To my beloved friends

I dedicate this work

Manal Touirat

Dedication

First and foremost, I thank ALLAH for all the will and courage He has given me to complete this work and face the differences in life.

To the purest hearts in my life, to those who taught me to give without waiting… My dear parents, may God prolong their lives for mom and dad

To my brothers…. who taught me that life without symbiosis, love and cooperation is worth nothing. To those who shared good and bad times with me, who taught me that success is worth the seriousness and effort, to my sister.

For whom I look forward to seeing their bright future, God willing……. Baraa El-Dine and Saif El-Dine.

To all my teachers, without whom I would not have reached where I am now for a crowd of relatives and friends.

I dedicate this humble work, and I pray that you will like it

Neguez Somia

Abstract

Hybrid power systems (HPSs) based on clean and renewable energies have become an effective alternative for reducing the use of fossil fuels in generation systems. One of the well-known HPSs dedicated to transportation applications is that formed by a PEMFC acting as the main source along with a lithium-ion battery and a supercapacitor acting as storage systems. This hybridization allows optimizing the fuel cell system to achieve better performance via an energy management strategy (EMS) that distributes the load power between the power sources. This EMS ensures optimal fuel economy while ensuring that each power source operates within its proper limits. The EMSs that have been considered herein are the state machine control strategy (SMC), PI controller strategy, equivalent consumption minimization strategy (ECMS), and external energy maximization strategy (EEMS). To this end, a simulation model was developed to validate the different EMSs and assess their performances.

Keywords: Fuel cell, Battery, Supercapacitor, DC-DC converter, Energy management strategy, Hybrid power system.

Résumé

Les systèmes hybrides d'énergie basés sur des énergies propres et renouvelables sont devenus une alternative efficace pour réduire l'utilisation des combustibles fossiles dans les systèmes de production d'énergie. L'un des systèmes hybrides les plus connus dédiés aux applications de transport est celui formé par une pile à combustible de type PEMFC agissant comme source principale avec une batterie lithium-ion et un supercondensateur agissant comme des systèmes de stockage. Cette hybridation permet d'optimiser le système de pile à combustible pour obtenir de meilleures performances. grâce à une stratégie de gestion de l'énergie (EMS) qui répartit la puissance de charge entre les sources d'énergie. Cette stratégie assure une économie de carburant optimale tout en garantissant que chaque source d'énergie fonctionne dans ses propres limites. Les EMSs considérées ici sont la stratégie de contrôle de la machine d'état (SMC), la stratégie du contrôleur PI, la stratégie de minimisation de la consommation équivalente (ECMS) et la stratégie de maximisation d'énergie externe (EEMS). Pour cela, un modèle de simulation a été développé pour valider les différentes EMSs et évaluer leurs performances.

Mots-clés : Pile à combustible, Batterie, Supercondensateurs, Convertisseur DC-DC, Stratégie de gestion d'énergie, Système hybride de puissance.

ملخص

لقد أصبحت أنظمة الطاقة الهجينة (HPS) القائمة على الطاقات النظيفة والمتجددة بديلاً فعالاً لتقليل استخدام الوقود الأحفوري في أنظمة التوليد. أحد أنظمة الطاقة الهجينة المعروفة والمخصصة لتطبيقات النقل هي تلك التي تتكون من خلية وقود PEMFC تعمل كمصدر رئيسي إلى جانب بطارية ليثيوم أيون ومكثف فائق يعملان كنظامي تخزين. يسمح هذا التهجين بتحسين نظام خلايا الوقود لتحقيق أداء أفضل من خلال استراتيجية إدارة الطاقة (EMS) التي توزع طاقة الحمل بين مختلف مصادر الطاقة. تضمن هذه الاستراتيجية الاقتصاد الأمثل للوقود مع ضمان عمل كل مصدر طاقة ضمن حدوده المناسبة. استراتيجيات إدارة الطاقة المذكورة هنا هي إستراتيجية التحكم في آلة الحالة (SMC)، إستراتيجية وحدة التحكم PI، إستراتيجية تقليل الاستهلاك المكافئ (ECMS)، واستراتيجية تعظيم الطاقة اللحظية الخارجية (EEMS). تم تطوير نموذج محاكاة للتحقق من صحة استراتيجيات EMSs المختلفة وتقييم أدائها.

الكلمات المفتاحية: خلية وقود، بطارية، مكثف فائق، محول DC-DC، إستراتيجية إدارة الطاقة، نظام طاقة هجين.

Table of Contents

Table of Figures

Chapter 1: Fuel Cell/ Battery/ Supercapacitor Hybrid System Generalities

Chapter 2: Modeling and Control of Fuel Cell/ Battery/ Supercapacitor Hybrid System

Chapter 3: Fuel Cell/ Battery/ Supercapacitor Hybrid System's Energy Management Strategy

List of Tables

List of Abbreviations

ABC	Artificial Bee Colony.
AC	Alternating Current.
AFC	Alkaline Fuel Cell.
AIS	Artificial Intelligence Strategy.
ANN	Artificial Intelligence Network.
ANFIS	Adaptive Neuro Fuzzy Inference System.
CCM	Continuous Conduction Mode.
D	Duty-Cycle.
DC	Direct Current.
DCM	Discontinuous Conduction Mode.
DE	Differential Evolution.
DMC	Dimethyl Carbonate.
DP	Dynamic Programming.
DG	Distributed Generation.
DRBS	Deterministic Rule-Based Strategy.
EC	Ethylene Carbonate.
ECMS	Equivalent Consumption Minimization Strategy.
EEMS	External Energy Maximization Strategy.
EDLC	Electrochemical Double Layer Capacitor.
EMS	Energy Management Strategy.
FC	Fuel cell.
FCHS	Fuel Cell Hybrid System.

FD	Frequency Decoupling.
FRBS	Fuzzy Rule-Based Strategy.
FBC	Filter-Based Control.
GA	Genetic Algorithm.
GOS	Global Optimization Strategy.
GP	Genetic Programming.
HHO	Harris Hawks Optimization.
HPS	Hybrid Power System.
IOS	Instantaneous Optimization Strategy.
MCFC	Molten Carbonate Fuel Cell.
MILP	Mixed-Integer Linear Programming.
MINLP	Mixed-Integer Non-Linear Programming.
ML	Machine Learning.
MPC	Model Predictive Control.
MRO	Manta Ray Optimization.
MAS	Multi-Agent System.
MS	Management System.
NN	Neural Network.
OS	Optimization Strategy.
PAFC	Phosphoric Acid Fuel Cell.
PEMFC	Proton Exchange Membrane Fuel Cell.
PI	Proportional-Integral.
PMP	Pontryagin’s Minimum Principle.
PSO	Particle Swarm Optimization.
PV	Photovoltaic.

PWM	Pulse Width Modulated.
RBS	Rule-Based Strategy.
RC	Robust Control.
RL	Reinforcement Learning.
RNN	Recursive Neural Network.
SA	Simulated Annealing.
SC	Supercapacitor.
SDP	Stochastic Dynamic Programming.
SMC	State Machine Control.
SOC	State of Charge.
SOFC	Solid Oxide Fuel Cell.
SPS	Sim Power System.
WT	Wind Turbines.

List of Symbols

H^+	Hydrogen ion.
O_2	Oxygen atom.
H_2	Hydrogen atom.
H_2O	Water molecule.
Li^+	Lithium ion.
$LiCoO_2$	Lithium oxide cobalt.
C	Carbon atom
CoO_2	Oxide Cobalt.
e^-	Electron
E_n	Nernst voltage.
K_c	Voltage constant at nominal condition of operation.
P_{H_2}	Partial pressure of hydrogen.
P_{O_2}	Partial pressure of oxygen.
P_{H_2O}	Partial pressure of water.
P_{fuel}	Fuel pressure.
P_{air}	Air pressure.
R	Ideal gas constant.

$U_{f_{H_2}}$	Hydrogen utilization.
$U_{f_{O_2}}$	Oxygen utilization.
χ	Percentage of hydrogen in the fuel.
y	Percentage of oxygen in the air.
V_{fuel}	Fuel flow rate.
V_{air}	Air flow rate.
i_{fc}	Cell current.
η_{act}	Activation loss.
i_0	Exchange current.
A	Tafel slope.
ΔG	Activation energy barrier.
K	Boltzmann's constant.
h	Planck's constant
T	Temperature of operation.
z	Number of moving electrons.
α	Charge transfer coefficient.
F	Faraday's constant.
T_d	Cell settling time.
η_{ohmic}	Ohmic loss.
R_{ohmic}	FC internal resistance.

N	Number of FC cells.
v_{batt}	Battery voltage.
E_{ob}	Battery open circuit voltage.
E_0	Battery constant voltage.
K	Polarization constant.
Q_{batt}	Battery capacity.
$i*$	Filtered battery current.
it	Actual battery charge.
A_0	Exponential zone amplitude.
B	Exponential zone time constant inverse.
R_{batt}	Battery internal resistance.
Pol_{res}	Polarization resistance.
C_H	Helmholtz capacitance.
C_{GC}	Gouy-Chapman capacitance.
N_e	Number of electrode layers.
ε	Permittivity of the electrolyte material.
ε_0	Permittivity of free space.
A_i	Inter-facial area between electrodes and electrolyte.
D_n	Helmholtz layer length.

Q_C	SC cell electric charge.
c	Molar concentration.
N_s	Supercapacitor module cells in series.
N_p	Supercapacitor module cells in parallel.
C_T	SC total capacitance.
V_{sc}	Supercapacitor output voltage.
Q_T	Total electric charge.
R_{sc}	Supercapacitor module resistance.
i_{sc}	Supercapacitor module current.
V_{in}	Input voltage.
V_L	Voltage across the Inductance.
i_L	Inductance current.
V_{out}	Output voltage.
L	Inductance.
C	Capacitance.
R	Resistor load.
i_c	Capacitor current.
T_s	Switching period.
$I_{L\max}$	Maximum current of the inductor.
$I_{L\min}$	Minimum current of the inductor.

Δi_L	Inductor current ripple.
ΔQ	Variation of the electric charges in the capacitor C.
f_s	Switching frequency.
ΔV_{out}	Voltage ripple.
K_{bpi}, K_{kpi}	Proportional gains of current regulator of boost and buck converters, respectively.
K_{bii}, K_{kii}	Integral gains of current regulator of boost and buck converters, respectively.
K_{bpv}, K_{kpv}	Proportional gains of voltage regulator of boost and buck converters, respectively.
K_{biv}, K_{kiv}	Integral gains of voltage regulator of boost and buck converters, respectively.
ω_{bni}, ω_{kni}	Natural frequency for current regulator of boost and buck converters, respectively.
ξ_{bi}, ξ_{ki}	Damping coefficient for current regulator of boost and buck converters, respectively.
ω_{bnv}, ω_{knv}	Natural frequency for voltage regulator of boost and buck converters, respectively.
ξ_{bv}, ξ_{kv}	Damping coefficient for voltage regulator of boost and buck converter, respectively.
V_{fc}	Full cell output voltage.
T_{sc}	Scope period.
C_{dc}	Capacitor of the converter.
L_{b_fc}	Inductance of boost converter (full cell).
ω_{bni_fc}	Natural frequency for current regulator of boost converter (fuel cell).
ξ_{bi_fc}	Damping coefficient for current regulator of boost converter (fuel cell).
$i_{L\,fc}$, $i_{L\,fcref}$	Fuel cell currant and its reference.
P_{fc} , P_{fc_ref}	Fuel cell power and its reference.

d_{fc} Duty cycle of boost converter (fuel cell).

L_{k_batt} Inductance of buck converter (battery).

L_{b_batt} Inductance of boost converter (battery).

ω_{kni_batt} Natural frequency for current regulator of buck converter (battery).

$\xi_{\mathrm{ki\_batt}}$ Damping coefficient for current regulator of buck converter (battery).

$\xi_{\mathrm{bi\_batt}}$ Natural frequency for current regulator of boost converter (battery).

$\omega_{\mathrm{bni\_batt}}$ Damping coefficient for current regulator of boost converter (battery).

d_{buck}, d_{boost} Buck and boost duty cycles.

i_{Lboost} Current of boost converter.

i_{Lref} Reference current.

i_{Lbuck} Current of buck converter.

$\mathrm{L_{k\_sc}}$ Inductance of buck converter (SC).

$\mathrm{L_{b\_sc}}$ Inductance of boost converter (SC).

$\omega_{\mathrm{kni\_sc}}$ Natural frequency for current regulator of buck converter (SC).

$\xi_{\mathrm{ki\_sc}}$ Damping coefficient for current regulator of buck converter (SC).

$\omega_{\mathrm{bni\_sc}}$ Natural frequency for current regulator of boost converter (SC).

$\xi_{\mathrm{bi\_sc}}$ Damping coefficient for current regulator of boost converter (SC).

V_{SC} Supercapacitor voltage.

p_{sc} , p_{scref} Supercapacitor power and its reference.

P_{fc_min}	Minimum FC power.
P_{fc_max}	Maximum FC power.
P_{fc_nom}	Nominal FC power.
P_{batt}	Battery power.
P_{batt_char}	Maximum charge battery power.
P_{load}	Load power.
SOC_{min}	Minimum state of charge.
SOC_{max}	Maximum state of charge.
SOC_{ref}	Reference state of charge of battery.
i_{batt}	Battery current.
k_p	Proportional gain.
k_i	Integral gain.
ΔT	Sampling time.
α_p	Penalty coefficient.
μ	Balance coefficient.
ΔV	Supercapacitor charge/discharge voltage.
C_r	Rated capacitance of the supercapacitor.
V_{DC_min}	Minimum of the DC-bus voltage.
V_{DC_max}	Maximum of the DC-bus voltage.

t	Time.
i_{out}	Output current.
V_{cell}	Cell output voltage of FC.
E_{oc}	Cell open circuit voltage of FC.
u_{ab}^*, u_{bc}^*	Line-to-line reference voltage.
v_a^*, v_b^*, v_c^*	Reference voltages.
i_a, i_b, i_c	Load currents.
$V_{nom\text{-}rms}$	Nominal rms phase voltage.
F	Frequency.
P_{AC}	AC power.
S	Apparent power.
P	Active power.
Q	Reactive power.
Z	Impedance module.
v_s	Load voltage vector.
v_a, v_b, v_c	Three phase voltages.
C_s	Cell capacity of SC.
C_{bv}, C_{kv}	Transfer function for voltage regulator of boost and buck converters, respectively.
C_{bi}, C_{ki}	Transfer function for current regulator of boost and buck converters, respectively.

General Introduction

Recent global challenges, such as the Russia-Ukraine conflict, worldwide Covid-19pandemic, climate change, and supply chain disruptions, have driven up oil and gas costs, severely impacting various applications [1]. As a result, numerous nations are seeking to attain sustainable development goals and switch from non-renewable energy sources to ones that are more effective and environmentally friendly [2]. Renewable and green energy sources are the auspicious solution for nowadays energy problems [3].

In this context, there is a promising technology that has the potential to use these renewable and green energy sources called a hybrid power system (HPS). The HPS is a technique to revolutionize the way energy is stored and used, so it consists of interconnected loads, power sources, and energy storage systems [4].

The power energy sources include renewable energy sources such as photovoltaic (PV), wind turbines (WT), biomass, and tidal and wave power sources, in addition to fuel cell (FC) as clean sources [4]. The energy storage system can be divided into mechanical systems, including compressed air, flywheel, and pumped hydro; electrochemical systems, including battery; electrical systems, including supercapacitor, and superconductive magnets; also thermal systems including hot water storage, thermal fuel storage, and ceramic thermal storage [4] [5].

An energy management strategy (EMS) is a primary part of an HPS [6] [7]. The EMSs play a critical role in system performance to attain several key goals, such as minimizing production costs, improving energy efficiency, and increasing durability and reliability [8].

Given that the majority of the EMSs have yet to be used in industry and are still in the stage of scientific research; they fall into two categories: industrial and scientific research. The former consists of a rule-based strategy (RBS), while the latter consists of an optimization strategy (OS) [9]. The RBS mainly subcategorized the deterministic rule-based control strategies (DRBS), in which usually include look-up tables, filter-based control (FBC), and wavelet transform (frequency decoupling FD), load follow control known as state machine control (SMC) [10], and the fuzzy rule-based strategy (FRBS) [11], which can be traditional, adaptive or predictive fuzzy control strategy [7]. Furthermore, OS may be split into global optimization strategies (GOSs), including linear programming, dynamic programming, and

stochastic strategy [7]; also instantaneous optimization strategy (IOS) [9] typically including the equivalent consumption minimization strategy (ECMS) [12], external energy maximization strategy (EEMS) [13], model predictive control (MPC) [14], artificial neural network [15], particle swarm optimization (PSO) [16], and Pontryagin's minimum principle (PMP) [17]. Other methods can also be included like sliding mode control [18], robust control (RC) [9], manta ray optimization (MRO) [19], and Harris Hawks optimization (HHO) [20].

The HPS can be used in a variety of applications, including in vehicles [9], in which it is used to generate electricity for powering electric motors. In aircraft [21], in which it is used as an emergency power system. In remote locations [22], in which it provides a reliable source of electricity for military bases [23], university campus [4], buildings [24], hospitals, police stations, industrial locations, and other essential services.

In accordance with global energy transition trends, Algeria increases its bet on investment in renewable energies; and it has a tendency to adopt hydrogen as "Algeria's clean energy choice". Hydrogen called also "energy of the future" is a future fuel free of emissions to reach carbon neutrality and limit climate change. It can be used as a hydrogen fuel cell, a promising hydrogen-related technology, to act as the main source in the HPSs. Hydrogen fuel cell technology may be used in a wide range of applications, such as electric vehicles [9], trains [25], tramways [26] [27], aircraft [21], and powering buildings [28]. Not only that, laptops and mobile phones [29], and drones [30] may also be powered by tiny hydrogen fuel cells.

Subsequently, the proposed HPS consists of a proton exchange membrane fuel cell that is presented as the primary source, as well as a storage system comprised of a lithium-ion battery and a supercapacitor acting as a secondary source.

So, the objectives of this study are the modeling, control, and management of the fuel cell hybrid power system, in which a simulation model is established based on the average model of the unidirectional and bidirectional DC-DC converters and DC-AC inverter as well. To fulfill these objectives, this work will be subdivided into three chapters, which are organized as follows:

Chapter 1 goes through relevant literature on the topic of HPS, with a focus on the concept of hybridization and the main energy sources principles.

As described in chapter two, the system components and the basic operation of the converters are described with the objective of reaching a mathematical model of the HPS. Actually, the modeling phase is indispensable for the power converter's sizing and control

design. For this end, two DC-DC converters are considered: the boost converter is used to control the fuel cell output power, and the bidirectional DC-DC converter is used to control the bidirectional power flow from or to the battery/ supercapacitor.

The presence of multiple power sources requires the design of an EMS to distribute the power load between the fuel cell and battery. Chapter three will discuss this problem statement. The design of such EMS should be made in such a way as to achieve the minimization of fuel usage to ensure each energy source operates within its limits and guarantee the longevity of the whole hybrid power system. There are several EMSs that have been reported in the literature; we will study many of them, including the state machine control strategy, PI-based energy management strategy, equivalent consumption minimization strategy, and external energy maximization strategy.

At the end of this manuscript, a general conclusion is given to conclude the obtained findings, and give some relevant suggestions for further work.

Chapter 1:
Fuel Cell/ Battery/ Supercapacitor Hybrid System Generalities

---

In many applications, using conventional electricity is neither economically nor technically feasible. Hybrid power systems are increasingly being used as alternatives. Utilizing the plentiful fuel cell supply and all renewable energy sources can be crucial in ensuring ecologically friendly and clean electricity. However, due to their sporadic nature, these sources frequently do not provide enough power to meet the demand from the load. As a result, energy storage is a necessary condition to provide a steady supply of electricity. While lowering operating costs, HPSs utilizing clean and renewable energy sources can offer effectiveness, dependability, and security. This chapter presents an overview of the suggested HPS. It starts with focusing on the concept itself followed by presenting the different possible configurations. In these configurations, the fuel cell is considered as the main source. The battery and supercapacitor are regarded as storage systems. Subsequently, more details about fuel cell source and storage energy sources are given.

1.1 Hybrid power system overview

Fossil fuel supplies are disappearing over the world today, which raises the price of producing them [31]. As a result, renewable energy creates an essential function in future power supply due to its availability in most zones, and even people's cognition is increased about dangerous environmental emissions [32]. However, owing to the irregular nature of these sources, a hybrid of these with an energy storage system can ensure reliability by continuous supply, in which energy storage is an integral element of the system. Furthermore, proper HPSs configuration selection, control techniques, and source dimensions are vital to forming a powerful HPS [33].

1.2 Concept and topologies of hybrid power system

The hybrid power system has its generation sources that are connected with the loads [34]; subsequently, the fuel cell (FC) is considered as the main source in the hybrid fuel system, while the battery and supercapacitor (SC) are considered as the storage devices.

As shown in Figure (1.1), FC possesses a slow dynamic due to its tardy inner electrochemical and thermodynamic responses [35], contrary to the storage energy sources that have faster dynamics. Furthermore, SC provides a too-quickly dynamic than to battery [36]. As a result, the SC operates at a transient peak and the battery during continuous demand while the FC meets the average demand [21]. Hence, that hybridization delivers flexibility in managing the power demand from the fuel cell by protecting this last from harmful transition, thus achieving higher efficiency through this levelling [37].

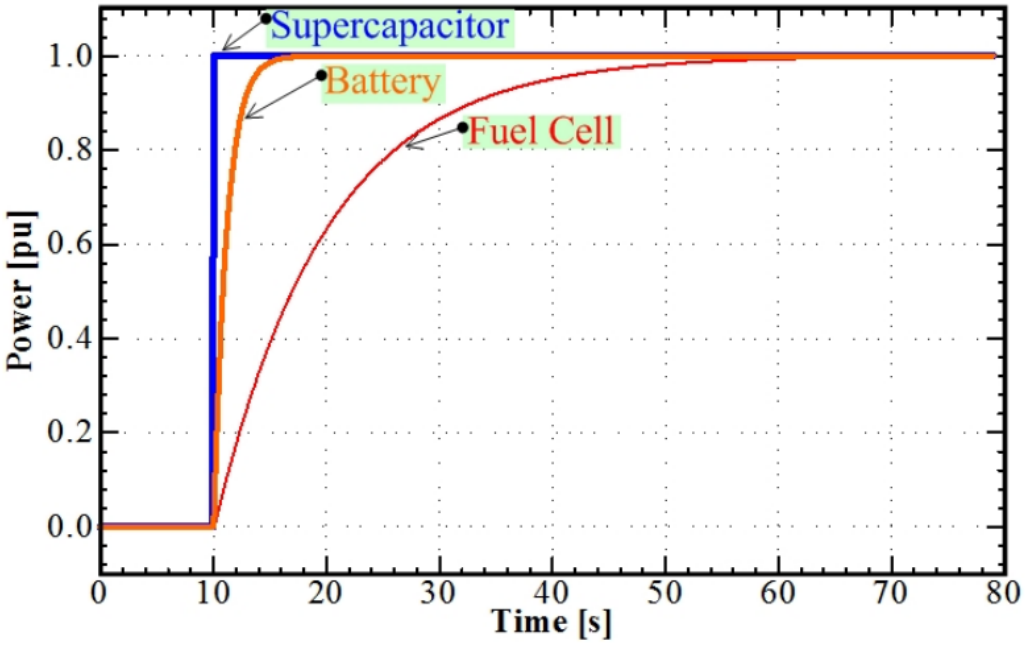

Figure 1.1: *Dynamic classification of the embedded sources [36].*

All these elements share the same DC-bus through suitable electronic power converters. As depicted in Figure (1.2), there are nine topologies for the power converter connections as suggested in [21].

To achieve a better DC coupling configuration in terms of power controllability, efficiency, cost, and weight, we should keep an eye on all of these components. For this purpose, a unidirectional DC/DC converter is always chosen to attach the FC to the DC-bus, and bidirectional DC/DC converters are required to connect the battery and SC.

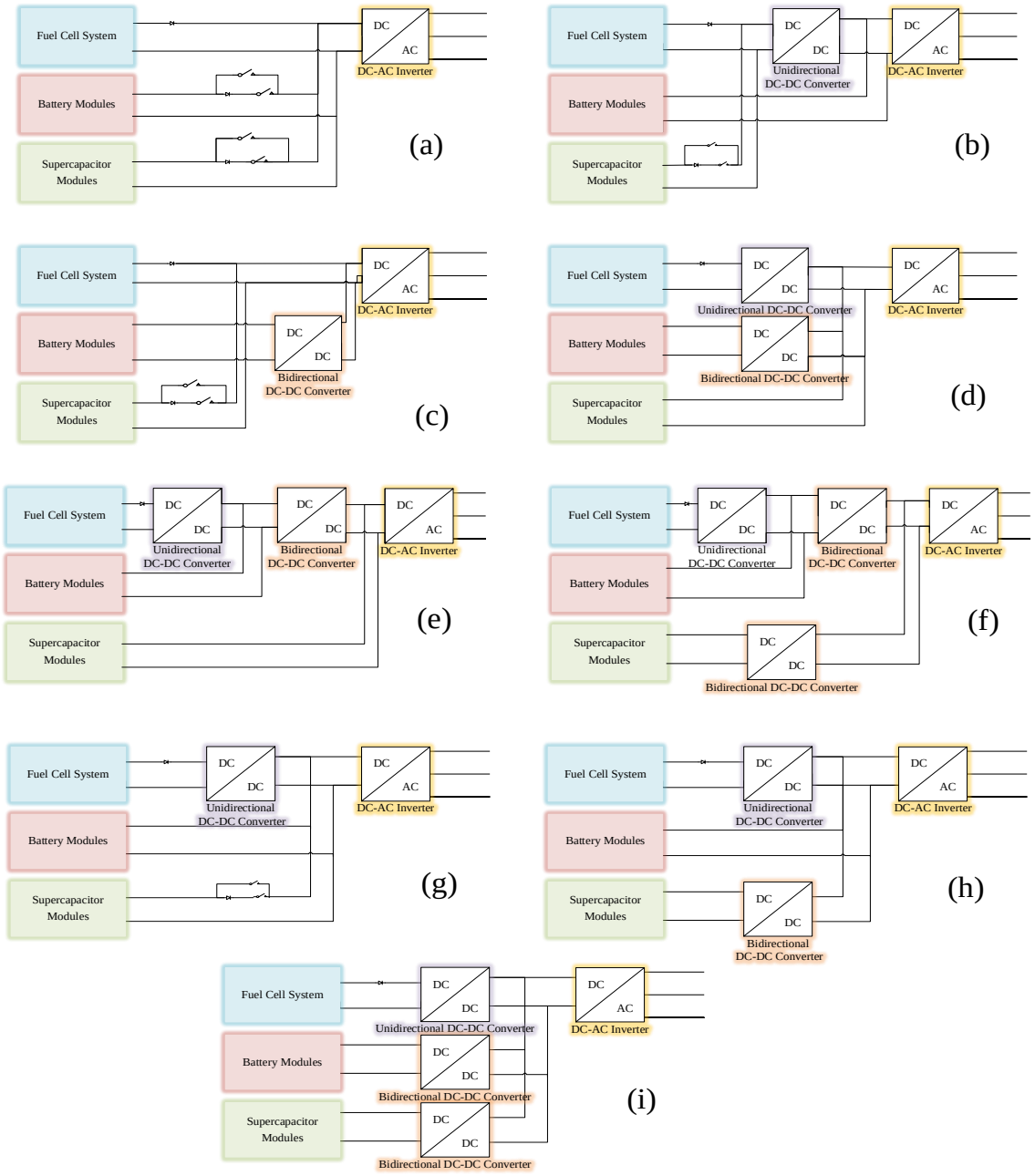

Figure 1.2: *Hybrid power system topologies.*

1.3 Main energy source

1.3.1 Fuel cell description

Various techniques can be used to convert hydrogen into electricity, including FCs and combustion reactions. Compared to combustion reactions, FCs offer the advantage of superior conversion efficiencies [38].

FCs are stationary energy-converting devices that transform chemical energy straight into DC electrical energy [34]. All FCs share a similar basic structure; it mainly consists of an

anode and a cathode on both sides, which are supplied them by fuel and oxidant, respectively, and an electrolyte is located between these, in addition to an external circuit [39]. There are different sorts of FCs according to the type of electrolyte used, and the operating temperature considered [40].

A single FC voltage is typically in the field of $0.6-0.9\ V$ in actual applications, while the theoretical value is nearly $1.23\ V$ [41]. For this reason, the FC stack must be created by series (to increase the potential) or parallel (for a more current to be dragged) connection [39].

1.3.2 Fuel cell components

FC has different layers, as seen in Figure (1.3). They all contribute with different functions to achieve the goal of a well-functioning FC.

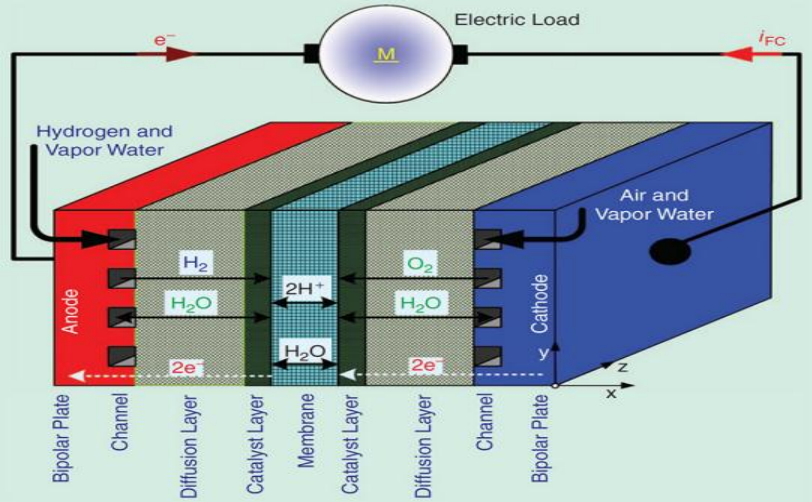

Figure 1.3: *Fuel cell components [36].*

- **Electrodes (anode and cathode)**

The electrodes of the FC are an essential part of the electrochemical reaction as they are composed of two components; an anode and a cathode. The former is responsible for the oxidation of the fuel; the latter is responsible for the reduction of the oxidant. They are usually made of a bipolar plate, which allows the fuel and oxidant to pass through into the cell, and are coated with a catalyst layer, which facilitates oxidation and reduction reactions. They also contain diffusion layers, which ensure that the reactants are evenly distributed throughout the FC [41].

❖ **Bipolar plates**

Bipolar plates are typically made of graphite, stainless steel, or polymers [42]. There are two main types of bipolar plates: solid and porous. Solid plates are made of a single material; they are better for high-temperature applications, while porous plates have a layer of porous material between two solid layers; they are better for low-temperature applications [43].

They have ability to conduct electricity; these plates contain channels that dispense oxidant and fuel to the cell. The plates must also be coated with a material that is resistant to corrosion in order to maintain their structural integrity, and provide a good conductivity [41].

❖ **Diffusion layer**

There are two main types of diffusion layers. Microporous layers that are made up of a thin membrane with tiny pores that allow the reactants to pass through. They are typically used in low-temperature FCs and placed between the catalyst layer and the gas diffusion layer. Their major roles are to border the lack of catalyst into the gas diffusion layers, furthermore, get better managing water [44]. Gas diffusion layers are made up of a thicker membrane with larger pores that allow the reactants to pass through. They are hence used in high-temperature FCs. They are arranged between the bipolar plates and microporous layers [39], and provide several key benefits; as well, their primary procedures are equivalent to those of microporous layers. They help to ensure that the reactants are evenly distributed throughout the cell and that the reaction is as efficient as possible [45]. This layer is used to conduct current between the catalyst layer and the bipolar plates, and it is utilized to empty the produced water to avoid its collection [46].

❖ **Catalyst layer**

A catalyst is a material used to accelerate the reaction of FCs. Platinum is the most commonly used catalyst, whereas other metals such as palladium and ruthenium can also be used. It is a precious metal, which can be expensive. It facilitates the electrochemical reactions by reducing the activation energy to allow happened them at a lower temperature; this makes the process more efficient [47].

❖ **Electrolyte**

Electrolyte is the medium that facilitates the ionic transport between the two electrodes of the FC; so, it should be able to maintain a high ionic conductivity. The sort of electrolyte used in an FC includes a solid or liquid material. It also acts as a barrier to prevent the crossover of reactants and products between the electrodes [48].

- **External circuit**

Its process is to circulate electric charges and ease their flow among the electrodes.

1.3.3 Classification of fuel cells

FCs are developed in a diversity of forms, each with unique benefits, drawbacks, and possible applications. The classification of FC is based on many factors, among them the electrochemical reactions, temperature field, and type of fuel and electrolyte required, where the latter mainly determines how they are classified [10] [41], as detailed in Table (1.1).

Fuel cell kind	Electrolyte employed	Mobile ion	Temperature °C	Electrical efficiency %	Typical power kW	Applications
PEMFC Proton Exchange Membrane Fuel Cell	Polymer membrane	H^+ Hydrogen ion	50 to 100	60 to 65	0.5 to 250	-Backup power -Portable power -DG -Transportation
AFC Alkaline Fuel Cell	Aqueous alkaline solution *KOH*	OH^- Hydroxide ion	$\simeq 100$	60 to 70	50 to 150	-Military -Space
PAFC Phosphoric Acid Fuel Cell	Liquid phosphoric acid H_3PO_4	H^+ Hydrogen ion	150 to 220	40 to 45	50 to 11000	-DG (distributed generation)
MCFC Molten Carbonate Fuel Cell	Molten carbonate salt Li_2CO_3	CO_3^{2-} Polyatomic ion	600 to 700	53 to 57	10 to 2000	-Electric utility -DG
SOFC Solid Oxide Fuel Cell	Yttria-Stabilized Zirconia ZrO_2	O^{2-} Oxide ion	$\simeq 1000$	55 to 65	1 to 2000	-Auxiliary power -Electric utility -DG

Table 1. 1: *Classifications of fuel cell.*

1.3.3.1 Proton exchange membrane fuel cell

Proton exchange membrane fuel cell (PEMFC), which is called polymer electrolyte membrane fuel cell, is a kind of FC that is being made for transportation, stationary, and portable FC applications [41]. It uses porous carbon electrodes with platinum catalysts and a solid polymer as a medium. For functioning, it only requires oxygen from the air as an oxidant and pure hydrogen supplied by reformers or storage tanks as a fuel [49].

1.3.3.1.a Operating principle of the PEMFC

The operating principle of this FC can be explained through the following [39]:

1. Hydrogen undergoes oxidation at the anode, therefore, is divided into two ions and two electrons by the formula shown in equation (1.1).

$$Anodic\ reaction: \quad H_2 \rightarrow 2\,H^+ + 2\,e^- \tag{1.1}$$

2. These electrons track an external circuit and make a direct electric current when they move to a different side. Besides, ions pass directly through the membrane.

3. Subsequently, oxygen is reduced at the cathode using ions and electrons. Thus, water is the end product plus heat, according to the equation (1.2).

$$Cathodic\ reaction: \quad \frac{1}{2}\,O_2 + 2\,H^+ + 2\,e^- \rightarrow H_2O \tag{1.2}$$

4. The cell is then cleared of extra water and air, in addition to the electrical energy as presented in the equation (1.3).

$$Overall\ reaction: \quad H_2 + \frac{1}{2}\,O_2 \rightarrow H_2O + Heat + Electrical\ Energy \tag{1.3}$$

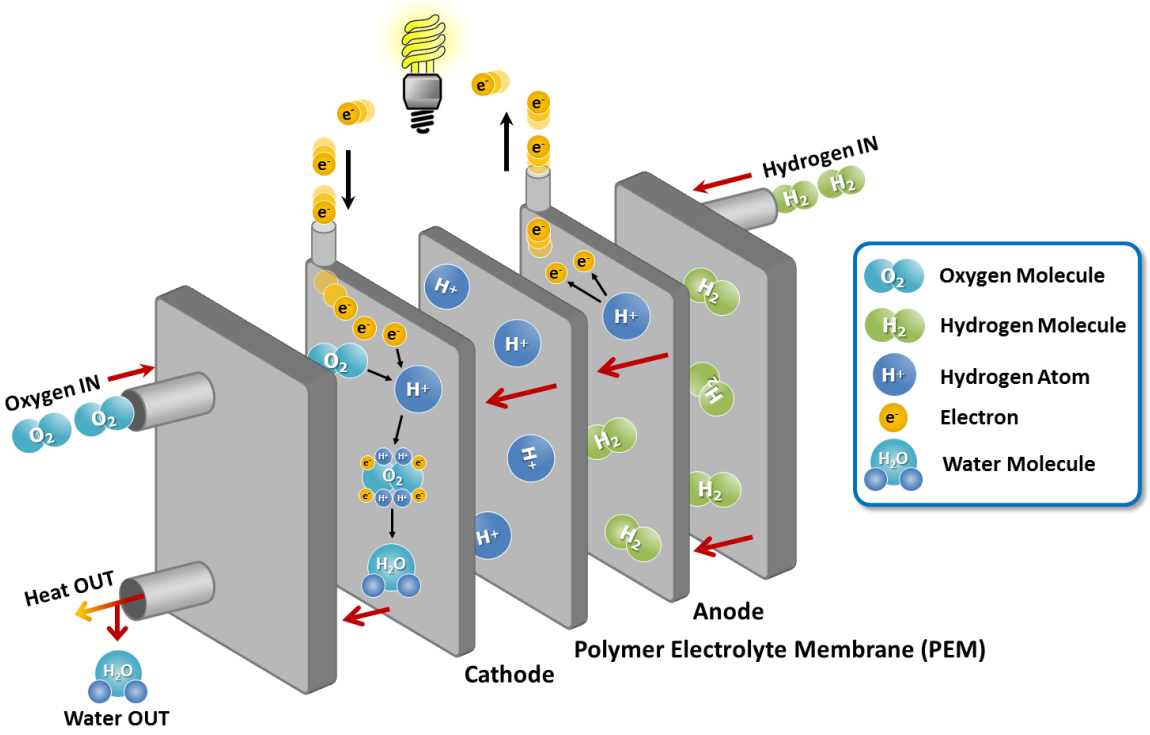

Figure 1.4: *Operation of the PEMFC [50].*

1.3.3.1.b Advantages and limitations of the PEMFC

- **Advantages [51]**
  - Zero emissions through the use of green energy (hydrogen); therefore, the FC vehicles are environmentally friendly.
  - More effective.
  - Deliver flexibility because of the production of hydrogen from different methods.
  - Offer security via elimination of oil requirement.
  - Scalability of this fuel cell (various sizes, thus, there are produced diverse power).
  - Lower weight than batteries.
- **Limitations [38]**
  - Lifetime limits are not confirmed validities.
  - Drop in electrical efficiency within passing her lifetime.
  - Special fuel treatment (H_2) is required.
  - Platinum-used catalyst is expensive.

1.4 Storage energy sources

The storage system used consists of two components, a battery and supercapacitor.

1.4.1 Battery

1.4.1.1 Description of battery

Batteries are an essential part of the hybrid system, and they offer the perfect aid to deliver power and help FCs with sudden load needs [39]. They are electrochemical devices that can be classified into non-rechargeable (primary battery) and rechargeable (secondary battery) batteries [52]. For these latter, a transformation of electrical energy into chemical energy is possible during charging mode, while in discharging mode, the chemical energy is converted back into electric energy [36]. They are used to store and supply power from and to renewable energy and clean energy-based power systems, and should be reliable, durable, and safe, including lead-acid, lithium-ion and sodium-sulfur batteries [32].

Batteries formed from a single electrochemical cell are referred to as cells. Therefore, these cells can be assembled in series or parallel to form batteries to obtain the desired voltage and storage capacity [52].

1.4.1.2 Components of battery

❖ **Negative and positive electrodes**

The two electrodes are the seats of the redox reactions [53]. Furthermore, the negative electrode is created from a mixture of carbon-based materials, while the positive electrode is constructed out of metal oxides.

❖ **Electrolyte**

The electrolyte allows ions to pass and lets them exclusively flow, and it can be in the form of a liquid, polymeric, or solid. Currently, liquid electrolytes are supported for multiple applications [54].

❖ **Separator**

To avoid internal short circuits between the electrodes, separator insulation must be inserted between the electrodes when the electrolyte is liquid [53], and this is a microporous membrane whose role is to allow the exclusive flow of ions [55].

Multiple battery forms can be either cylindrical, pouch or prismatic cells [56], as depicted in Figure (1.5).

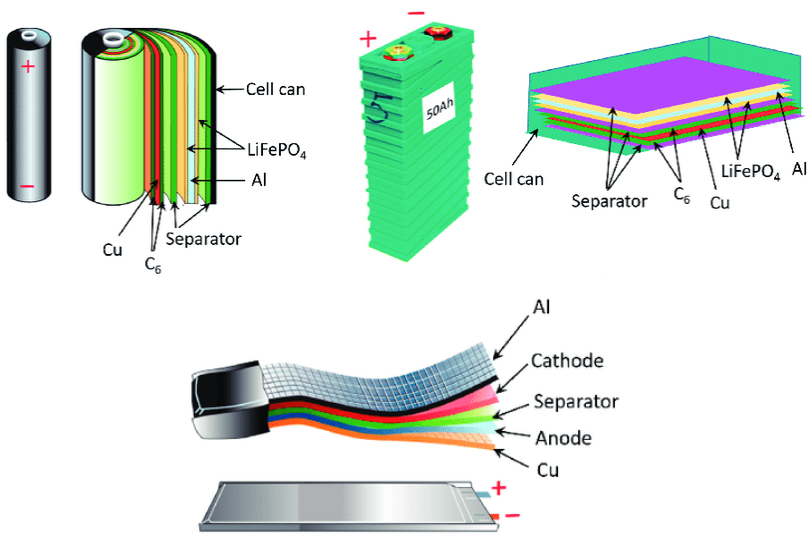

(a) (b) (c)

Figure 1.5: *Representation of the shape and components of various Li-ion battery configurations. Cylindrical (a), prismatic (b), and pouch cell (c) [57].*

1.4.1.3 Classification of batteries

Depending on the materials used for electrodes, one can find many promising battery technologies [10] [58] [59] , as described in Table (1.2).

Type	Lithium-ion	Lead-acid	Nickel-cadmium	Nickel-metal
Negative electrode	*Graphite*	*Pb*	*Cd*	*MH*
Positive electrode	$LiCoO_2$	PbO_2	$Ni(OH)_2$	$Ni(OH)_2$
Electrolyte	*Organic*	H_2SO_4	*KOH*	*KOH*
Nominal voltage (V)	3.6	2	1.25	1.25
Energy density (Wh/Kg)	110-160	30-50	45-80	60-120
Power density (W/Kg)	1800	180	150	250-1000
Overcharge tolerance	Very low	High	Moderate	Low
Self-discharge rate	Very low	Low	Moderate	High
Operating temperature (°C)	-20 to 60	-20 to 60	-40 to 60	-20 to 60
Number of cycle life	500-1000	200-300	1500	300-500

Table 1.2: *Classifications of batteries.*

1.4.1.3.1 Lithium-ion battery (Li-ion battery)

Due to lithium's lightweight and quick-response nature, the lithium-ion battery is the finest commercially available battery in terms of power density [5]. It functions similarly to a capacitor and possesses three layers: negative and positive electrodes, and an electrolyte.

The typical material used at the negative electrode is graphite as an intercalation material of lithium (LiC6), as viewed in Figure (1.6). In other words, graphite, which is one of the allotropic forms of carbon, has a hexagonal structure (i.e., the most stable phase

thermodynamically) and forms planar layers that allow the lithium to be wedged and stored between the layers. Thus, the technical term for this is intercalation [58].

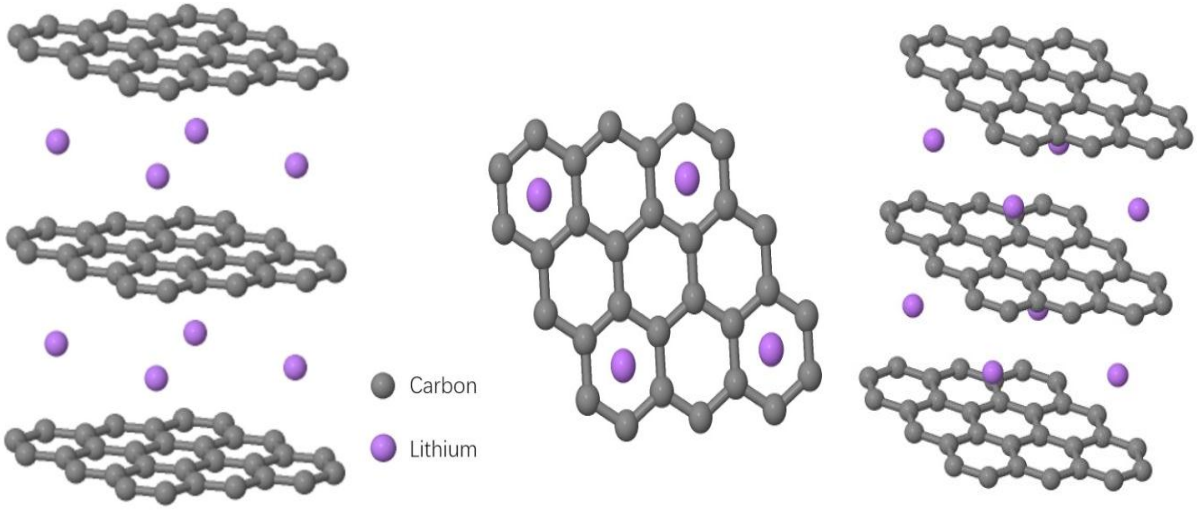

Figure 1.6: *Representation of Li-ion battery negative electrode [60].*

Positive electrode materials are divided into three main categories. The most studied ones are oxides of spinal structure, metal oxides of polyanionic structure (given in olivine-like structural materials, iron phosphates), and lamellar transition metal oxides [58]. Based on the latter, LiCoO2 (lithium cobalt oxide) is the most common positive electrode material used in commercial and rechargeable lithium batteries [61]. This material has a lamellar structure, and the crystalline mesh is rhombohedral and is formed by oxygen atoms with alternating layers of lithium and cobalt ions [62], as presented in Figure (1.7); this structure allows lithium ions to be easily inserted into the matrix.

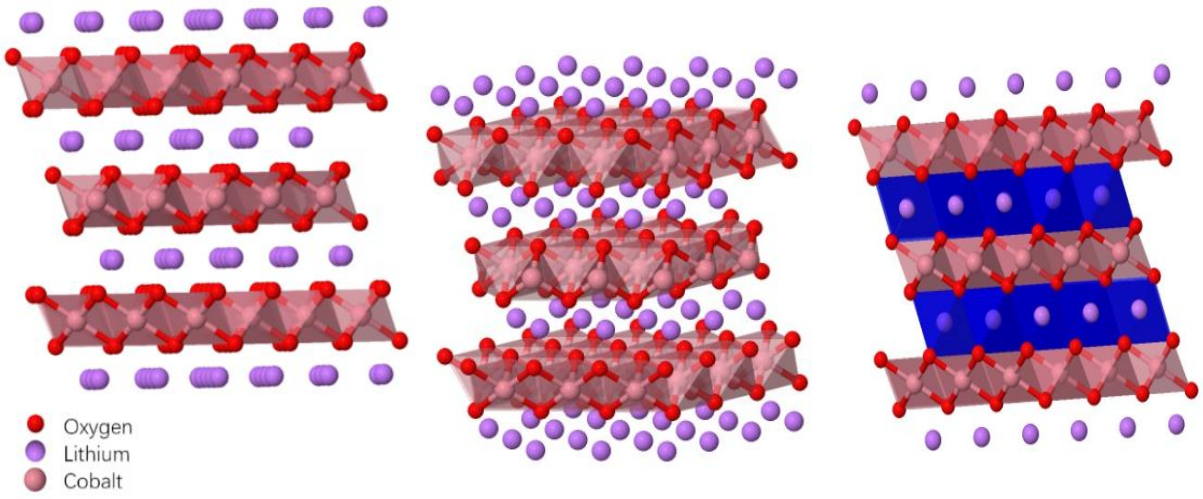

Figure 1.7: *Representation of Li-ion battery positive electrode [60].*

The thing to be known is that graphite and cobalt peroxide materials are not good at collecting or distributing electrons; thus, a conductive copper layer is added to the graphite [63], and a conductive aluminum layer next to the cobalt oxide [64]. These two layers are called collectors.

Additionally, an electrolyte is created by dissolving lithium salts in organic (non-aqueous) solvents [54]. Salts are abbreviated in lithium hexafluoroarsenic (LiAsF6), lithium perchlorate (LiClO4), lithium tetrafluoroborate (LiBF4), and in particular, lithium hexafluorophosphate (LiPF6) is the most widely used salt on an industrial scale [65], as it offers a good compromise between ionic conductivity, stability, and cost compared to other salts. Shortened solvents in propylene carbonate (PC) and ethylene carbonate (EC) are the most commonly used solvents. Co-solvents included dimethyl carbonate (DMC) and diethyl carbonate (DEC). The composition usually used is premised on LiPF6 disbanded in a combination of ethylene carbonate (EC) and dimethyl carbonate (DMC), known as designation "LP30" [58] and described in Figure (1.8 (a)).

Thus, Li^+ is primarily coordinated with polarizable carbonyl groups; Li^+ ions bind to the oxygen atoms of the DMC, with bonds making and breaking in parts of a second, and the same is true for EC [66], and it is aggregated in ion pairs with PF^{-6}. Combining these observations, one can rationalize that the presence of a Li+ ion, which is coordinated with a carbonyl group, will orient the corresponding EC or DMC molecule with its carbonyl group slightly towards the next layer [67], as shown in Figures (1.8 (b)) and (1.8 (c)).

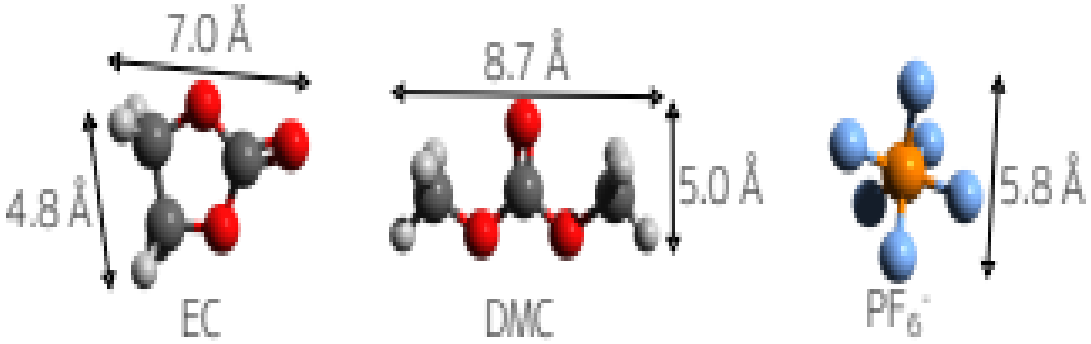

(a) Sketches of the molecules of the individual species comprising the investigated LiPF6 in EC: DMC electrolyte solution, the arrows indicate the molecular size, and include the molecules' van-der-Waals radii [67].

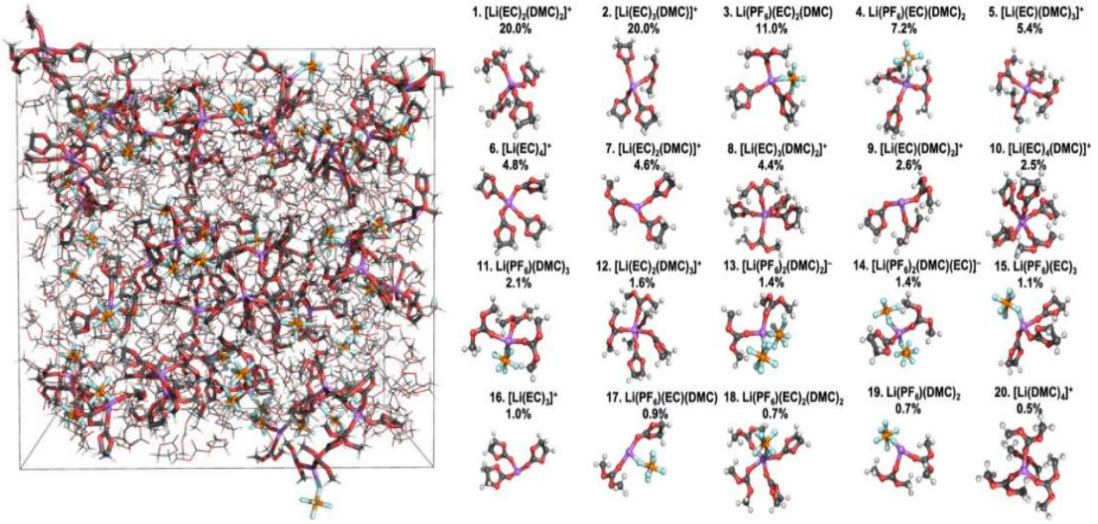

(b) the overall structure of LP30 [68]. *(c) the 20 most common Li^+ 1st solvation shell structures, and Li^+ probabilities (in percentages) [68].*

Figure 1 8: *Representation of Li-ion battery electrolyte.* The principal contributors to the (Li+) ion transport: are purple: Li; orange: P; cyan: F; red: O; grey: C; white: H.

Since the electrolyte is an organic solvent, it contains a key battery element to ensure its good safety, which is called the separator with a plastic nature; to give more accuracy, polyethylene (PE) is the most common in Li-ion batteries [69].

1.4.1.3.1.a Operating principle of the Li-on battery

The operating principle of the Li-ion battery [54] is detailed in the following:

During discharge (use), the negative electrode will yield electrons to the external circuit via an electrochemical oxidation reaction, which kicks out those electrons into an external circuit also accompanied by the deintercalation of lithium ions from the graphitic planes, according to the ensuing oxidation reaction presented in equation (1.4).

$$Li_x C_6 \rightarrow 6\,C + x\,Li^+ + x\,e^- \qquad (1.4)$$

Throughout the discharge process, Li+ ions are therefore produced with the negative electrode, then migrated from one electrode to another through the ionic conductive electrolyte and consumed by the positive electrode via an insertion reaction, according to the subsequent reduction reaction viewed in equation (1.5).

$$Li_{1-x}CoO_2 + x\,Li^+ + x\,e^- \rightarrow LiCoO_2 \qquad (1.5)$$

During the charge, an opposite current is imposed employing an external generator; therefore, an opposite phenomenon will take place; oxidation to the positive electrode (lithium extraction) and reduction to the negative electrode (lithium insertion).

The overall equation for this procedure is described in equation (1.6).

$$Li_xC_6 + Li_{1-x}CoO_2 \underset{Charge}{\overset{Discharge}{\rightleftharpoons}} LiCoO_2 + 6\,C \qquad (1.6)$$

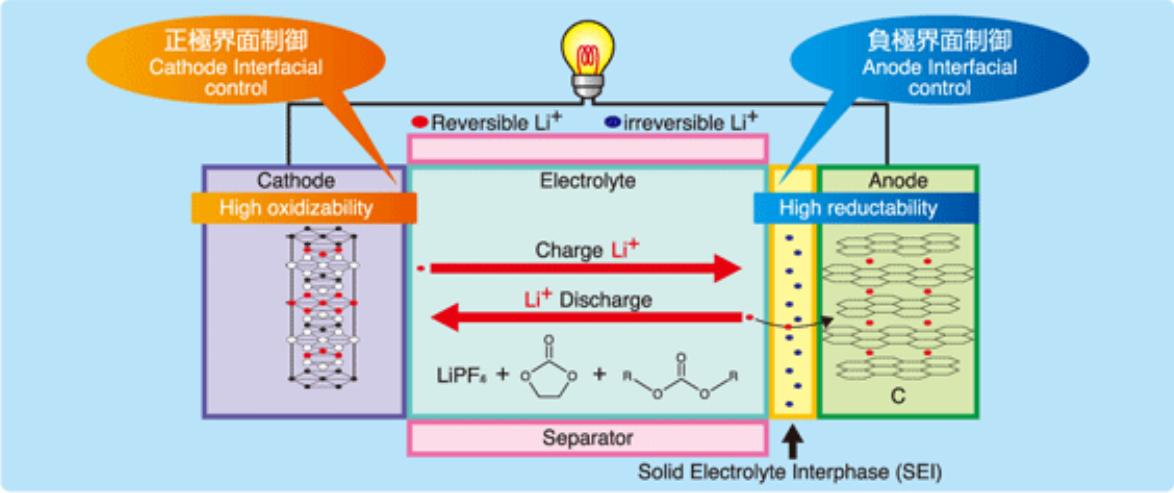

Figure 1.9: *Operation of the Li-ion battery [66].*

1.4.1.3.1.b Advantages and limitations of Li-ion batteries

- **Advantages**
  - High energy density [70].
  - Relatively low self-discharge [70].
  - Low-down maintenance [70].
  - Adequate performance even in low temperatures [46].
  - Long longevity of service [71].
- **Limitations**
  - Expensive to fabricate than other kinds [70].
  - Require costly surveillance criteria; utilized to evade explosion when their temperature is too hot [71].

1.4.2 Supercapacitor

1.4.2.1 Description of supercapacitor

A supercapacitor as a store energy system is used to support energy storage elements that do not have sufficient power for use like batteries, FCs, etc. This SC energy is stored in electrostatic form by charge accumulation between two electrodes. The electrodes are made of porous carbons, and they are separated by a dielectric material. In the SC, there is no oxidation-reduction reaction between the electrodes and the dielectric material. Thanks to this energy storage process, the SC has a high specific power (W/kg) and a long lifespan [72].

1.4.2.2 Components of supercapacitor

The composition of the SC is undertaken simply, as shown in Figure (1.10). In fact, the SC consists of two electrodes, which are immersed in the electrolyte. A separator separates the two electrodes. The latter in turn lets the ions migrate in the electrolyte [72]. A practical SC for energy storage in a microgrid requires a stack of many single cells connected in series [73]. Each cell consists of five layers with a porous separator in the center, a pair of porous electrodes on each side of it, and a pair of current collectors that congregate charges located at the end of each cell [5].

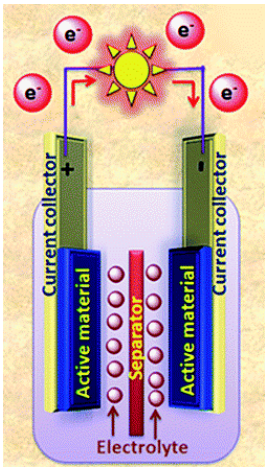

Figure 1.10: *Supercapacitor components [74].*

- **The electrode**

Electrode materials should have high capacitance because they are of great priority in the performance of SCs. These materials might be fabricated from various materials on the basis of the type of energy storage and capacity ranges required for use. Thus, by reference to the SC sorts [75], electrochemical double-layer capacitors **(**EDLCs) used can be activated carbon,

carbon aerogels, graphene, or carbon nanotubes (CNT); the pseudo-capacitors based on metal oxides or conducting polymers (CPs); and hybrid capacitors are focused on combinations regarding conducting polymers or metal oxides with carbon materials [76].

- **The electrolyte**

Electrolyte is employed for the movement or conduction of ions, and it is selected by the type and size of ions, concentration, and electrode materials. It is presented in organic and aqueous electrolytes like acid, alkaline, and neutral electrolytes [77] or ionic liquid electrolytes [78].

- **The separator**

It is an electrical insulator that prevents physical contact between electrodes but allows ion transfer between them [79].

- **The cells**

They are packed and immersed in an electrolytic solution, forming the double-layer charge distribution.

1.4.2.3 Classification of supercapacitors

Supercapacitors can be divided into three general classes: electrochemical double-layer capacitors, pseudocapacitors, and hybrid capacitors. As indicated in Figure (1.11), each class is characterized by its unique mechanism for storing charge [80].

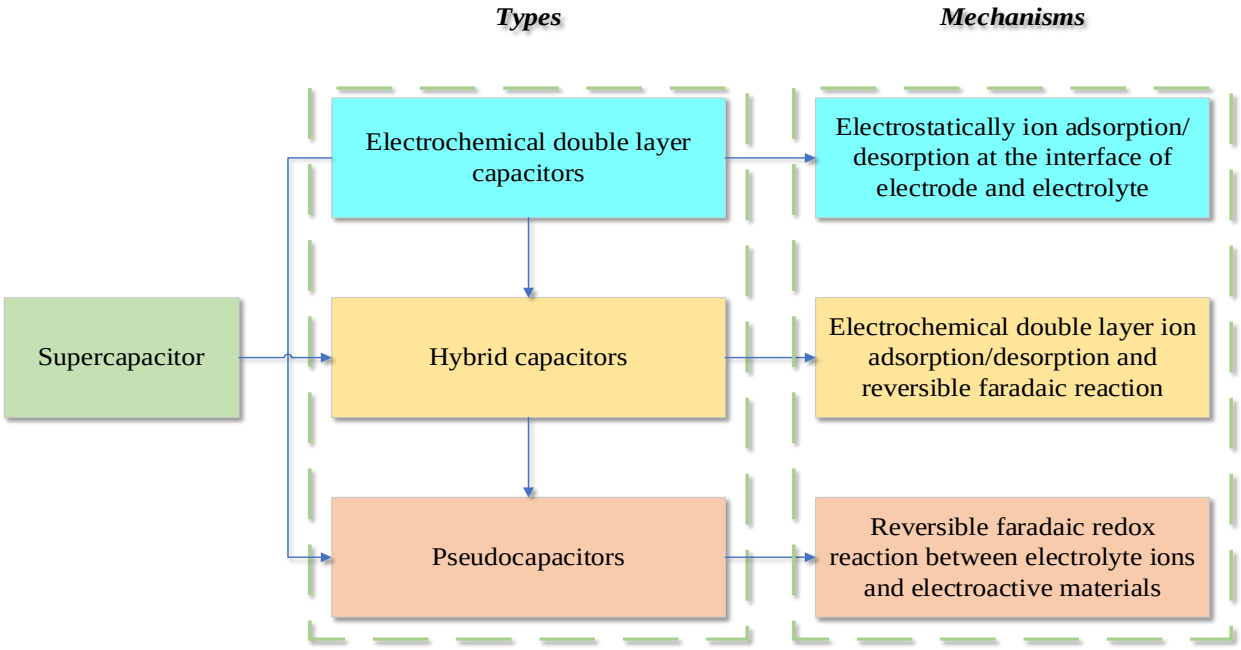

Figure 1.11: *Supercapacitors types based on the mechanism of energy storage.*

1.4.2.3.a Pseudocapacitors

Pseudocapacitor is a type of SC with metal oxide or conducting polymer electrodes with high electrochemical pseudocapacitance material [75]. Pseudocapacitors store Faradaically through the transfer of charge between electrode and electrolyte. This is accomplished through electrosorption and reduction-oxidation reactions [82]. In the case of applying a potential to the pseudo-capacitor reduction, the oxidation happens on electrode material that includes the charge's passage across a double layer, leading to the fact that the Faradic current passes through an SC cell. In addition, the Faradic mechanism involved in pseudocapacitors allows them to achieve a great specific capacitance as well as energy densities in comparison to EDLCs [83].

1.4.2.3.b Hybrid capacitors

Hybrid Capacitors is a type of SC with asymmetric electrodes that utilize both Faradaic and non-Faradaic processes to store charge [80]. In addition, the hybrid capacitors have a combination of performance properties that was previously unachievable. Also, they are combining the best features related to pseudo-capacitors and EDLCs into a unified structure [77].

1.4.2.3.c Electrochemical double-layer capacitors

EDLCs include an electrolyte; two carbon-based materials use an electrode as well as a separator. EDLCs are either able to electro-statically store the charges or via a non-faradic process that does not need charge transfers between the electrolyte and electrode [81]. Usually, the storage capacity of a SC is 20-1000 times that of a common capacitor. It has high power density and high energy conversion efficiency. Hence, it has attracted widespread attention. However, since the voltage of a single cell is low, a SC consists of numerous capacitors arranged in parallel or in series. Strictly speaking, the internal parameters of each capacitor are different, and thus a voltage imbalance may exist in the SC and affect its operational reliability [5].

1.4.2.3.c.1 Operating principle of the electrochemical double-layer capacitors

EDLCs utilize an electrochemical double-layer of charge to store energy. As voltage is applied, charge accumulates on the electrode surfaces. Following the natural attraction of unlike charges, ions in the electrolyte solution diffuse across the separator into the pores of the electrode of the opposite charge. However, the electrodes are engineered to prevent the recombination of the ions. Thus, a double-layer of charge is produced at each electrode. These double-layers, coupled with an increase in surface area and a decrease in the distance between electrodes, allow EDLCs to achieve higher energy densities than conventional capacitors [84]. Because there is no transfer of charge between electrolyte and electrode, there are no chemical or composition changes associated with non-Faradaic processes. For this reason, charge storage in EDLCs is highly reversible, which allows them to achieve very high cycling stability. EDLCs generally operate with stable performance characteristics for a great many charge-discharge cycles, sometimes as many as 106 cycles. On the other hand, electrochemical batteries are generally limited to only about 103 cycles. Because of their cycling stability, EDLCs are well suited for applications that involve non-user serviceable locations, such as deep sea or mountain environments [80].

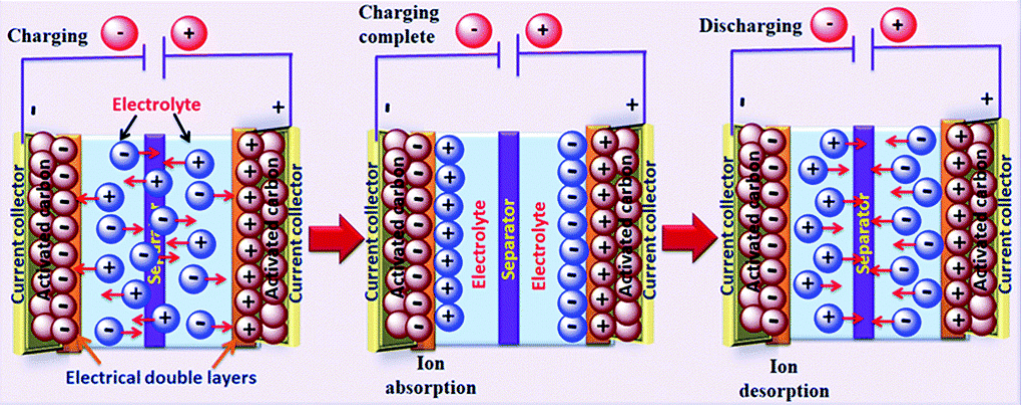

Figure 1.12: *Operation of the electrochemical double-layer capacitors [74].*

1.4.2.3.c2 Advantages and limitations of electrochemical double-layer capacitors

- **Advantages [59]**
  - High power density.
  - Can withstand extreme temperature conditions.
  - Quick dynamics (fast charging and unloading times).
  - Long service life (very high cycle).
- **Limitations [59]**
  - Low energy density.
  - Lowly nominal voltage, which requires multiple modules to be serialized.
  - High cost.

1.5 Conclusion

This chapter provides a synopsis of a fuel cell hybrid power system. A comprehensive review of its components is given, along with the reason for choosing them and some details of their operation. In the current chapter, the modeling of the PEM fuel cell hybrid power system, in which PEMFC represents the fundamental power source, will be considered alongside a Li-ion battery and supercapacitor as an energy storage system. For the record, they are all controlled by DC-DC power converters.

Chapter 2:

Modeling and Control of Fuel Cell/ Battery/ Supercapacitor Hybrid System

---

Hybrid power system modeling, required for computer simulation and controller synthesis, is usually based on a theoretical analysis of the various physical processes occurring in the system. Indeed, mathematical models describing the system characteristics are formulated and translated into computer codes to be used in the simulation process. The modeling of the components of the HPS involves the knowledge of various disciplines (power sources, power electronics, etc.) and requires a good understanding of the interactions between them. In the first part of this chapter, the modeling of fuel cell, battery, and supercapacitor is presented. These sources need to be interfaced with the DC-bus by means of DC-DC converters. So, these converters are also modeled and controlled in the second part of this chapter. Finally, simulation results of each power source connected to a constant DC-bus source via an appropriate converter are illustrated and discussed.

2.1 Fuel cell modeling

The Proton Exchange Membrane fuel cells have shown great promise for use as distributed generation sources [85]. They are a good source of energy, providing a reliable source in a steady state. However, they cannot respond to a transient electrical load as quickly as desired, due to slow electrochemical and internal thermal reactions [32]. They have highly nonlinear behavior and depend on a combination of factors such as temperature, reactant pressure, membrane hydration, reactant concentrations, and electrical load [86].

The overall reaction of PEMFC can be written as follows:

$$H_2 + \frac{1}{2}O_2 \rightarrow H_2O + heat + electrical\ energy \tag{2.1}$$

where H_2, O_2 and H_2O are hydrogen, oxygen and water molecule, respectively.

The output voltage of a fuel cell is given as the algebraic sum of the open circuit voltage E_{oc}, activation losses η_{act}, ohmic losses η_{ohmic}, and concentration losses, as follows [86]:

$$V_{cell} = E_{oc} - \eta_{act} - \eta_{ohmic} - \eta_{conc} \quad (2.2)$$

The PEMFC equivalent electrical circuit describing the above equation is shown in Figure (2.1).

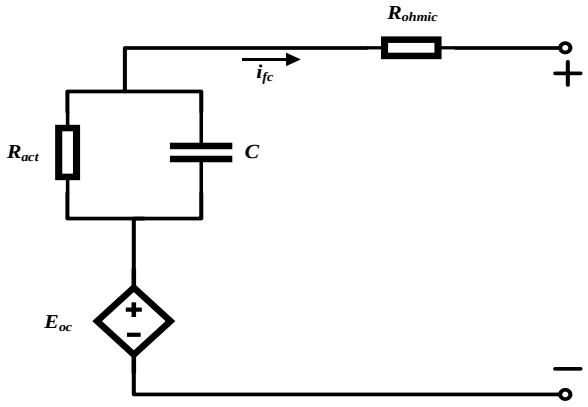

Figure 2.1: *Equivalent electrical circuit of a PEMFC.*

The open circuit voltage is expressed as:

$$E_{oc} = K_c E_n \quad (2.3)$$

Where K_c is the voltage constant at nominal condition of operation and, En is the Nernst voltage.

The Nernst equation is calculated as follows:

$$E_n = \begin{cases} 1.229 + (T - 298).\frac{-44.43}{2F} + \frac{RT}{2F}\ln\left[P_{H_2}\left(P_{O_2}\right)^{0.5}\right] & when\ T \le 100C^0 \\ 1.229 + (T - 298).\frac{-44.43}{2F} + \frac{RT}{2F}\ln\left[\frac{P_{H_2}\left(P_{O_2}\right)^{0.5}}{P_{H_2O}}\right] & when\ T > 100C^0 \end{cases} \quad (2.4)$$

where:

- P_{H_2} : is the partial pressure of hydrogen.
- P_{O_2} : is the partial pressure of oxygen.
- P_{H_2O} : is the partial pressure of water. Notice that $P_{H_2O} = 1$ for T<100°C; for that, it is not used in the first equation od (2.4).
- R : is the ideal gas constant equal to $8.3143\ J/(mol.K)$.
- F : is the Faraday constant equal to 96487 coulombs/mol.
- T: Operating temperature (K).

The partial pressures of hydrogen, oxygen and water are expressed as [87]:

$$P_{H_2} = (1 - U_{f_{H_2}}) x\% P_{fuel} \tag{2.5}$$

$$P_{O_2} = (1 - U_{f_{O_2}}) y\% P_{air} \tag{2.6}$$

$$P_{H2O} = (W - 2y\% U_{f_{O_2}}) P_{air} \tag{2.7}$$

where $U_{f_{H_2}}$ and $U_{f_{O_2}}$ are the hydrogen and oxygen utilizations, x and y are the percentages of hydrogen and oxygen in the fuel and air (%), W percentage of water vapor in the oxidant (%).

The hydrogen and oxygen utilization factors are expressed by:

$$U_{f_{H_2}} = \frac{60000 RT i_{fc}}{2F P_{fuel} V_{fuel} x\%} \tag{2.7}$$

$$U_{f_{O_2}} = \frac{60000 RT i_{fc}}{2F P_{air} V_{air} y\%} \tag{2.9}$$

where V_{fuel} and V_{air} are the fuel and air flow rates (l/min), i_{fc} is the cell current of FC (A).

2.1.1 Activation loss

Activation loss or overvoltage in activation is the result of electron transfer breaks that form chemical bonds on the electrodes [88]. Activation loss is the portion of available energy that is lost during the transfer of electrons to and from the electrodes [89]. The reaction of hydrogen oxidation at the anode is very fast, while the reaction of oxygen reduction at the cathode is much slower [90]. Therefore, cathode reactions are dominated by voltage drop. The relationship between over-energization voltage and current density is described by the Tafel equation [39, 41] :

$$\eta_{act} = A \ln\left(\frac{i_{fc}}{i_0}\right) \frac{1}{s\frac{T_d}{3} + 1} \tag{2.10}$$

The exchange current and the Tafel slope are given by:

$$i_0 = \frac{2FK(P_{H_2} + P_{O_2})}{Rh} \exp\left(\frac{-\Delta G}{RT}\right) \tag{2.11}$$

where A is the Tafel slope and has a unit of volt and it is expressed by:

$$A = \frac{RT}{z\alpha F} \tag{2.12}$$

- i_0 is the exchange current.
- ΔG is the activation energy barrier (J).
- K and h are the Boltzmann's constant (J/K) and the Planck's constant (Js), respectively.
- z is the number of moving electrons (2 for the redox reaction).
- α is the charge transfer coefficient (0.18409).
- T_d is the cell settling time to a current step.

2.1.2 Ohmic loss

The ohmic loss is due to the resistance of the polymer membrane, the transport of protons, the resistance of the electrode and collector plate, and the transport of electrons. In the ohmic polarization region, the output voltage becomes linearly dependent on the current density with a slope determined by the ionic resistance of the electrolyte polymer [41].

$$\eta_{ohmic} = R_{ohmic} i_{fc} \tag{2.13}$$

where R_{ohmic} is the FC internal resistance.

The equivalent voltage of a number of stacked fuel cells is expressed as:

$$V_{fc} = N_{fc} V_{cell} \tag{2.14}$$

where N_{fc} is the number of the FC cells.

2.1.3 Concentration Loss

Concentration loss is the results of the change in the reactants concentration as they are consumed in the reaction. This loss is the reason for rapid voltage drop at high current density. The voltage drop resulting from concentration losses is approximated by [41]:

$$V_{conc} = I_{fc}\left(C_2 \frac{I_{fc}}{I_{\max}}\right)^{C_3} \tag{2.15}$$

where C_2 and C_3 are constants that depend on the temperature and the reactant partial pressure and can be determined empirically.

$I_{\max}$: is the current density that causes a precipitous voltage drop.

Figure (2.2) shows the scheme of the fuel cell stack model implemented in Specialized Power Systems (SPS). Block A represents equations (2.8) and (2.9). Block B represents equations (2.3) and (2.11). Block C represents equation (2.12). In this model, the concentration losses are neglected.

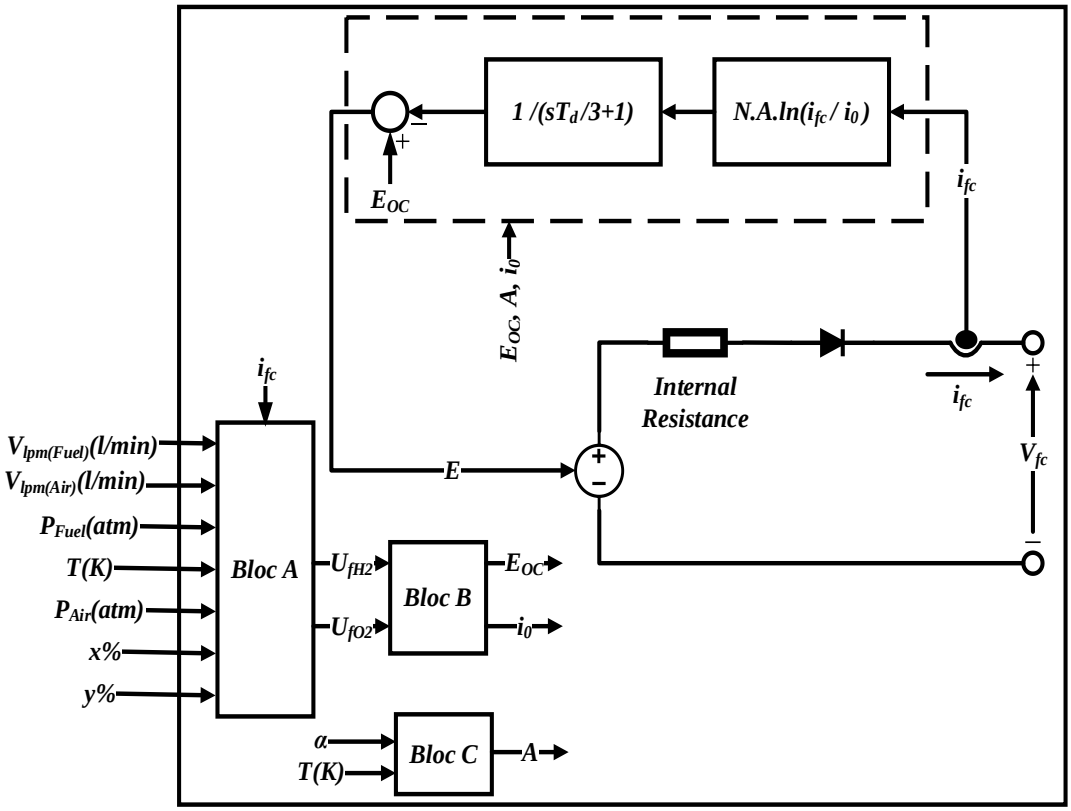

Figure 2. 2: *Fuel cell stack model [23].*

2.2 Battery modeling

The battery considered for this study is of the Li-ion type because. It has been shown to exhibit high energy density and efficiency compared to other battery types (such as lead-acid, NiCd or NiMH). This feature makes it more attractive for automotive or aircraft applications [91].

The battery voltage is expressed as:

$$V_{batt} = E_{ob} - R_{batt} i_{batt} \tag{2.16}$$

The battery open circuit voltage E_{ob} for charging and discharging modes is expressed as:

$$E_{ob} = \begin{cases} E_0 - K\frac{Q}{Q-it}i^* - K\frac{Q}{Q-it}it + A_0 e^{-(B.it)} & \text{when } i^* > 0 \quad \text{(discharge mode)} \\ E_0 - K\frac{Q}{0.1Q-it}i^* - K\frac{Q}{Q-it}it + A_0 e^{-(B.it)} & \text{when } i^* < 0 \quad \text{(charge mode)} \end{cases} \tag{2.17}$$

- E_0 : is the battery constant voltage (V).
- K : is the polarization constant (V/Ah).
- Q : is the battery capacity (Ah).
- i^* : is the filtered battery current (A),
- it : is the actual battery charge (Ah).
- A_0 : is the exponential zone amplitude (V).
- B : is the exponential zone time constant inverse $(Ah)^{-1}$.
- R_{batt} : is the battery internal resistance (Ω).

The term $K\frac{Q}{Q-it}.it$ from equation (2.17) is referred as polarization voltage, while the term $K\frac{Q}{Q-it}$ is the polarization resistance (Pol_{res}).

During charging mode, the battery voltage increases abruptly after being fully charged, this behavior is represented by modifying the polarization resistance (only during charging) as follows:

$$K\frac{Q}{it-0.1Q} \tag{2.18}$$

The transfer function of the current filter is as follows:

$$G = \frac{1}{6.67s+1} \tag{2.19}$$

Figure (2.3) shows the block diagram of the battery model implemented in SPS.

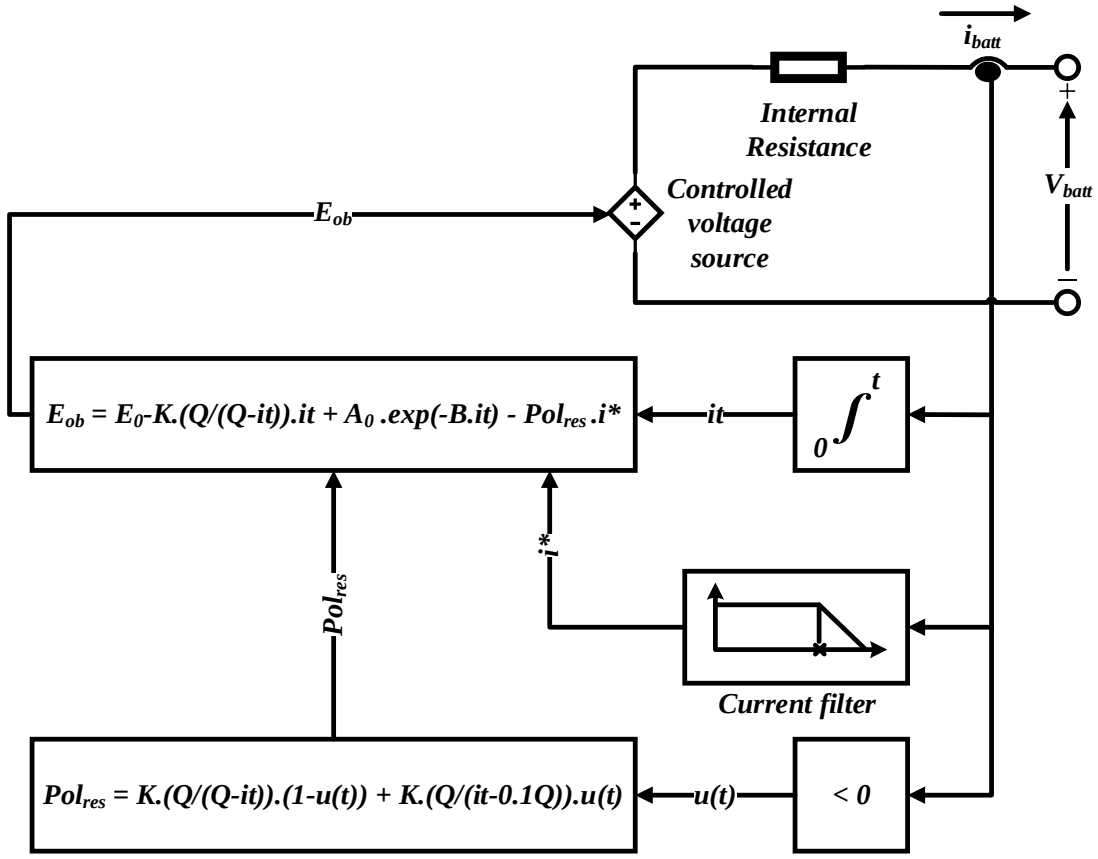

Figure 2.3: *Li-ion battery model [23].*

In charging mode u(t)=1 and in discharging mode u(t)=0.

❖ **State of charge**

State of charge (SOC) is defined as the remaining available capacity in the battery, expressed as a percentage of the rated capacity. It is a very important characteristic that informs us about the battery load level. The ability to estimate charge status avoids deep discharges or overcharges that would damage batteries [92]. The SOC is defined by:

$$SOC\ (\%) = 100\ (1 - \frac{1}{Q}\int_0^t i_{batt}(t))dt \tag{2.20}$$

2.3 Supercapacitor modeling

A Electric Double Layer Capacitors (EDLC) is used in HPS for its capability of delivering high power for short periods of time without damaging its internal structure, and also operates for a long cycle life with high efficiency, which exceeds Li-ion battery performance [93]. Also, EDLC maintains Li-ion battery discharge current within the battery limits, which extends the life cycle of a Li-ion battery by compensating for high load current [94]. The

adopted SC model is based on the Stern model, which combines the Helmholtz and Gouy-Chapman models. The EDLC cell capacity is expressed as [72]:

$$C_s = \left[\frac{1}{C_H} + \frac{1}{C_{GC}} \right]^{-1} \tag{2.21}$$

where C_H and C_{GC} are the Helmholtz and Gouy-Chapman capacitance (F), respectively defined by:

$$C_H = \frac{N_e \varepsilon \varepsilon_0 A_i}{D_h} \tag{2.22}$$

$$C_{GC} = \frac{FQ_c}{2N_e RT} \sinh\left(\frac{Q_c}{N_e^2 A_i \sqrt{8RT\varepsilon\varepsilon_0 c}} \right) \tag{2.23}$$

where:

- N_e: is the number of electrode layers.
- ε and ε_0 are the permittivities (F/m) of the electrolyte material and free space, respectively.
- A_i: is the inter-facial area between electrodes and electrolyte (m^2).
- D_h: is the Helmholtz layer length (or molecular radius) (m).
- Q_C: is the cell electric charge (C).
- c: is the molar concentration (mol^{-3}).

For a SC module of N_s cells in series and N_p cells in parallel, the total capacitance is given by:

$$C_T = \frac{N_p}{N_s} C \tag{2.24}$$

The SC output voltage is expressed considering resistive losses as:

$$V_{sc} = \frac{Q_T}{C_T} - R_{sc}.i_{sc} \tag{2.25}$$

with:

$$Q_T = N_p Q_c = \int i_{sc} dt \tag{2.26}$$

where Q_T is the total electric charge (C), R_{sc} is the SC module resistance (Ω) and i_{sc} is the SC module current (A).

2.4 Power converters modeling and control

The FC and storage elements are connected to the DC-AC inverter through DC-DC converters. This allows voltage conversion (from low voltage to high voltage) as well as full control of the fuel cell/battery/ supercapacitor current and DC-bus voltage. The FC is controlled by a DC-DC boost converter [95]. Similarly, the Li-ion battery and SC are controlled by bidirectional DC-DC buck-boost converters, since during operation they are charging and discharging [93]. The converter operates in boost mode when the battery / SC discharges and it works in buck mode when the battery / SC charges [92]. DC-DC converters can be represented by two types of models, which are: the switching models and the average-value models. The switching models are mainly used for design purpose and to investigate types of pulse-width-modulated (PWM) schemes with regards to switching harmonics and losses. These models require small sampling time to observe all the switching actions, which makes the simulation very time consuming [21]. In the averaged model, the power electronic switch and diode are replaced by a combination of controlled current and voltage sources. This gives the same performance as the detailed circuit model at less time [34].

2.4.1 DC-DC boost converter model and control

2.4.1.1 Model of boost converter

In this subsection, a unidirectional DC-DC boost converter is considered to convert the DC power generated by the PEMFC stack to an output controlled DC power [37].

As illustrated in Figure (2.4), the DC-DC boost converter circuit consists of a semiconductor power switch, diode and inductor to transfer the energy from input to output. Control circuitry is added to the boost converter to handle the energy transfer and to maintain the current and/or voltage in normal operating range [96].

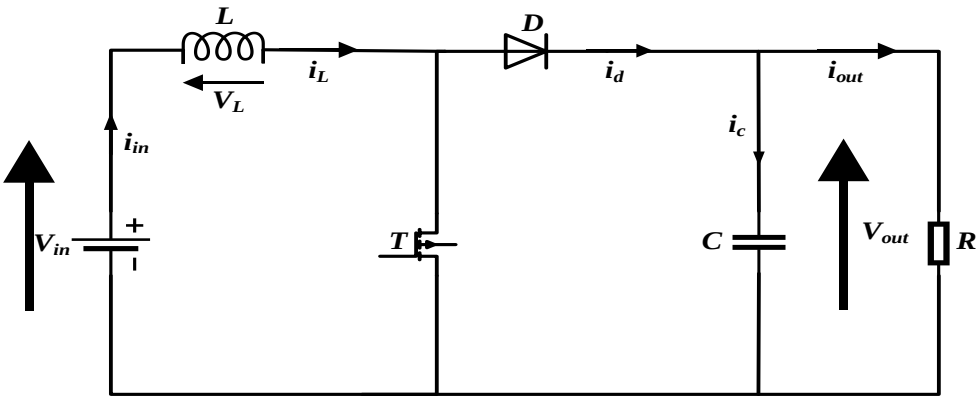

Figure 2.4: *Structure of a classic boost converter.*

Depending on the shape of the current of the inductance, we have two operating modes of the DC-DC converter [97]:

- Discontinuous conduction mode (DCM), in which the inductance current is periodically canceled.
- Continuous conduction mode (CCM), in which the inductance current is never cancelled.

The adopted mathematical model of the DC-DC boost converter is obtained using the Kirchhoff's voltage and current laws in continuous mode. Based on the switching position function (S=1 (Figure (2.5)) or S=0 (Figure (2.6))).

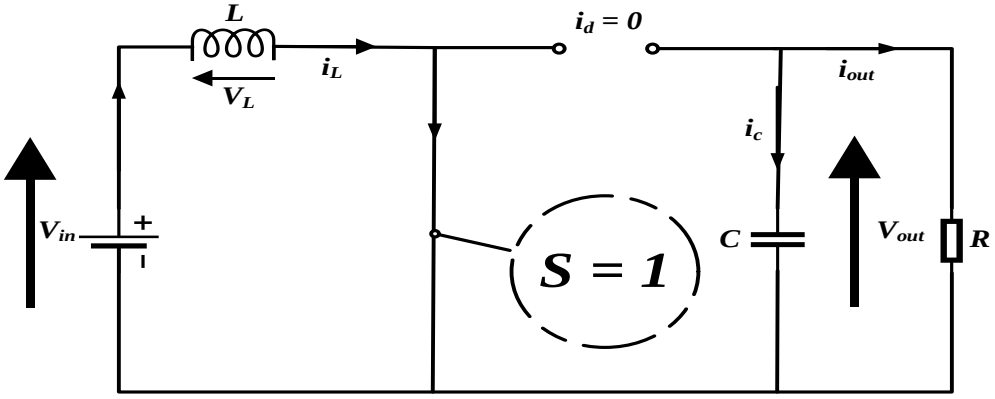

Figure 2.5: *Equivalent circuit of the classic boost converter when the switch is closed.*

When the switch position function is set to S=1, the following equations are obtained [98].

$$V_{in} = V_{L} = L\frac{di_L}{dt} \tag{2.27}$$

$$C\frac{dV_{out}}{dt} = -\frac{V_{out}}{R} \tag{2.28}$$

$$y = C_1\begin{bmatrix} i_L \\ V_{out} \end{bmatrix} = Ri_C = CR\frac{dV_{out}}{dt} = -V_{out} \tag{2.29}$$

Using the matrix form, the above equations can be rewritten as:

$$\begin{bmatrix} \frac{di_L}{dt} \\ \frac{dV_{out}}{dt} \end{bmatrix} = \underbrace{\begin{bmatrix} 0 & 0 \\ 0 & \frac{-1}{RC} \end{bmatrix}}_{A_1} \begin{bmatrix} i_L \\ V_{out} \end{bmatrix} + \underbrace{\begin{bmatrix} \frac{1}{L} \\ 0 \end{bmatrix}}_{B_1} V_{in} \tag{2.30}$$

$$y = \underbrace{[0 \quad -1]}_{C_1} \begin{bmatrix} i_L \\ V_{out} \end{bmatrix} \tag{2.31}$$

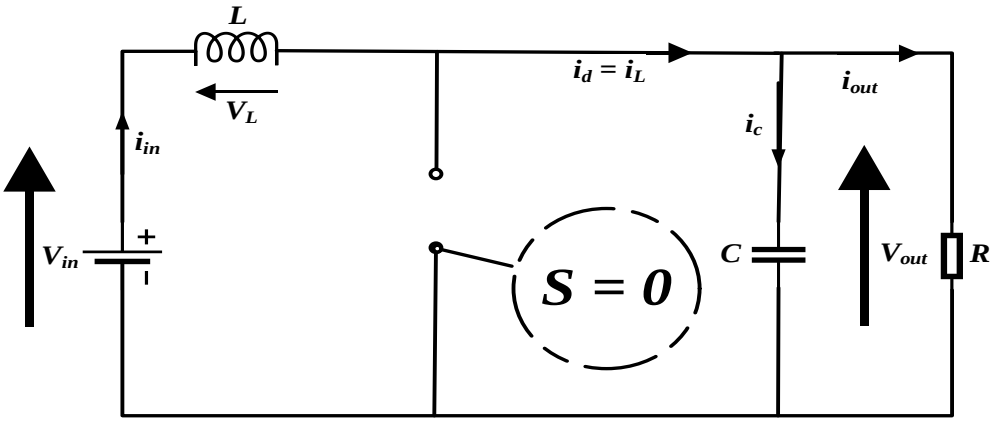

Figure 2. 6: *Equivalent circuit of the classic boost converter when the switch is opened.*

When the switch position function is set to S=0, the following equations are obtained:

$$\begin{cases} L\frac{di_L}{dt} = V_L = V_{in} - V_{out} \\ C\frac{dV_{out}}{dt} = i_c = i_L - i_{out} \end{cases} \tag{2.32}$$

$$y = V_{out} = Ri_{out} \tag{2.33}$$

$$i_{out} = i_L - i_C = i_L - C\frac{dV_{out}}{dt} = \frac{1}{R}V_{out} \tag{2.34}$$

Using the matrix form, the above equations can be rewritten as:

$$\begin{bmatrix} \frac{di_L}{dt} \\ \frac{dV_{out}}{dt} \end{bmatrix} = \underbrace{\begin{bmatrix} 0 & -\frac{1}{L} \\ \frac{1}{C} & \frac{-1}{RC} \end{bmatrix}}_{A_2} \begin{bmatrix} i_L \\ V_{out} \end{bmatrix} + \underbrace{\begin{bmatrix} \frac{1}{L} \\ 0 \end{bmatrix}}_{B2} V_{in} \tag{2.35}$$

$$y = \underbrace{[0 \quad 1]}_{C_2} \begin{bmatrix} i_L \\ V_{out} \end{bmatrix} \tag{2.36}$$

Assuming the duty cycle of the converter is D $(0 \le D \le 1)$, the state space average model can be expressed as:

$$\frac{dx}{dt} = [DA_1 + (1-D)A_2]x + [DB_1 + (1-D)B_2]V_{in} \tag{2.37}$$

$$y = \left[C_1 D + C_2(1-D)\right]x \tag{2.38}$$

where $x = \begin{bmatrix} i_L \\ V_{out} \end{bmatrix}$, the detailed model of boost converter is expressed by:

$$\begin{cases} L\dfrac{di_L}{dt} = V_{in} - (1-D)V_{out} \\ C\dfrac{dV_{out}}{dt} = (1-D)i_L - i_{out} \end{cases} \quad \text{with} \quad i_{out} = \frac{V_{out}}{R} \tag{2.39}$$

$$y = \begin{bmatrix} 0 & (1-2D) \end{bmatrix} \begin{bmatrix} i_L \\ V_{out} \end{bmatrix} \tag{2.40}$$

Switching converters are nonlinear systems that need to be linearized in order to ease the controller design. An advantage of such linearized model is that for a constant duty cycle, the model is time invariant. There is no switching or switching ripple to manage, and only the DC components of the waveforms are modeled. This is achieved by perturbing and linearizing the average model about a quiescent operating point to obtain a small signal model [99]. Introducing small AC perturbation and separation of AC and DC components, it yields:

$$V_{in} = v_{in} + \tilde{v}_{in} \tag{2.41}$$

$$x = X + \tilde{x} \tag{2.42}$$

$$D = D + \tilde{d} \tag{2.43}$$

$$D' = D' - \tilde{d} \rightarrow D' = 1 - D \tag{2.44}$$

By introducing these perturbations in (2.37), it yields:

$$\tilde{x} = A\tilde{x} + \left(\left(A_1 - A_2\right)x + \left(B_1 - B_2\right)V_{in}\right)\tilde{d} + B\tilde{V}_{in} \tag{2.45}$$

where:

$$\begin{aligned} A &= A_1 D + A_2 D' \\ B &= B_1 D + B_2 D' \end{aligned} \tag{2.46}$$

$$A = \begin{bmatrix} 0 & -(1-D) \\ \dfrac{1-D}{C} & \dfrac{-1}{RC} \end{bmatrix}; B = \begin{bmatrix} \dfrac{1}{L} \\ 0 \end{bmatrix} \tag{2.47}$$

Finally, one can get:

$$\frac{d}{dt}\begin{bmatrix}\tilde{i}_L\\ \tilde{V}_{out}\end{bmatrix}=\begin{bmatrix}0 & -\frac{(1-D)}{L}\\ \frac{1-D}{C} & -\frac{1}{RC}\end{bmatrix}\begin{bmatrix}\tilde{i}_L\\ \tilde{V}_{out}\end{bmatrix}+\begin{bmatrix}0 & \frac{1}{L}\\ -\frac{1}{C} & 0\end{bmatrix}\begin{bmatrix}i_L\\ V_{out}\end{bmatrix}\tilde{d}+\begin{bmatrix}\frac{1}{L}\\ 0\end{bmatrix}\tilde{V}_{in} \quad (2.48)$$

where *L*, *C*, *R* denote the inductance of the input circuit, capacitance of the output filter and the output load resistance, respectively.

The circuit shown in Figure (2.7) illustrates the averaged-value model of the boost converter, where the switch is essentially replaced by a voltage-controlled source at the low voltage side and a current controlled source at the high voltage side.

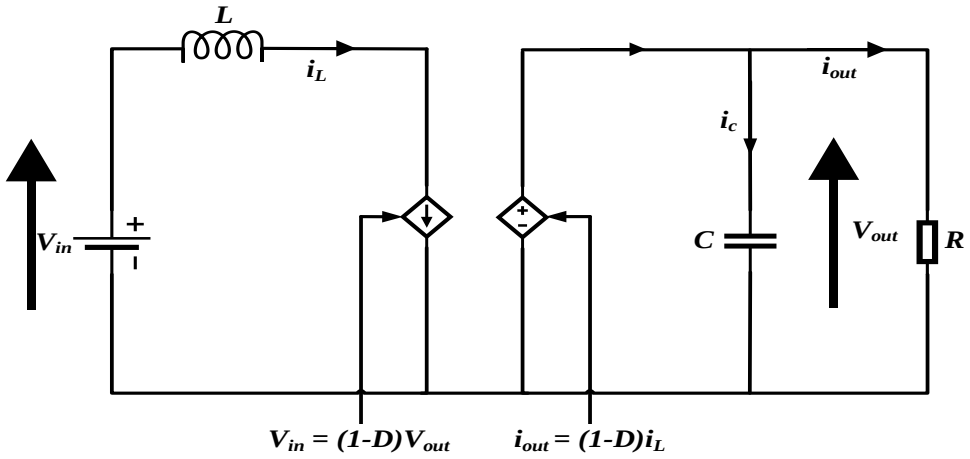

Figure 2. 7: *Equivalent circuit of averaged-value boost converter.*

2.4.1.1.a Boost converter inductance and capacitance Sizing

When the switch is closed S=1, the inductance current is given by:

$$i_L(t)=\frac{V_{in}}{L}t+I_{L\min} \quad (2.49)$$

The maximum value of the current is calculated by:

$$I_{L\max}=i_L(DT_s)=\frac{V_{in}}{L}DT_s+I_{L\min} \quad (2.50)$$

The current ripple is defined by:

$$\Delta i_L=\frac{V_{in}}{L}DT_s \quad (2.51)$$

When the switch is opened S=0, the inductance current is given by:

$$i_L(t)=\frac{V_{in}-V_{out}}{L}t+I_{L\max} \quad (2.52)$$

The minimum value of the current is calculated by:

$$I_{L\min} = i_L((1-D)T_s) = \frac{V_{in} - V_{out}}{L}(1-D)T_s + I_{L\max} \tag{2.53}$$

The current ripple is defined by:

$$\Delta i_L = \frac{V_{out} - V_{in}}{L}(1-D)T_s \tag{2.54}$$

As $V_{in} = (1-D)V_{out}$, one can write:

$$\Delta i_L = \frac{V_{out}(1-D)D}{Lf_s} \tag{2.55}$$

From equation (2.53) and as the current ripple Δi_L is maximal for D = 0.5, the inductance L must satisfy the following inequality:

$$L \geq \frac{V_{out}}{4 f_s \Delta i_L} \tag{2.56}$$

Where f_s = 25000 Hz, V_{out} = 270V, Δi_L is generally fixed in the interval of $[1\% i_L, 10\% i_L]$.

The voltage ripple across capacitor C can be calculated as follows:

$$\Delta V_{out} = \frac{\Delta Q}{C} = \frac{i_{out} D T_s}{C} \tag{2.57}$$

As $i_{out} = (1-D)i_L$, we can write:

$$\Delta V_{out} = \frac{\bar{i}_L(1-D)D}{Cf_s} \tag{2.58}$$

From this we calculate the value of the capacitor as follows:

$$C = \frac{\bar{i}_L(1-D)D}{f_s \Delta V_{out}} \tag{2.59}$$

where, D=0.5, f_s=25000Hz, ΔV_{out} is generally fixed in the interval of $[5\% V_{out}, 20\% V_{out}]$, which gives $C = 185 \times 10^{-6} F$

2.4.1.1.b Inductance value ensuring a continuous operation

In continuous mode, the current flowing through the inductor is not zero over a switching period T_s. In this situation, the mean boundary current flowing through the coil verifies:

$$\bar{i}_L = \frac{1}{T_s}\int_0^{T_s} i_L dt = \frac{i_{L\max}}{2} = \frac{\Delta i_L}{2} \tag{2.60}$$

The continuous conduction limit being reached for $I_{L\min} = 0$

$$I_{L\max} = \frac{V_{in}}{L} DT_s \tag{2.61}$$

The average value of inductance current becomes:

$$\bar{i}_L = \frac{V_{in}}{2L} DT_s \tag{2.62}$$

And we have:

$$V_{in} = (1-D)V_{out} \tag{2.63}$$

From (2.59) and (2.60), the average current of the inductance is expressed as follows:

$$\bar{i}_L = \frac{D(1-D)V_{out}}{2L} T_s \tag{2.64}$$

By replacing the duty cycle value $D = 1/2$ in (2.61), the maximum value of the average current of the inductance $\bar{i}_{L\max}$ can be calculated as follows:

$$\bar{i}_{L\max} = \frac{V_{out}}{8L} T_s \tag{2.65}$$

Equation (2.65) can be used to calculate the minimum value of the inductance, which ensures that the converter always operates in the continuous conduction mode. The value of this inductance can be calculated by the following equation:

$$L_{\min} = \frac{V_{out}}{8\bar{i}_{L\max}} T_s \tag{2.66}$$

with $T_s = \frac{1}{f_s}$, $f_s = 25000Hz$, $\bar{i}_{L\max} = 250A$, $V_{out} = 270V$, it results $L_{\min} = 5.4\times10^{-6} H$.

2.4.1.2 Control of boost converter

The converter control objective is to maintain a constant bus voltage and/or a constant current despite variations in the load and the input (FC, battery, SC) [37]. The control system

has to protect power components such as switches, which are sensitive to over-current, hence the system current should be controlled [6].

The converter is modeled by using first order transfer functions, which can be controlled using simple PI controllers.

- **Output voltage control of boost converter**

A proportional-integral (PI) type regulator whose transfer function is symbolized by $C_{bv}(s)$ is used to adjust the output voltage of the converter (load voltage). The output of this regulator gives the reference of the current to be imposed in the capacitor C.

The transfer function of voltage controller is given by:

$$C_{bv}(s) = \frac{K_{bpv}s + K_{biv}}{s} \tag{2.67}$$

The capacitor voltage in Laplace domain is given by:

$$V_{out} = \frac{(1-D)i_L - i_{out}}{Cs} \tag{2.68}$$

Figure (2.8) shows the boost converter output voltage regulation loop.

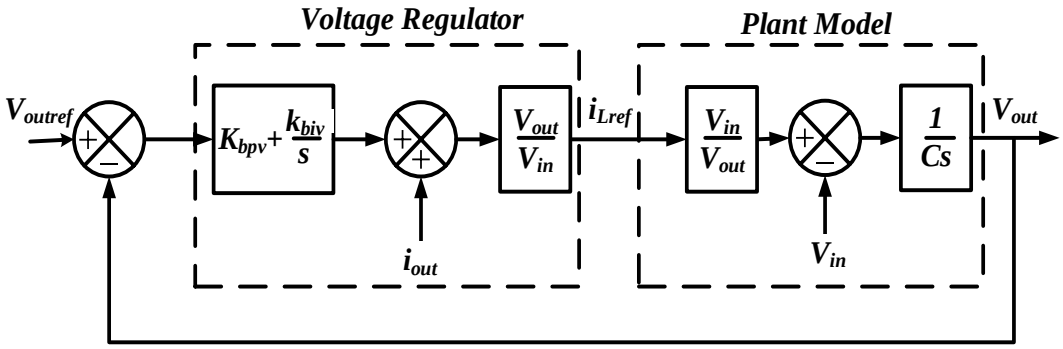

Figure 2.8: *Voltage regulator of the boost converter.*

The closed loop transfer function is given by:

$$B_{v_{close}}(s) = \frac{\frac{K_{bpv}}{C}s + \frac{K_{biv}}{C}}{s^2 + \frac{K_{bpv}}{C}s + \frac{K_{biv}}{C}} \tag{2.69}$$

To calculate the PI boost voltage regulator gains, the pole placement method is used. We want that the transfer function (2.69) exhibits the same dynamic behavior as a second-order system of the following transfer function:

$$H_{bv}(s) = \frac{{\omega_{bnv}}^2}{s^2 + 2\xi_{bv}\omega_{bnv}s + {\omega_{bnv}}^2} \tag{2.70}$$

The proportional gain K_{bpv} and integral gain K_{biv} are determined by identifying term by term the two characteristic equations of (2.70) and (2.69), which results in:

$$\begin{cases} K_{bpv} = 2\xi_{bv}\omega_{bnv}C \\ K_{biv} = \omega^2{}_{bnv}C \end{cases} \tag{2.71}$$

where ω_{bnv} is the natural frequency and ξ_{bv} is the damping coefficient of the boost output voltage loop.

- **Inductor current control of boost converter**

A proportional-integral (PI) type regulator whose transfer function is symbolized by $C_{bi}(s)$ is makes it possible to correct the error between the measured current and its reference. The output of each regulator makes it possible to determine the voltage reference to be imposed on the terminals of the inductor.

The transfer function of current controller is given by:

$$C_{bi}(s) = \frac{K_{bpi}s + K_{bii}}{s} \tag{2.72}$$

The inductor current in Laplace domain are given by:

$$I_L = \frac{V_{in} - (1-D)V_{out}}{Ls} \tag{2.73}$$

Figure (2.9) shows the boost converter output current regulation loop.

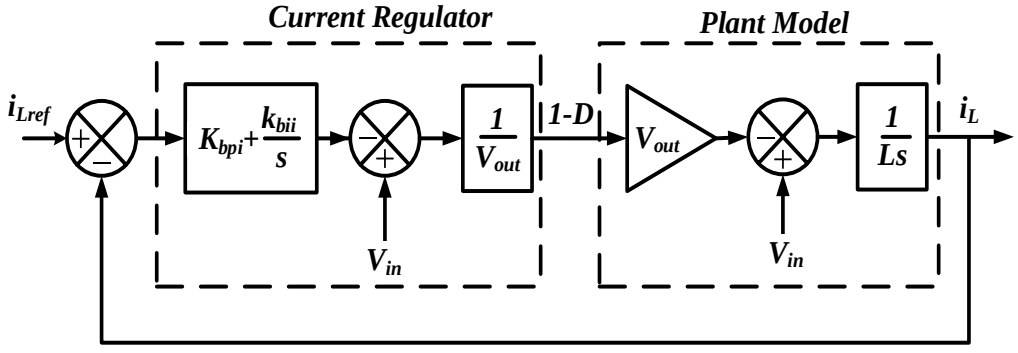

Figure 2. 9: *Current regulator of the boost converter.*

The closed loop transfer function is given by:

$$B_{i\,close}(s) = \frac{\frac{K_{bpi}}{L}s + \frac{K_{bii}}{L}}{s^2 + \frac{K_{bpi}}{L}s + \frac{K_{bii}}{L}} \tag{2.74}$$

To calculate the gains of the PI regulator, the closed loop transfer function (2.74) has to exhibit the same dynamic behavior as a second-order system defined by the following transfer function:

$$H_{bi}(s) = \frac{{\omega_{bni}}^2}{s^2 + 2\xi_{bi}\omega_{bni}s + {\omega_{bni}}^2} \tag{2.75}$$

The proportional gain K_{bpi} and integral gain K_{bii} are determined by identifying term by term the two characteristic equations of (2.74) and (2.75), which results in:

$$\begin{cases} K_{bpi} = 2\xi_{bi}\omega_{bni}L \\ K_{bii} = {\omega^2}_{bni}L \end{cases} \tag{2.76}$$

where ω_{bni} is the natural frequency and ξ_{bi} is the damping coefficient of the boost input current loop.

2.4.2 DC-DC buck converter model and control

2.4.2.1 Model of buck converter

Buck converter, depicted in Figure (2.10), is a simple and widely used voltage step-down device with high efficiency. Typically, a buck converter consists of a filter consisting of an inductor and a capacitor, and a switching component such as a MOSFET or an IGBT. There are two states in the operation process of buck converter: the on-state and off-state of the switch S.

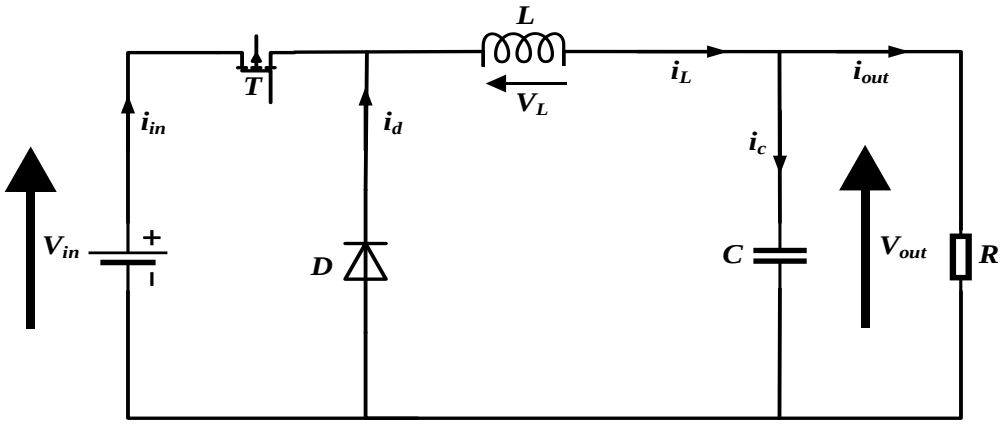

Figure 2. 10: *Structure of a buck converter.*

As shown in Figure (2.11), when the switch is closed, the current flowing through the inductor increases linearly. The diode is reverse biased and there is no current flowing through it.

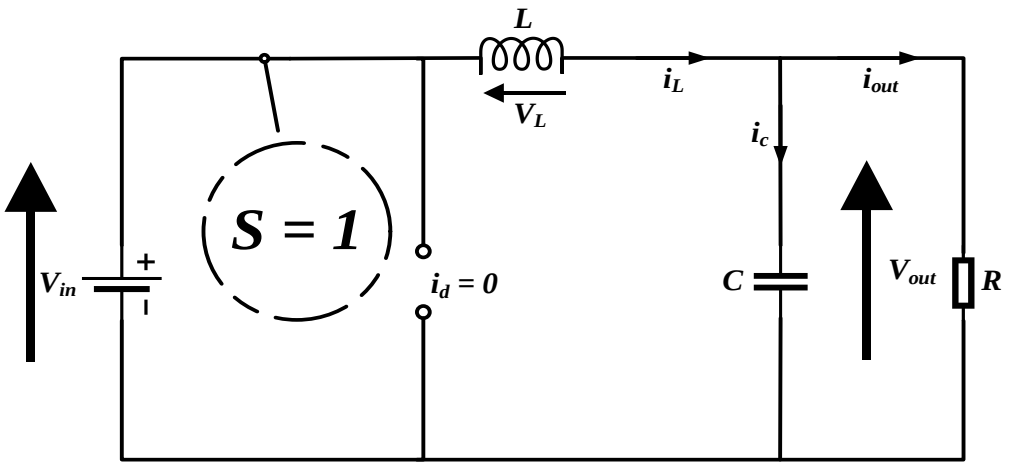

Figure 2.11: *Equivalent circuit of the buck converter when the switch is closed.*

When the switch position is set to S=1, the following equations are obtained:

$$\begin{cases} L\dfrac{di_L}{dt} = V_{in} - V_{out} = V_L \\ C\dfrac{dV_{out}}{dt} = i_c = i_L - \dfrac{V_{out}}{R} \end{cases} \tag{2.77}$$

$$y = V_{out} = R i_{out} \tag{2.78}$$

$$i_{out} = i_L - i_C = i_L - C\frac{dV_{out}}{dt} = \frac{1}{R}V_{out} \tag{2.79}$$

These equations can be rewritten in the following matrix from:

$$\begin{bmatrix} \dfrac{di_L}{dt} \\ \dfrac{dV_{out}}{dt} \end{bmatrix} = \underbrace{\begin{bmatrix} 0 & -\dfrac{1}{L} \\ \dfrac{1}{C} & -\dfrac{1}{RC} \end{bmatrix}}_{A_3} \begin{bmatrix} i_L \\ V_{out} \end{bmatrix} + \underbrace{\begin{bmatrix} \dfrac{1}{L} \\ 0 \end{bmatrix}}_{B_3} V_{in} \tag{2.80}$$

$$y = \underbrace{\begin{bmatrix} 0 & 1 \end{bmatrix}}_{C_3} \begin{bmatrix} i_L \\ V_{out} \end{bmatrix} \tag{2.81}$$

As shown in Figure (2.12), when the switch S is opened, the inductor acts as a source and maintains current through a load resistor. During this period, the current continues to flow in the inductor through the diode D. As the magnetic field collapses, the energy stored in the inductor as well as the current through it decrease. In continuous mode, the switch S is closed and the diode D is opened before the inductor is completely discharged.

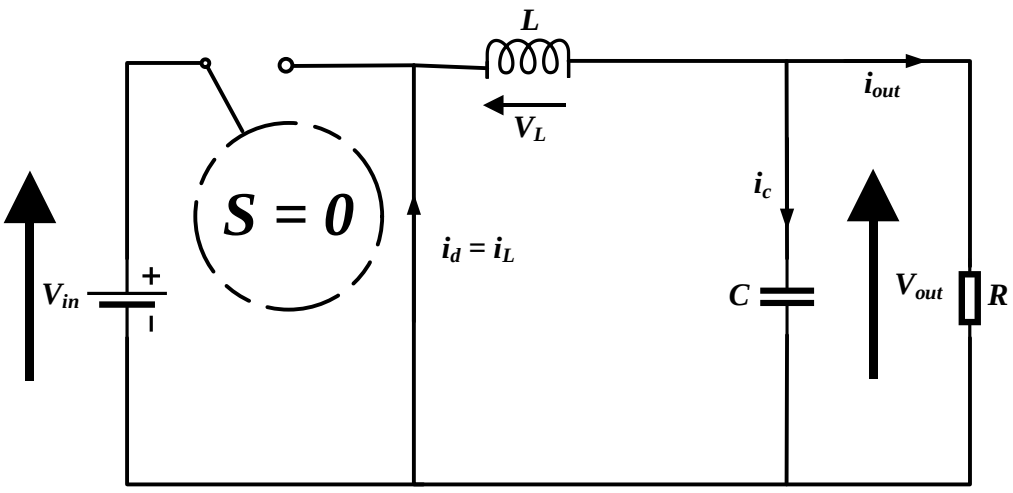

Figure 2.12: *Equivalent circuit of the buck converter when the switch is opened.*

When the switch position is set to S=0, the following equations are obtained:

$$\begin{cases} L\dfrac{di_L}{dt} = V_L = -V_{out} \\ C\dfrac{dV_{out}}{dt} = i_c = i_L - \dfrac{V_{out}}{R} \end{cases} \tag{2.82}$$

$$y = V_{out} = R\,i_{out} \tag{2.83}$$

$$i_{out} = i_L - i_C = i_L - C\frac{dV_{out}}{dt} = \frac{1}{R}V_{out} \tag{2.84}$$

These equations can be rewritten in the following matrix from:

$$\begin{bmatrix} \dfrac{di_L}{dt} \\ \dfrac{dV_{out}}{dt} \end{bmatrix} = \underbrace{\begin{bmatrix} 0 & -\dfrac{1}{L} \\ \dfrac{1}{C} & \dfrac{-1}{RC} \end{bmatrix}}_{A_4} \begin{bmatrix} i_L \\ V_{out} \end{bmatrix} + \underbrace{\begin{bmatrix} 0 \\ 0 \end{bmatrix}}_{B_4} V_{in} \tag{2.85}$$

$$y = \underbrace{\begin{bmatrix} 0 & 1 \end{bmatrix}}_{C_4} \begin{bmatrix} i_L \\ V_{out} \end{bmatrix} \tag{2.86}$$

Combining (2.85) with (2.80) and (2.86) with (2.81), state space average model can be obtained by:

$$\frac{dx}{dt} = [DA_3 + (1-D)A_4]x + [DB_3 + (1-D)B_4]V_{in} \tag{2.87}$$

$$y = [C_3 D + C_4(1-D)]x \tag{2.88}$$

where $x = \begin{bmatrix} i_L \\ V_{out} \end{bmatrix}$ is the state space vector and D is the duty cycle.

The detailed model of buck converter is expressed by:

$$\begin{cases} L\dfrac{di_L}{dt} = DV_{in} - V_{out} \\ C\dfrac{dV_{out}}{dt} = i_L - i_{out} \end{cases} \quad \text{with} \quad i_{out} = \frac{V_{out}}{R} \tag{2.89}$$

$$y = \begin{bmatrix} 0 & 1 \end{bmatrix} \begin{bmatrix} i_L \\ V_{out} \end{bmatrix} \tag{2.90}$$

The resultant averaged model is nonlinear and time-invariant. This model is linearized at the operating point to obtain a small signal model. The linearization process produces a linear time invariant small-signal model [100].

Introducing small perturbation, it yields:

$$V_{in} = v_{in} + \tilde{v}_{in} \tag{2.91}$$

$$x = X + \tilde{x} \tag{2.92}$$

$$D = D + \tilde{d} \tag{2.93}$$

$$D' = D' - \tilde{d} \rightarrow D' = 1 - D \tag{2.94}$$

By replacing these perturbations in equation (2.87), it yields:

$$\dot{\tilde{x}} = A\tilde{x} + \left(\left(A_3 - A_4 \right) x + \left(B_3 - B_4 \right) V_{in} \right) \tilde{d} + B\tilde{V}_{in} \tag{2.95}$$

Where

$$A = A_3 D + A_4 D' \tag{2.96}$$

$$B = B_3 D + B_4 D' \tag{2.97}$$

$$A = \begin{bmatrix} 0 & -\dfrac{1}{L} \\ \dfrac{1}{C} & \dfrac{-1}{RC} \end{bmatrix}; B = \begin{bmatrix} \dfrac{1}{L} \\ 0 \end{bmatrix} \tag{2.98}$$

The following equation represents the small signal model.

$$\frac{d}{dt} \begin{bmatrix} \tilde{i}_L \\ \tilde{V}_{out} \end{bmatrix} = \begin{bmatrix} 0 & -\dfrac{1}{L} \\ \dfrac{1}{C} & \dfrac{-1}{RC} \end{bmatrix} \begin{bmatrix} \tilde{i}_L \\ \tilde{V}_{out} \end{bmatrix} + \begin{bmatrix} \dfrac{1}{L} \\ 0 \end{bmatrix} V_{in}\tilde{d} + \begin{bmatrix} \dfrac{1}{L} \\ 0 \end{bmatrix} \tilde{V}_{in} \tag{2.99}$$

Figure (2.13) shows the block diagram of the buck averaged-value model.

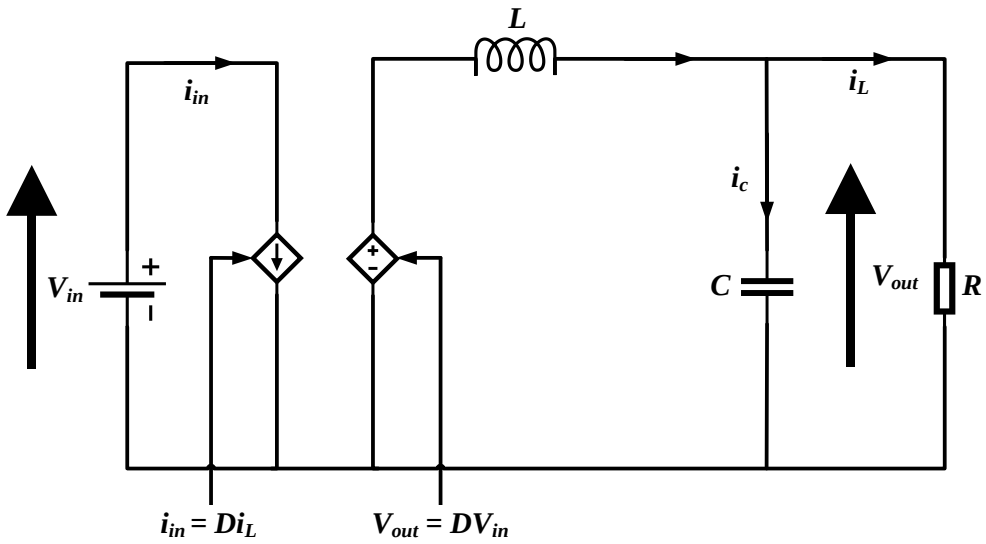

Figure 2.13: *Equivalent circuit of averaged-value buck converter.*

2.4.2.1.a Buck converter inductance and capacitance Sizing

The *LC* filter is used to smooth the output voltage and current ripples.

When the switch is closed S=1, the inductance current is expressed by:

$$i_L(t) = \frac{V_{in} - V_{out}}{L} t + I_{L\min} \tag{2.100}$$

This current reaches its maximum at $t = DT_s$, which results in:

$$I_{L\max} = i_L(DT_s) = \frac{V_{in} - V_{out}}{L} DT_s + I_{L\min} \tag{2.101}$$

The current ripple Δi_L is the difference between the maximum and the minimum values of the inductance current as in:

$$\Delta i_L = I_{L\max} - I_{L\min} = \frac{V_{in} - V_{out}}{L} DT_s \tag{2.102}$$

When the switch is opened S=0, the inductance current is expressed by:

$$i_L(t) = -\frac{V_{out}}{L} t + I_{L\max} \tag{2.103}$$

This current reaches its maximum at $t = (1-D)T_s$, which results in:

$$I_{L\min} = i_L((1-D)T) = -\frac{V_{out}}{L}(1-D)T_s + I_{L\max} \tag{2.104}$$

In this case, the current ripple Δi_L is calculated by:

$$\Delta i_L = \frac{V_{out}}{L}(1-D)T_s \tag{2.105}$$

Note that from equations (2.102) and (2.105), the current ripple is directly proportional to the duty-cycle and inversely proportional to the inductance. So, the current ripple can be controlled by a proper selection of the inductor.

The expressions for the maximum and minimum inductor currents are written as:

$$I_{L\max} = i_{out} + \frac{\Delta i_L}{2} = \frac{V_{out}}{R} + \frac{V_{out}}{2L}(1-D)T_s \tag{2.106}$$

$$I_{L\min} = i_{out} - \frac{\Delta i_L}{2} = \frac{V_{out}}{R} - \frac{V_{out}}{2L}(1-D)T_s \tag{2.107}$$

When the buck converter operates in the continuous conduction mode, there is always a non-null current in the inductor. The minimum inductor value that ensures continuous conduction mode can be obtained by imposing $I_{L\min} = 0$. So, it results:

$$L_{\min} = \frac{(1-D)}{2}RT_s = \frac{(1-D)}{2f_s}R = \frac{(1-0.5)}{2\times 25000}\times 10 = 0.0001H \tag{2.108}$$

The output voltage ripples depend on the capacitor connected to the load. The voltage ripple ΔV_{out} is written as:

$$\Delta V_{out} = \frac{\Delta Q}{C} = \frac{\Delta I_L T_s}{8C} = \frac{V_{out}(1-D)T_s^{\,2}}{8LC} \tag{2.109}$$

Therefore:

$$C = \frac{V_{out}(1-D)T_s^2}{8L\Delta V_{out}} = 2.7\times 10^{-6}F \tag{2.110}$$

With $V_{out} = 270V$, $D = 0.5V$ and $\Delta V_{out} = 5\%V_{out}$.

2.4.2.2 Control of buck converter

The current passing through the inductor is controlled indirectly by acting on the duty cycle . To do this, the current is subtracted from its reference value. The resulting error is canceled by a PI compensator whose output corresponds to the duty cycle. In the same way, the DC voltage control is performed.

The converter is modeled by first order transfer functions that can be controlled using simple PI regulators.

- **Output voltage control of buck converter:**

A proportional-integral (PI) type regulator is used to adjust the output voltage of the converter. The output of this regulator imposes the reference of the capacitor current.

The transfer function of voltage controller is given by:

$$C_{kv}(s) = \frac{K_{kpv}s + K_{kiv}}{s} \tag{2.111}$$

The capacitor voltage in Laplace domain is given by:

$$V_{out} = \frac{i_L - i_{out}}{Cs} \tag{2.112}$$

Figure (2.14) represents the block diagram of the output voltage regulation loop of the buck converter.

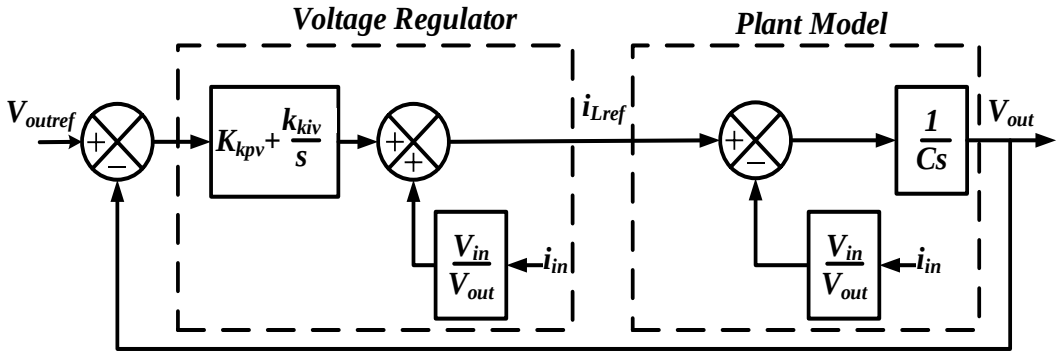

Figure 2.14: *Voltage control of the buck converter.*

From the diagram in Figure (2.14), the closed loop transfer function is written as:

$$k_{v_{close}}(s) = \frac{\frac{K_{kpv}}{C}s + \frac{K_{kiv}}{C}}{s^2 + \frac{K_{kpv}}{C}s + \frac{K_{kiv}}{C}} \tag{113}$$

To calculate the gains of the buck voltage regulator, the transfer function (2.113) has to exhibit the same dynamic behavior as a second-order system of the following transfer function:

$$H_{kv}(s) = \frac{{\omega_{knv}}^2}{s^2 + 2\xi_{kv}\omega_{knv}s + {\omega_{knv}}^2} \tag{2.114}$$

The proportional gain K_{kpv} and integral gain K_{kiv} are calculated by matching the characteristic equation of (2.114) with that of (2.115), which gives:

$$\begin{cases} K_{kpv} = 2\xi_{kv}\omega_{knv}C \\ K_{kiv} = {\omega^2}_{knv}C \end{cases} \tag{2.115}$$

where ω_{knv} is the natural frequency and ξ_{kv} is the damping coefficient of the buck output voltage loop.

- **Inductor current control of the buck converter**

Figure (2.14) represents the block diagram of the inductance current control loop of the buck converter.

Using Laplace transform, the inductor current in Laplace domain is given by:

$$i_L = \frac{DV_{in} - V_{out}}{Ls} \tag{2.116}$$

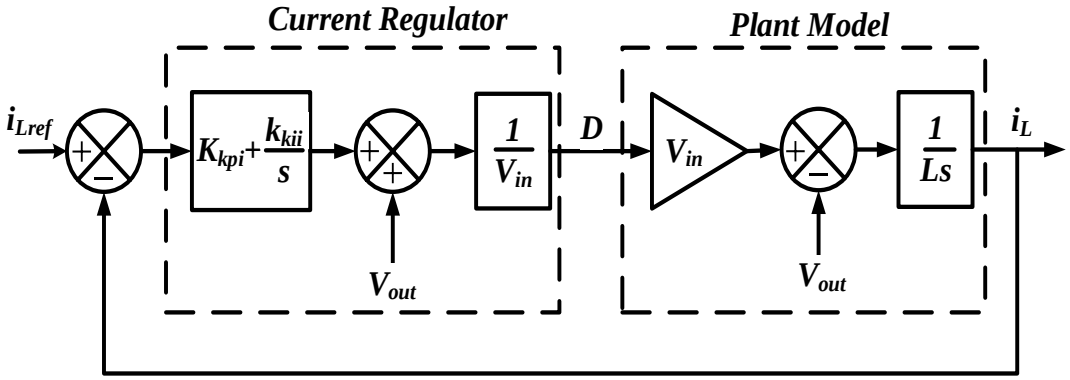

Figure 2.15: *Current control of the buck converter.*

From the diagram in Figure (2.15), the closed loop transfer function is written as:

$$k_{i\,close}(s) = \frac{\frac{K_{kpi}}{L}s + \frac{K_{kii}}{L}}{s^2 + \frac{K_{kpi}}{L}s + \frac{K_{kii}}{L}} \tag{2.117}$$

To calculate the gains of the PI regulator, the transfer function (2.117) has to exhibit the same dynamic behavior as a second-order system of the following transfer function:

$$H_{ki}(s) = \frac{{\omega_{kni}}^2}{s^2 + 2\xi_{ki}\omega_{kni}s + {\omega_{kni}}^2} \tag{2.118}$$

The proportional gain K_{kpi} and integral gain K_{kii} are determined by identifying term by term the two characteristic equations of (2.117) and (2.118), which results in:

$$\begin{cases} K_{kpi} = 2\xi_{ki}\omega_{kni}L \\ K_{kii} = {\omega^2}_{kni}L \end{cases} \tag{2.119}$$

where ω_{kni} is the natural frequency and ξ_{ki} is the damping coefficient of the buck output current loop.

2.4.3 Bidirectional DC-DC converter modeling

In this study, the average model of the bidirectional DC-DC converter is obtained jut by connecting in parallel the boost and buck converters as shown in Figure (2.16), in which each converter is modeled in its turn by its average model.

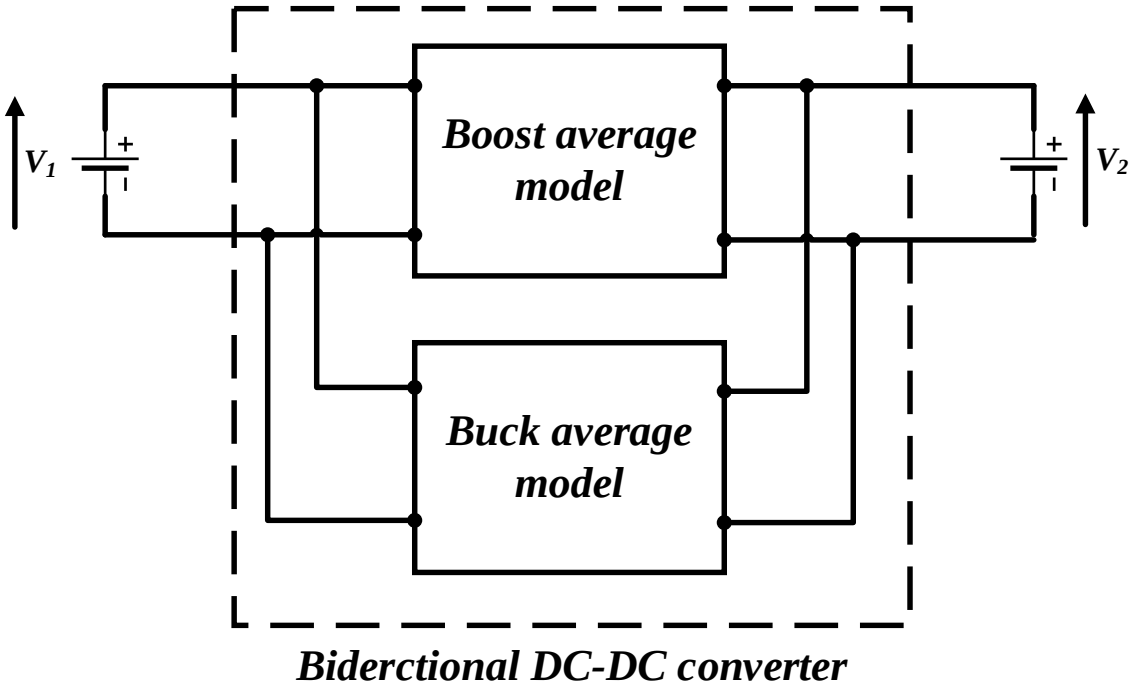

Figure 2.16: *Equivalent circuit of the averaged model of the bidirectional DC-DC converter.*

2.5 Simulation results

2.5.1 Simulation of the Fuel Cell System

As shown in Figure (2.17)**,** the FC is connected to the DC-bus via a DC-DC boost converter to set-up the FC output voltage V_{fc}. The power control of the DC-DC boost converter is achieved by controlling the inductance current using a PI controller.

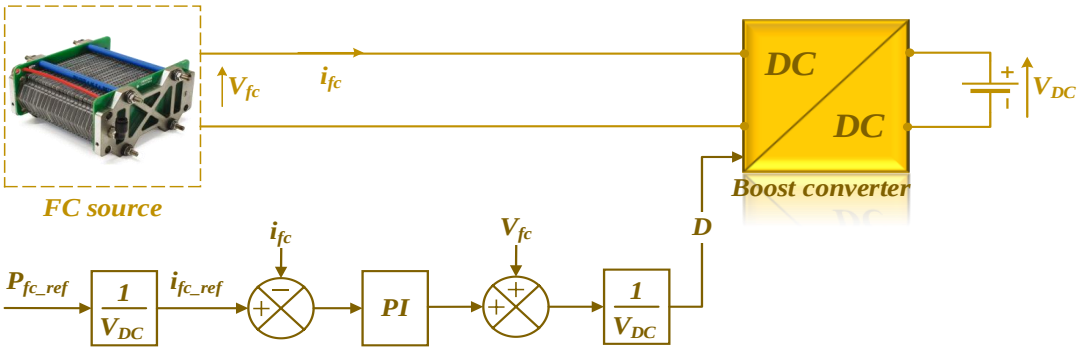

Figure 2.17: *Fuel cell system control.*

The model parameters for the fuel cell system are summarized in the Table (2.1).

T_s (µs)	T_{sc} (µs)	C_{dc} (mF)	L_{b_fc} (µH)	ω_{bni_fc} (rad/s)	r_{L_fc} (mΩ)	ξ_{bi_fc}	Number of cells N	Temperature (°C)
15	150	0.8	100	50	0.1	0.707	65	45

Table 2.1: *Parameters for the fuel cell system.*

Figure (2.18) shows the results for fuel cell system with current control using PI controller.

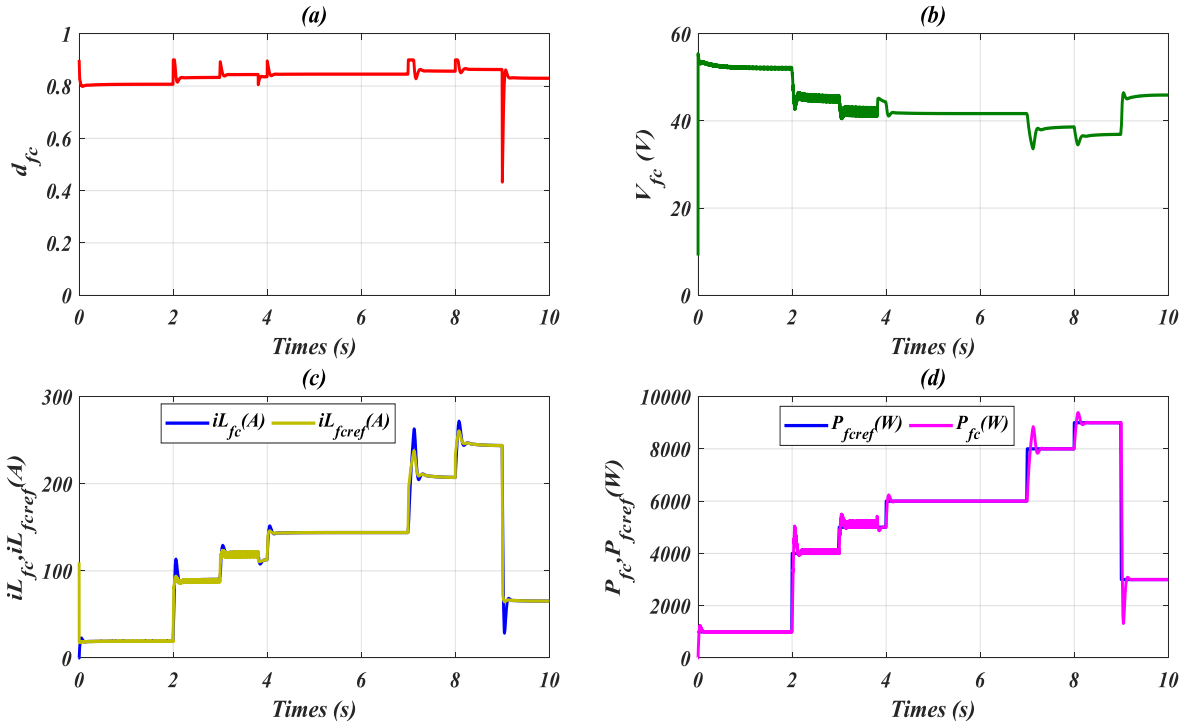

Figure 2.18: *Simulation results of the fuel cell system.*
(a) Duty cycle d_{fc} (b) Fuel cell voltage V_{fc}, (C) Fuel cell currant iL_{fc} with its reference iL_{fcref}, (d) Fuel cell power P_{fc} with its reference P_{fcref}.

❖ Interpretations

The simulation results in Figure (2.18) show a decrease in FC system voltage from 52 V at t = 0 s to 44 V at t = 2 s with a duty cycle of 0.8. From t = 2 s to 4s, the voltage decreases to 41V and remain almost constant until t = 7 s, then it decreases to approximately 37 V until 9 s followed by an increase to 46 V . The FC current has the same evolution as the FC power and the error between the FC output current and its reference is almost equal 0 thanks to the PI controller that works to match the FC current with i_{Lfcref} of approximately 20 A till t = 2 s. Inside the window [2, 3] s, the FC current is equal to 87 A, while between t = 4 s to 7 s the currant

begins to increase to approximately 140A. Over the remaining simulation time the current follows exactly the power profile. Furthermore, even the power tracks perfectly its desired value there are overshoots and undershoots at instants of reference power variations.

2.5.2 Simulation of the Battery Based Storage System

As shown in Figure (2.19), a Li-ion battery is connected to the DC-link through a bi-directional DC-DC converter. This converter is controlled so that it can control the charging and discharging modes of the battery.

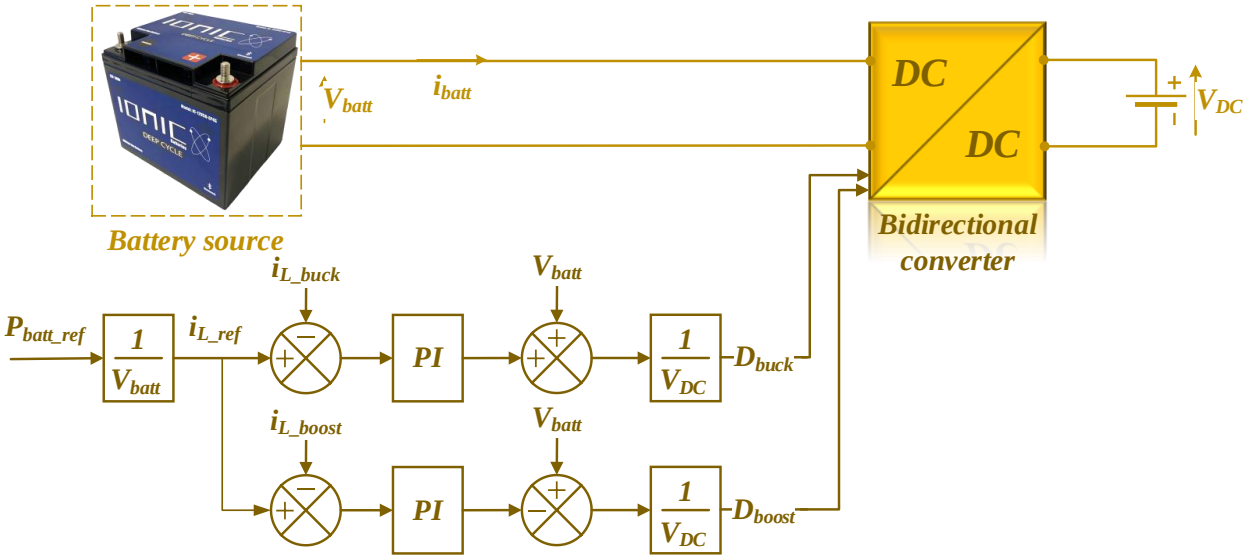

Figure 2.19: *Battery system control.*

The simulation is performed using the battery system parameters gathered in Table (2.2)

T_s (µs)	C_{dc} (mF)	L_{k_batt} (mH) (buck converter)	L_bat1 (µH) (boost converter)	ω_{kni_batt} (rad/s) (buck converter)	ξ_{ki_batt} (buck converter)	ξ_{bi_batt} (boost converter)	ω_{kni_batt} (rad/s) (Boost converter)	r_Lbat (mΩ)
15	3.2	10	100	7	0.995	0.995	390.270	0.1

Table 2.2: *Parameters for the battery system.*

Figure (2.20) shows the simulation results of the PI based current control of the battery system connected to a constant DC-link.

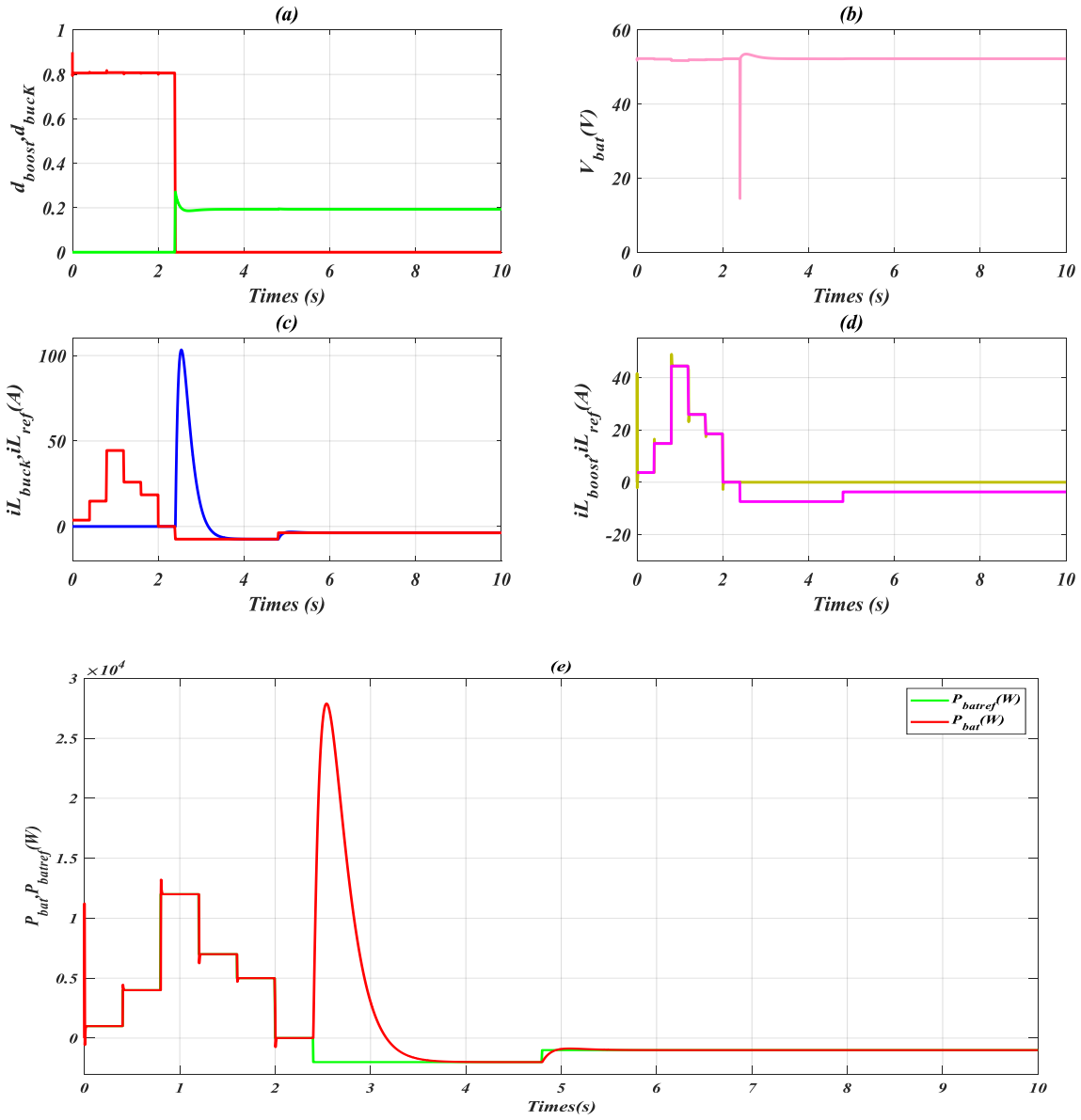

Figure 2.20: *Simulation results of the battery system.: Buck and boost duty cycles d_{buck}, d_{boost}, (b) Battery voltage V_{bat}, (c) Currant i_{Lboost} with reference current i_{Lref}, (d)Currant i_{Lbuck} with reference current i_{Lref}, (e) Battery power P_{bat} with reference power P_{batref}.*

❖ Interpretations

The simulation result in Figure (2.20.a) represents the duty cycles of buck and boost converters inside the window [0, 2.3] s. At t=0, the buck converter is out of operation meanwhile the boost converter operates with d_{boost}=0.8. From Figure (2.20.b), it can be seen that the battery voltage decreases slowly due to the fact that the battery is in discharging mode. During this time, the current of the boost converter tracks its reference value imposed by the reference power while the current of buck converter is set to zero since the reference power is positive. At t=2.3 s, the reference power changes to become negative; as consequence the boost converter is out of operation and the buck converter starts operating with d_{buck}=0.19. From this moment,

the battery voltage increases to reach 52.4V and the battery is in charging mode inside the window [2.3, 10] s. Thanks to the adopted PI controller, the buck converter current as well as its power track their references accept during the transition phase between buck and boost operating modes. During this transient, the current take and undesirable peak at t=2.3 s, which impacts in its turn the converter power shape.

2.5.3 Simulation of Supercapacitor Based Storage System

As shown in Figure (2.21), the SC is connected to the DC-link with a bi-directional DC-DC converter. This converter is used to control the charging and discharging modes of the supercapacitor storage system.

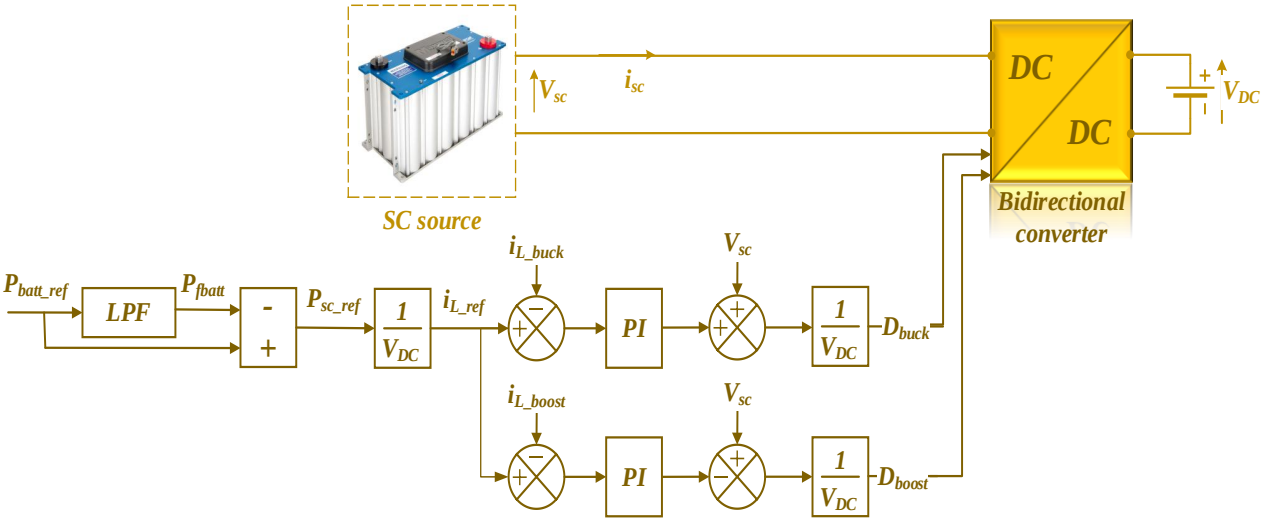

Figure 2.21: *Supercapacitor system control.*

The simulation model is built using the supercapacitor system parameters recapped in the Table (2.3):

T_s (µs)	C_{dc} (mF)	L_{k_sc} (mH) (buck converter)	L_{b_sc} (mH) (boost converter)	ω_{kni_sc} (rad/s) (buck converter)	ξ_{ki_sc} (buck converter)	ξ_{bi_sc} (boost converter)	ω_{bni_sc} (rad/s) (Boost converter)	r_Lsc (mΩ)
15	3.2	10	100	7	0.995	0.995	390.270	0.1

Table2.3: *Parameters for the supercapacitor system.*

Figure (2.22) portrays the simulation results of the current control of the supercapacitor system.

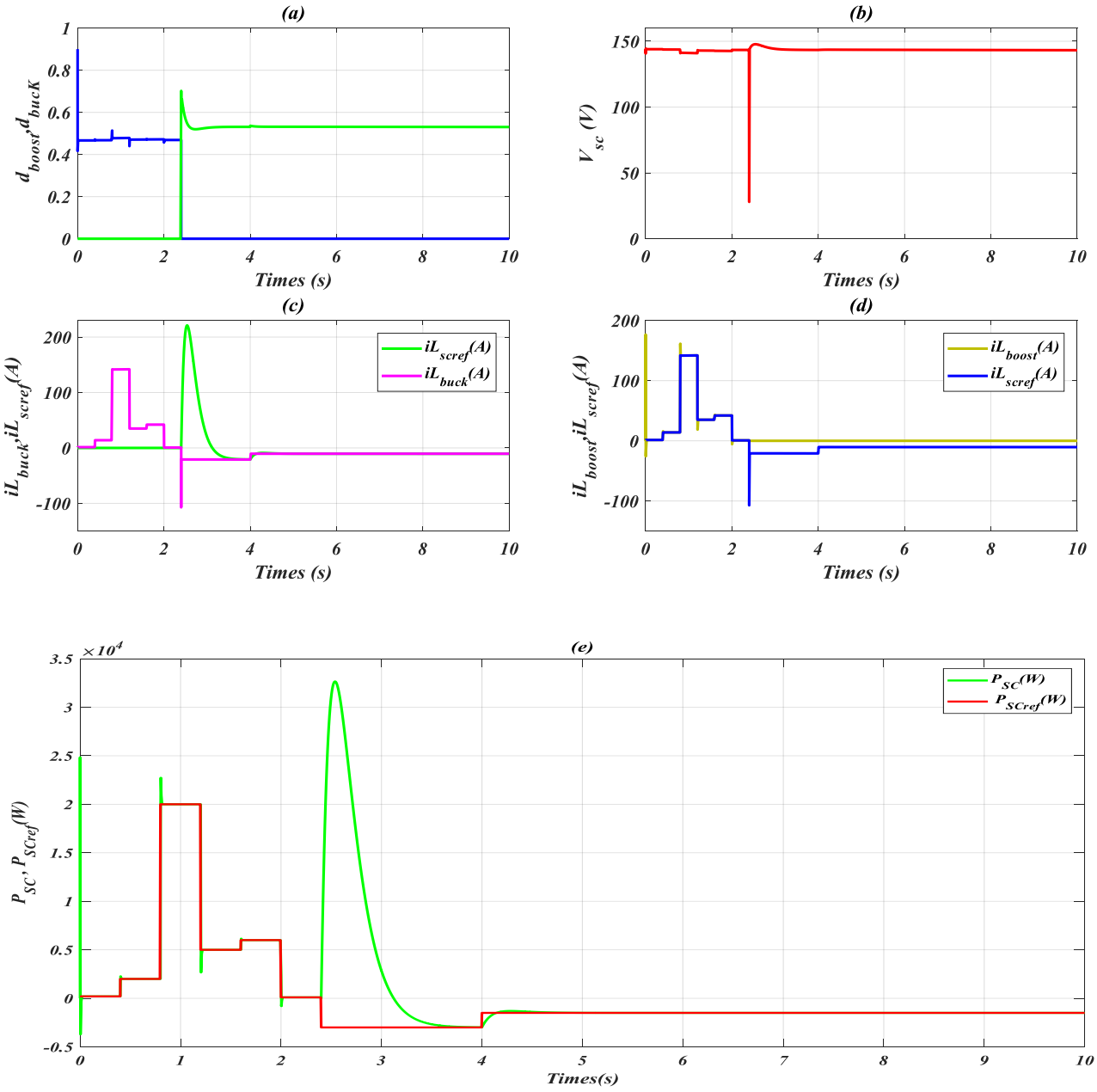

Figure 2.22: *Simulation results of the supercapacitor system: (a) Buck and boost duty cycles d_{buck}, d_{boost}. (b) Supercapacitor voltage V_{sc}, (c) Currant I_{Lboost} with its reference i_{Lref}, (d) Currant i_{Lbuck} with its reference i_{Lref}, (e)Supercapacitor power P_{sc} with its reference P_{scref}.*

❖ Interpretations

Simulation result depicted in Figure (2.22.a) represents the duty cycle of buck and boost converters during the time window of [0,2.4] s. Since the reference power is positive, the buck converter is excluded from operation starting from t=0; for that reason, the buck duty cycle is set to zero. However, the boost converter starts operating with d_{boost}=0.46. In the same time, we observe in Figure (2.21.b) that the voltage decreases slowly due to the fact that the supercapacitor is in discharging mode. During this time, the current of the boost converter tracks its reference value imposed by the power reference, while the current of the buck converter is

still 0 because the power reference is positive till now. At t=2.5 s, the reference power changes to become negative; as consequence the boost converter is out of operation and the buck converter starts operating with d_{buck}=0.53. From this moment, the supercapacitor voltage increases to reach 144.4 V due to the fact that the supercapacitor is in charging mode. An unwanted current peak of 219.71A appears at t=2.5 s, which impacts in its turn the converter power shape. Thanks to the adopted PI controller, the buck converter current as well as its power track their references accept during the transition phase between buck and boost operating modes.

2.5.4 Simulation of the fuel cell hybrid system

The fuel cell hybrid system shown in Figure (2.25) is a hybrid combination of three power sources, namely fuel cell, Li-ion battery, and supercapacitor. The DC-DC converter of the FC and that of SC operate on current control mode, whereas the DC-DC converter of the battery operates on voltage-current control mode. For both current and voltage controls, PI controllers are used. Figure (2.24) shows the control system of the fuel cell HPS. The reference current of the FC DC-DC converter is calculated knowing the fuel cell reference power P_{fc_ref}. A PI controller is used to generate the required duty cycle of the boost converter by forcing the output current of the converter to follow its reference. Regarding the SC converter control, the current control loop is similar to that of the FC. Concerning the battery converter control, the reference current needed for the inner current control loop is generated by the outer PI voltage control, which is responsible to maintain the DC-bus at 270V.

And, to solve the problem of slowness of the FC system, a filter is used to split the load demand fluctuation into different frequency components. This control method is very simple and has excellent performance [101].

The low pass filter transfer function shown in Figure (2.24) is defined as follows:

$$\frac{P_{fbatt}}{P_{batt-ref}} = \frac{1}{\tau s + 1} \tag{2.20}$$

where $\tau = 0.5$.

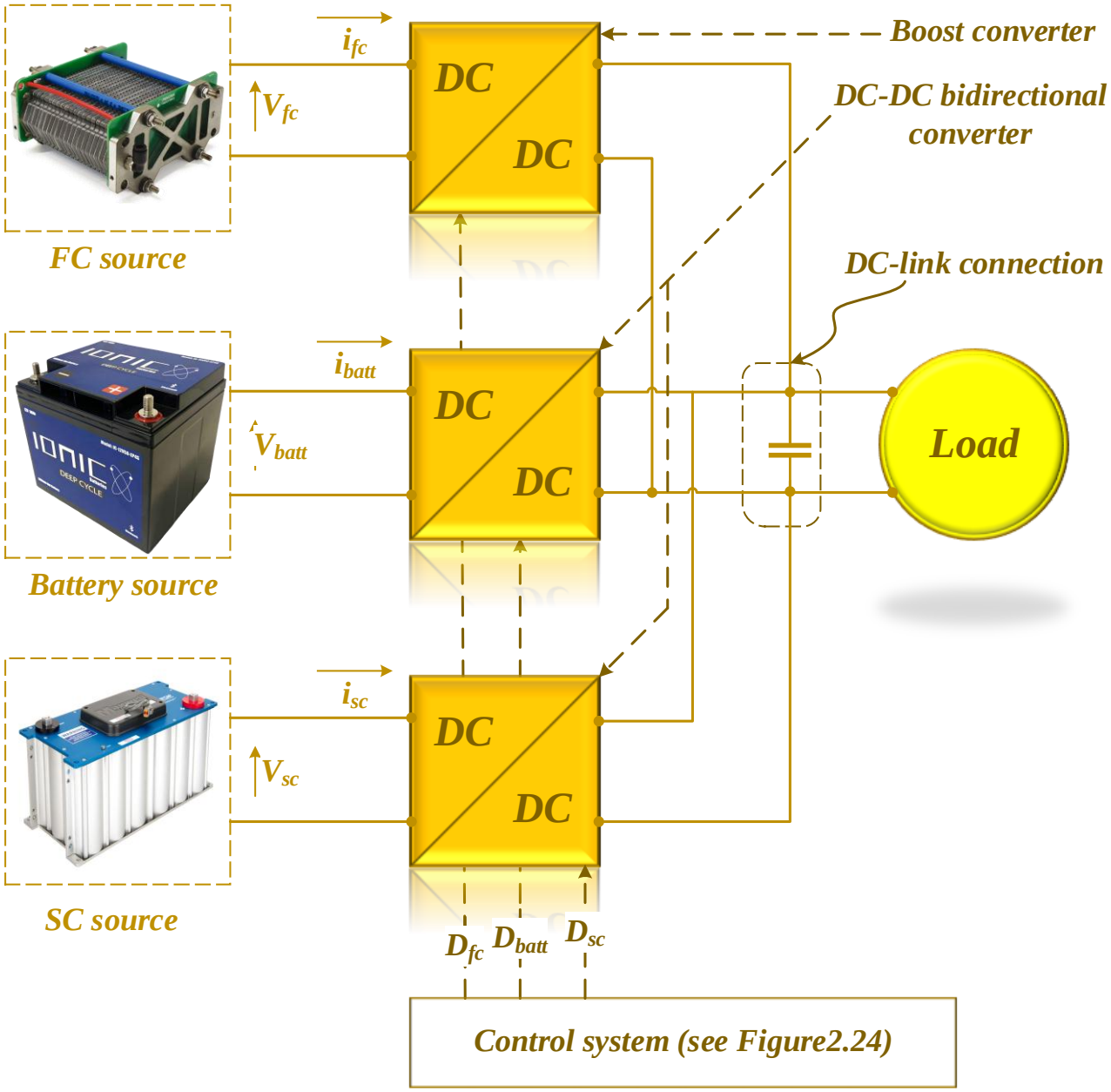

Figure 2.23: *Fuel cell hybrid system model in SPS.*

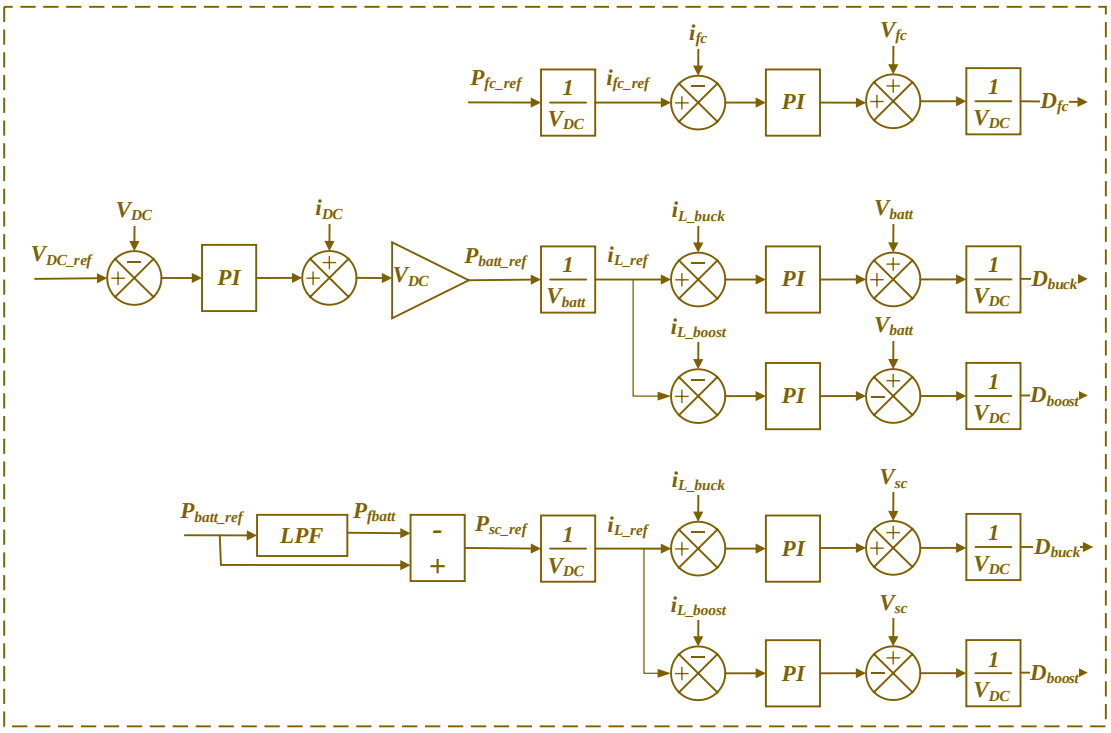

Figure 2.24: *Fuel cell hybrid system control.*

Figure (2.25) depicts the simulation results of the fuel cell system acting as a main source in the hybrid power system.

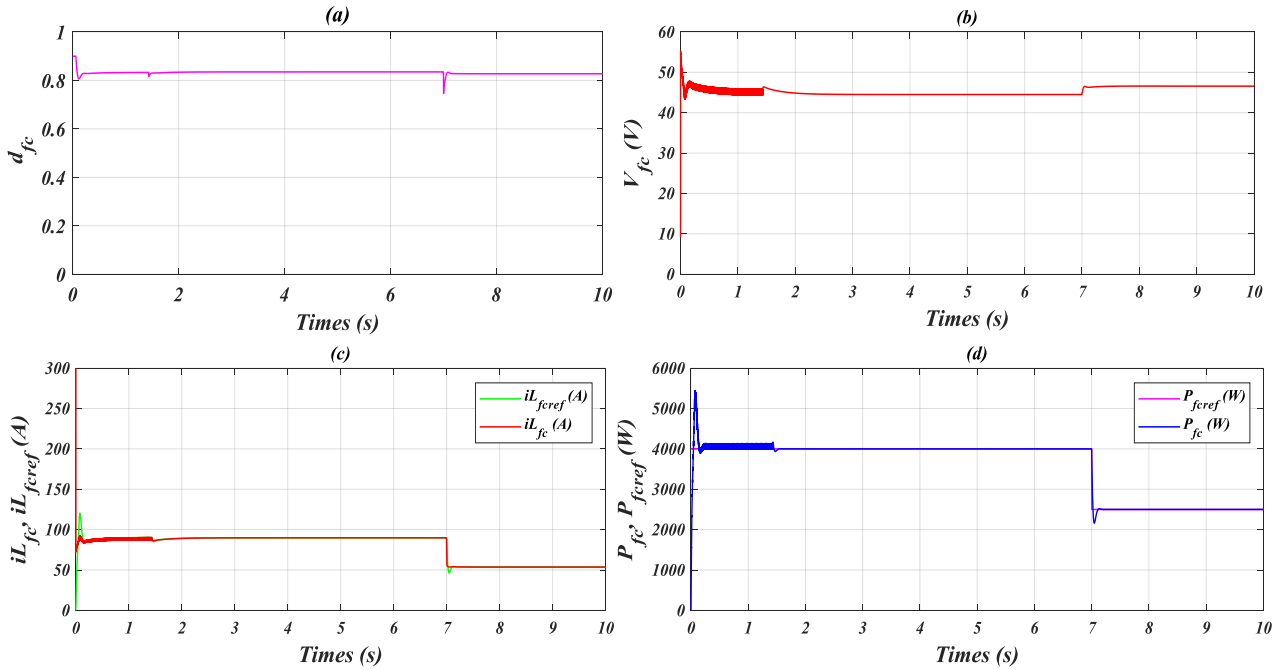

Figure 2.25: *Simulation results of the fuel cell hybrid system (fuel cell part): (a) Boost duty cycle d_{fc}, (b) Fuel cell voltage V_{fc}, (c) Current i_{Lfc} with its reference i_{Lfcref}, (d) Fuel cell power P_{fc} with its reference P_{fc_ref}.*

Figure (2.26) depicts the simulation results of the battery system acting as a storage system in the hybrid power system.

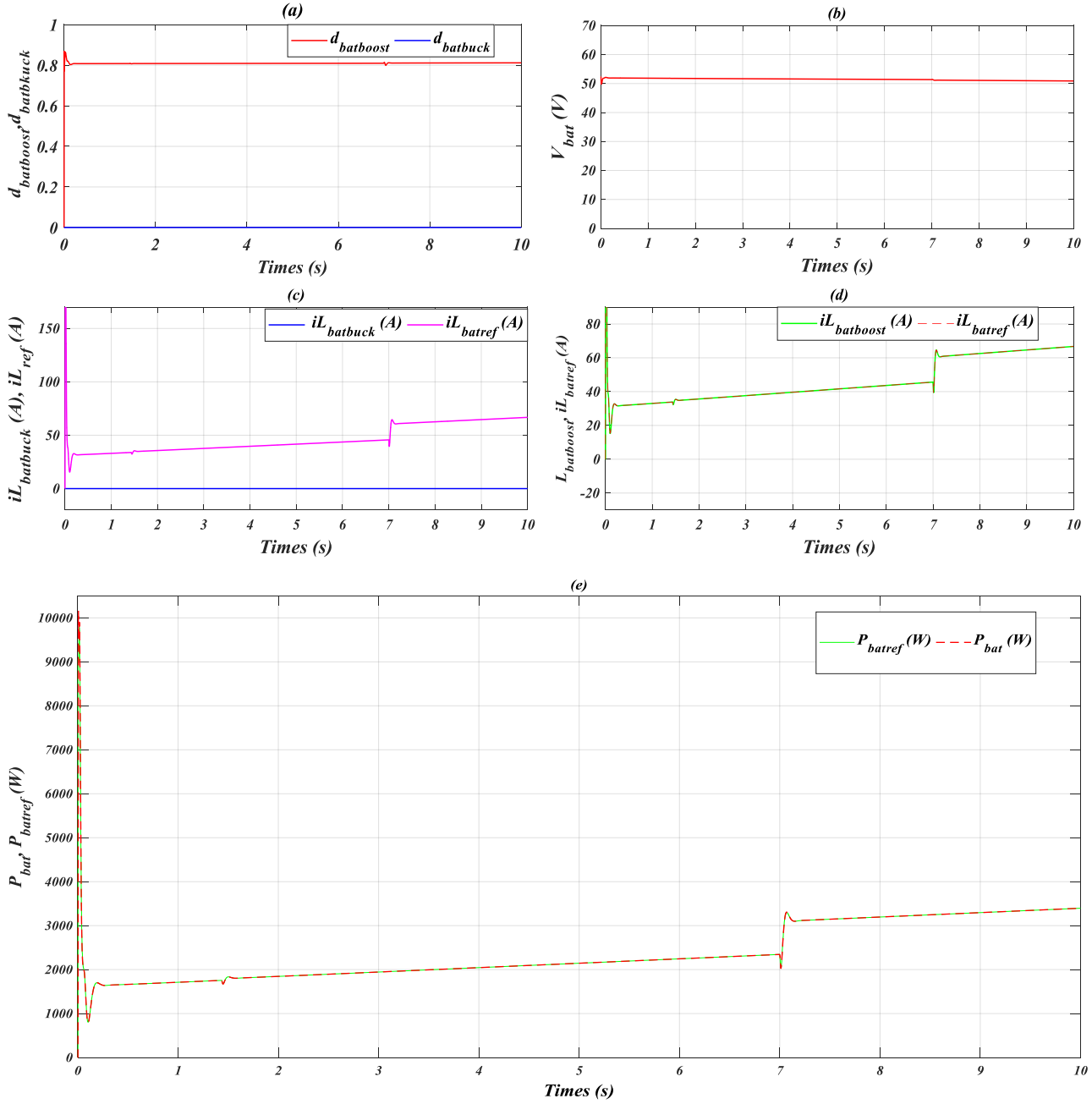

Figure 2.26: *Simulation results of the fuel cell hybrid system (battery system part): (a)Buck and boost duty cycles d_{buck}, d_{boost}, (b) Battery voltage V_{bat}, (C)Currant iL_{boost} with reference current i_{Lref}, (d) Currant i_{Lbuck} with reference current i_{Lref}, (e)Battery power P_{bat} with reference power P_{bat_ref}.*

Figure (2.27) depicts the simulation results of the supercapacitor system acting as a storage system in the hybrid power system.

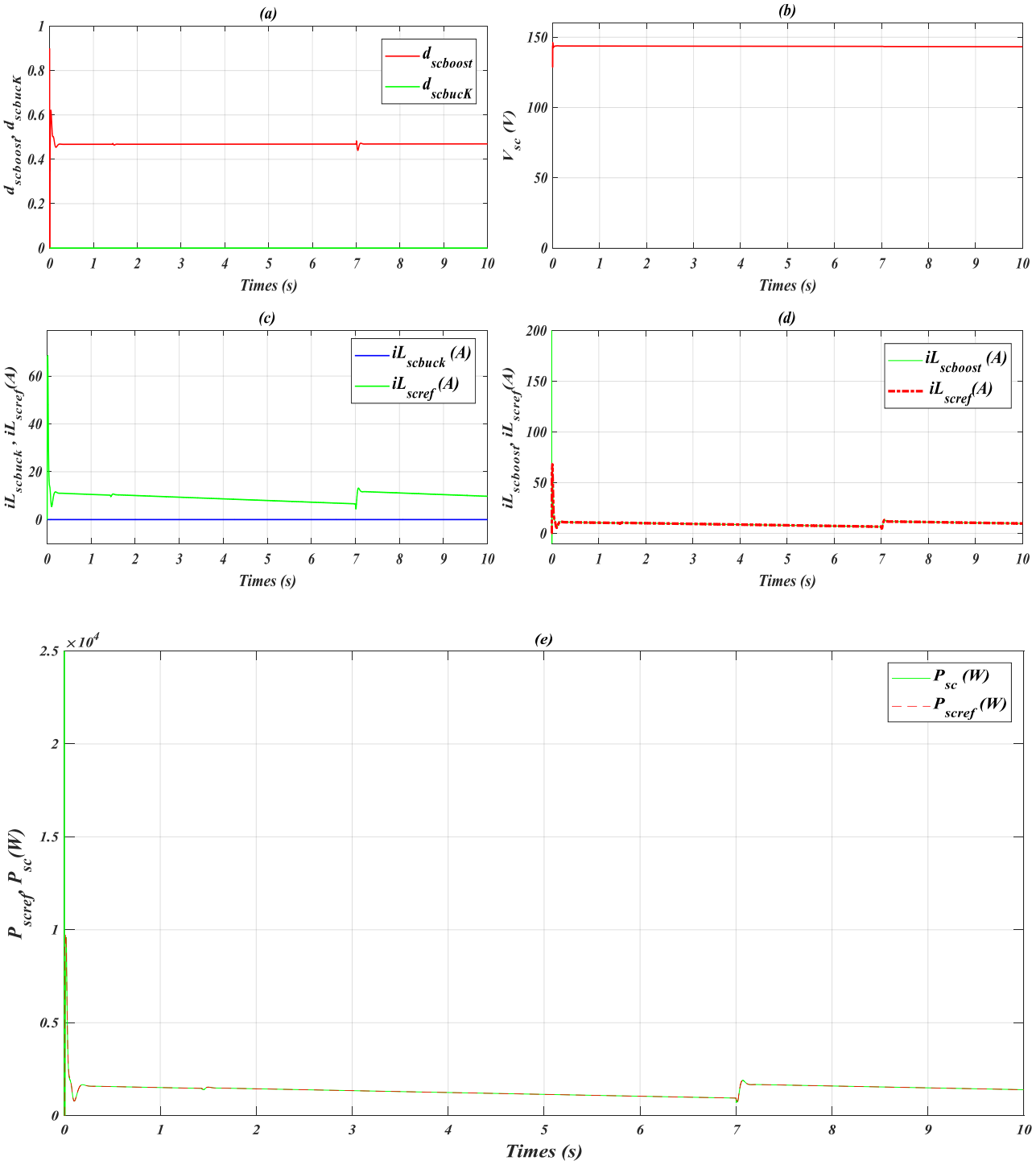

Figure 2. 27: *Simulation results of the fuel cell hybrid system (supercapacitor system): (a)Buck and boost duty cycles d_{buck}, $d_{boost.}$ (b) Supercapacitor voltage V_{sc}, (c) Currant i_{Lboost} with its reference i_{Lref}, (d) Currant i_{Lbuck} with its reference $i_{Lref,}$ (e) Supercapacitor power P_{sc} with its reference P_{sc_ref}.*

Figure (2.28) shows the simulation results of the DC-bus voltage.

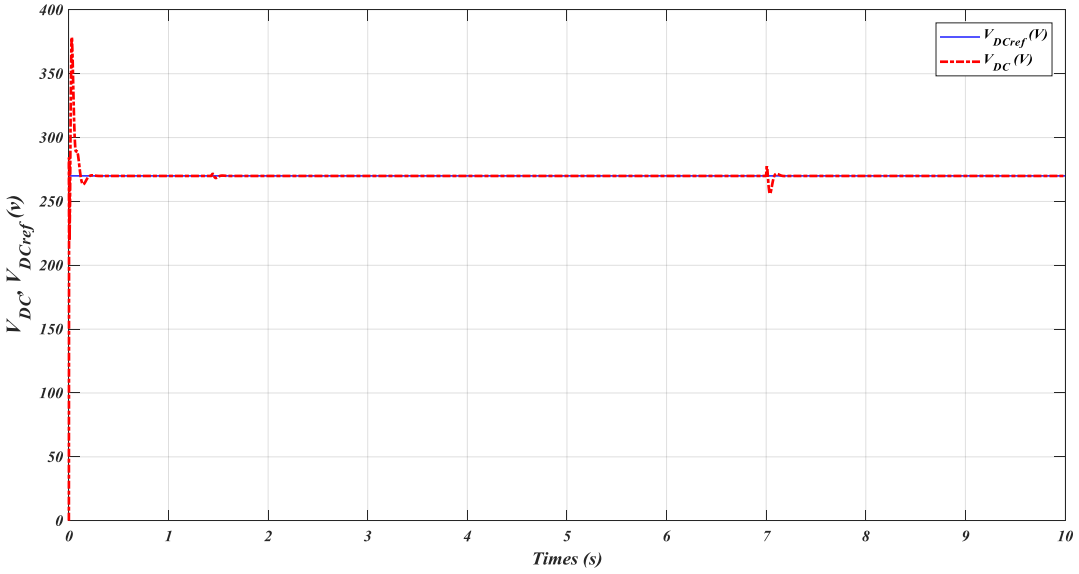

Figure 2.28: *DC-bus voltage.*

❖ **Interpretations**

The simulation results shown in Figures (2.25), (2.26), (2.27) and (2.28) present the behavior of the adopted HPS formed by an FC source with two storage systems. It can be seen that the energy generated by the FC system is used to feed the load and charge the storage systems as well.

Figure (2.25) presents the simulation results of the FC system, from which it can be seen that the inductance current changes according to the change of reference power. Furthermore, the FC voltage is equal to 45 V for a reference power equals to 5000 W and 48V for 3500 W.

From Figure (2.26) presenting the simulation results of the battery system, one can observe that the boost operates with d_{boost}=0.8 in all time, which is confirmed in Figure (2.26.a. The battery voltage is 52.4 V, and the battery current is i_{Lboost}=30A at t=0.1 s. This value increases slowly along the period [0.1, 10] s until it reaches at t=10 s the value iL_{boost}=70A. During this period, the boost current tracks its reference. It is worth mentioning that, in this period, the buck current is zero since the reference current is always positive.

In Figure (2.27), exhibiting the simulation results of the SC system, the duty cycle of the boost converter is $D_{scboost}$=0.47. Again, the boost converter is the only converter that operates, which leads to the decrease of its current from 20 A at t=0.1 s to 10A at t=10s.

Figure (2. 28) confirms that the PI controller is capable to maintain the DC-bus voltage at its reference of 270 V even during load change.

2.6 Conclusion

In this chapter, the modeling of the different elements that make up the proposed HPS are appropriately detailed. These mathematical models are used as tools to develop different PI based control algorithms needed to manage the power converters. Indeed, the FC is controlled by a DC–DC boost converter, whereas the Li-ion battery and SC are controlled by bidirectional DC-DC buck-boost converters. The simulation results of the fuel as well as the storage systems under reference power variations confirm the good performance of the adopted PI controllers in terms of tracking the output voltage and currents. In the following chapter, more focus will be given to the power management of the suggested HPS.

Chapter 3:

Fuel Cell/ Battery/ Supercapacitor Hybrid System's Energy Management Strategy

---

An energy management system (EMS) is an essential tool for a hybrid power system. Its strategies play an important role in system performance to achieve its key goals, such as minimization of production costs, improving energy efficiency, increasing durability and reliability, and dynamic response ability of the HPS. The EMS of the HPS is presented in this chapter. It begins with concentrating on the idea, then moves on to studying potential strategies. State machine control, PI-based energy management strategy, equivalent consumption minimization, and external energy maximization strategies are all considered in this study. A comparison of the suggested strategies is then provided.

3.1 Management system

Management system (MS) is a systematic framework designed to manage a set of policies, processes and procedures, so that it manages the interrelated parts of a system [102] in order to ensure that it can fulfill the tasks required to achieve its objectives, including [102]:

- Operational efficiency through better use of resources.
- Safety from risks by improved protection.
- Ability to provide consistent and improved services.

3.2 Energy management strategy

The MS oversees the operation of the HPS through various functions including creating and distributing the power reference for each controllable source, controlling the load to ensure the load leveling and securing the sources from critical operating conditions (peak shifting) [5] [103], charging and discharging storage systems, and maintaining the bus voltage within limits while ensuring each energy source operates within its boundaries. Along with these tasks, the MS also improves power flow, reduces operating costs, and takes into consideration emission reductions [10] [21]. The MS operational structure is described in Figure (3.1).

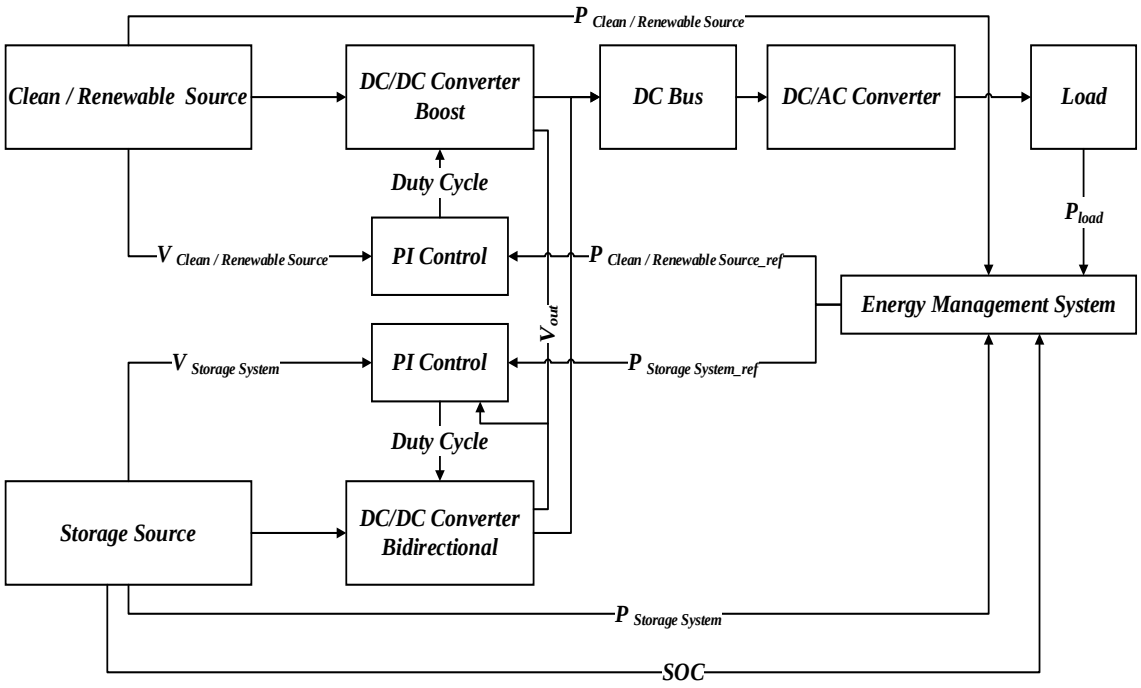

Figure 3.1: *MS operating scheme.*

The MS running relies on its embedded energy management strategy (EMS), which plays a critical role in ameliorating the performance and efficiency of the HPS [104]. In the literature, diverse EMSs for HPSs have been indicated, which can be categorized according to the topological structure shown in Figure (3.2). Considering that most of the strategies and algorithms did not deploy in industry and are still in the stage of scientific research, then EMSs fall under two categories, an industrial and a scientific research field [9]. The former includes a rule-based strategy (RBS), while the latter involves an optimization strategy (OS) [101] [7] [3]. Furthermore, based on the real-time implementation optimization strategy, OS can be divided into online and offline optimization [9].

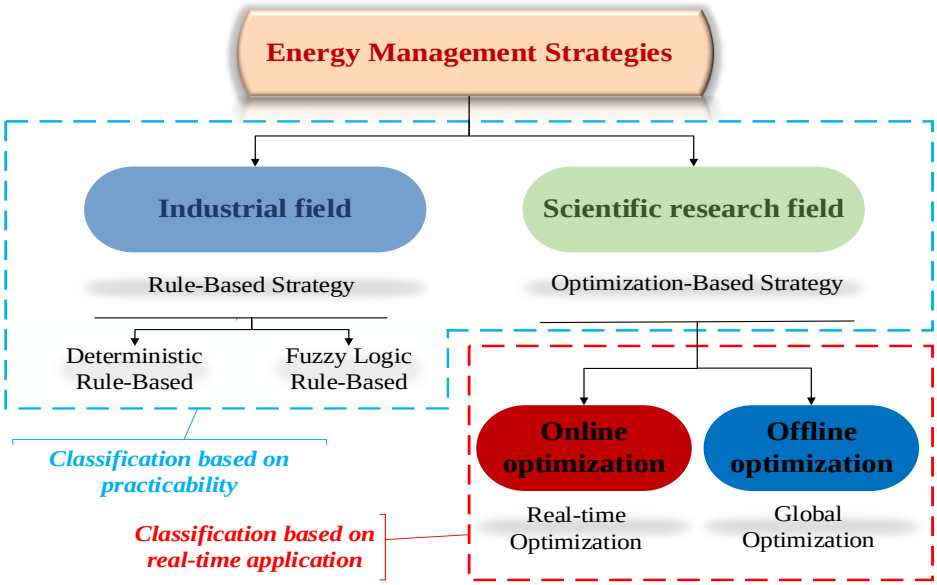

Figure 3.2: Energy management strategies classification.

The EMS was developed with objectives arranged in order of priority as follows [6]:

- Ensuring safe power supply operation by respecting the component maximum and minimum current limits.
- Delivering performance means meeting the load.
- Minimizing fuel usage for efficient fuel cell operation.
- Increasing FC longevity by preventing frequent load changes or switching on and off.

3.3 State of the research on energy management strategies

Although HPS configurations and operational tenets vary, their corresponding EMSs' fundamental ideas remain the same [9]. Rule-based and optimization EMSs are two categories of common EMSs.

3.3.1 Rule-based energy management strategy

The rule-based strategy (RBS) is a static controller that has been widely used; it is simple to execute it with a real-time controller for controlling power flow in an HPS, and its use mainly relies on the operating mode, this latter is decided using rule tables or flowcharts to satisfy the conditions of the HPS components as efficiently as possible [7]. Its rules were obtained in a variety of modes, frequently without prior knowledge of the load profile; these modes depend on human intelligence, heuristics, or mathematical models [10].

This strategy mainly subcategorized the deterministic rule-based strategy (DRBS) and the fuzzy rule-based strategy (FRBS) [11].

3.3.1.1 Deterministic rule-based strategy

Deterministic rule-based (DRBS), sometimes referred to as static logic threshold control strategies [9], in which the rules are designed based on predetermined objectives such as grid independence, cost economies, and reduced emissions. DRBS usually include look-up tables [105], filter-based control (FBC) [103], wavelet transform (frequency decoupling FD) [8], and load follow control is also named state machine control (SMC) [26]. The essential aspect of these strategies is their ease of control and minimal computational complexity [106]. We will go through a few of them below for more explanation.

- **State machine control strategy**

Because of its simplicity, state machine control is the most commonly employed approach [27]. Nevertheless, the decision is reliant on the load power and operational states of the components, causing it unstable with large input variation. Furthermore, it is incapable of responding to complex and changing operational circumstances [10] [26].

3.3.1.2 Fuzzy rule-based strategy

This approach FRBS, which is founded on fuzzy reasoning, may be used to reduce the challenging control problems in non-linear time-varying systems. The fuzzy controller frequently employed state variables as inputs, such as the SOC, also fuzzy reasoning to split the operating mode and decide the distribution of power output [9]. FRBS includes the conventional fuzzy control strategy [107], adaptive fuzzy control strategy [108], and predictive fuzzy control strategy [109].

3.3.2 Optimization energy management strategy

EMS of an HPS has to deal with optimization issues [9]. Optimization involves increasing the efficiency of the HPS [110]. Specifically, its goal is to minimize a cost function (objective function) including the emission, fuel consumption, and device degradation [111], in addition to other procedures depending on the use. Therefore, establishing and solving an optimization model based on an optimization algorithm is the primary responsibility of an OS [9]. According to numerous academics, these algorithms have been employed to get optimal solutions through numerous standard optimization methods [4]; well-known deterministic mathematical methods deal with and resolve issues swiftly and thoroughly [4]. Metaheuristic mathematical models, on the other hand, are another effective alternative option for HPS optimization [112], where heuristic methods are combined to find a satisfactory solution using

genetic algorithms, statistical mechanisms, and biological evolution to achieve optimal control [113]. The former comprises mixed-integer linear programming (MILP), mixed-integer non-linear programming (MINLP), and dynamic programming (DP), and the latter encompasses the artificial bee colony (ABC) solutions, particle swarm optimization (PSO), simulated annealing (SA), genetic programming (GP), differential evolution (DE) solutions, and genetic algorithm (GA) [4].

Two broad categories, global and instantaneous optimization, can be used to categorize these optimization techniques. In the parts that follow, these are thoroughly covered.

3.3.2.1 Global optimization (offline optimization)

Global optimization is a highly complex strategy that involves knowledge of all load profiles [10]. Due to the fact that it generates enormous amounts of data when calculated; it is an extremely complex approach that is challenging to execute in real-time applications [7]. Linear programming, dynamic programming, stochastic strategy, and so forth are used in this strategy. We will go through a few of them below for more explanation.

- **Linear programming**

Many convex nonlinear optimization problems are finally approximated by the linear programming method, which is also known as the LP method [7]. By applying linear programming to formulate fuel efficiency optimization problems, a global optimization solution can be found [114].

- **Dynamic programming**

The DP method, dynamic programming, is employed for numerous discretized and sequenced complex problems [4]. To deal with such issues, it is possible to classify these latter into optimally solvable sub-problems to address them. Following these findings' discussion, a suitable solution is developed [115] to optimize and address the main issue.

- **Stochastic control strategy**

Uncertainty-involved modeling and optimization problems can be framed using a stochastic strategy. Along with a genetic algorithm, a stochastic dynamic programming problem is formulated in this strategy [7].

- **Stochastic dynamic programming**

Stochastic optimization is a technique that employs random variables for solving optimization problems. Dynamic programming is referred to as stochastic dynamic programming if either the state or the decision can be expressed as a probability function. Therefore, the stochastic optimum control issue requires a high-performance computer approach to be solved [7].

- **Genetic algorithm**

For optimization and search problem, genetic algorithm is a reliable and robust solution, and it is a heuristic search algorithm with a broad scope of search space and an ability to quickly improve the parameters utilizing easy operations [7]. GA starts with a group of solutions (chromosomes) named a population. The solutions from one population are chosen based on their fitness to assemble new ones. The process is continued until the required condition is met, with the most appropriate solutions having a better chance of doing so than the less suitable solutions [116].

3.3.2.2 Instantaneous optimization (online optimization)

The cost function in these techniques is solely reliant on the system's current state [117]. In contrast to GOS methods, instantaneous optimization strategy requires less computing and has superior real-time performance, but it cannot accomplish global optimization [9]. It also does not require prior knowledge of all cycle circumstances [9]. Typically, these strategies include the equivalent consumption minimization strategy (ECMS) [12], external energy maximization strategy (EEMS) [13], model predictive control (MPC) [14], artificial neural network [15], particle swarm optimization (PSO) [16], and Pontryagin's minimum principle (PMP) [17]. Other methods also including sliding mode control [18], robust control (RC) [9], manta ray optimization (MRO) [19], and Harris Hawks optimization (HHO) [20]. We will go through a few of them below for more explanation.

❖ **Equivalent consumption minimization strategy**

To reduce fuel consumption and pollutant emissions, EMSs use the equivalent fuel consumption idea. Without harming fuel efficiency, this immediate reduction reduces harmful emissions [118]. Because it is real-time implementable and does not require previous information on the load profile to obtain an optimal solution; it transforms a global optimization issue into an instantaneous minimization problem and offers a solution at each instant [7] [117].

❖ **Model predictive control**

To predict electricity generation and efficiently manage the energy already in storage, predictive control techniques are required. This approach traditionally combines stochastic programming with control. The most significant of these techniques is predicting the deterioration of grid components, particularly energy storage systems [119].

❖ **Artificial intelligence strategies**

Artificial intelligence strategies (AISs) use clever techniques like neural networks and machine learning to build strategy [10].

- **Neural network**

The neural network is a potent computing technique that learns from training data and generalizes from there; it is made up of several blocks coupled together in a certain manner to carry out a particular task. Any lookup table may be fitted by a well-designed network, which can then adapt by coaching to update the table's data; it is best than rule-based controllers because of this property [7]. These strategies, such artificial neural networks (ANN), adaptive neuro fuzzy inference system (ANFIS), and recursive neural networks (RNN), are based on the neural network approach [10].

- **Machine learning**

This category, according to the author of [10], takes advantage of recent developments in machine learning, whose use has increased over the past ten years. It is widely used in other domains, such as energy management, in addition to having shown good results in some areas, particularly image classification. A database, which is not always accessible, is needed to train a model. Due to a lack of research in this relatively new sector, this is rather difficult. The fact that it cannot be guaranteed to operate with data other than those used for training is still a

limitation. It includes reinforcement learning (RL) [101], multi-agent systems (MAS) [110], and deep learning approach [120].

- **Particle swarm optimization**

As stated by [7]'s author, a quicker, less costly, and more reliable stochastic global optimization approach is particle swarm optimization (PSO). It is a heuristic progressing search algorithm, an iterative optimization technique that uses particles (populations of candidate solutions) and moves them around in the search space in accordance with a mathematical procedure upon the particle's place and velocity. These particles are directed into the best-known places in the search area as well as the best-known place of the entire swarm after they have been found.

- **Pontryagin's minimum principle**

In the existence of constraints for any state or input control, the Pontryagin's minimal principle (PMP) provides the optimal control to move a dynamic system from one state to another, according to the author of [7]. It is a particular case of calculus' Euler-Lagrange equation variations. Only the required requirements are provided by PMP for an optimal solution, and the Hamilton-Jacobi-Bellman equation satisfies sufficient conditions. The control based on PMP requires less computing time to get an ideal trajectory since the number of nonlinear second-order differential equations rises linearly with dimension. However, the optimal trajectory could only be a local optimal rather than a global one [121].

3.3.3 Brief comparison of energy management systems

Table 3.1 includes the advantages and disadvantages of each EMS approach.

Type	*Advantages*	*Disadvantages*
Deterministic rule-based	- Reliable, easy to develop, and simple to design [10]. - Nowadays, it is vastly used [10].	- Count on human expertise [101]. - Difficult to optimize [122].
Fuzzy rule-based	- Design simplicity and high performance [123]. - Extremely robust and highly effective in real time [10].	- Difficulty hitting the optimal and depending on human knowledge [123]. - The hardware and software for the control system are both complex [10].
Global optimization	- Owns a super performance and can be utilized as other strategies benchmark [124].	- Need prior load profile demand information, so high computation complexity [125].
Instantaneous optimization	- High real-time performance and each instant of its operating work is optimum, both enhance fuel cell lifetime and fuel efficiency [111].	- Require a high-processing controller for training the model [126].

Table 3.1: *Advantages/ disadvantages of various energy management strategies.*

3.4 Studied hybrid power system

The system under consideration in the current study is made up of a PEMFC acting as main source, a lithium-ion battery serving as a storage system, and a supercapacitor for handling sudden changes in power demand. While the power from the battery is processed by a specialized bidirectional DC-DC converter to assure charge-discharge operation, the power from the FC is handled by an energy management strategy based on unidirectional DC-DC converter. All sources are put together on one DC-bus. The Figure (3.3) shows the studied HPS included FC, battery and SC.

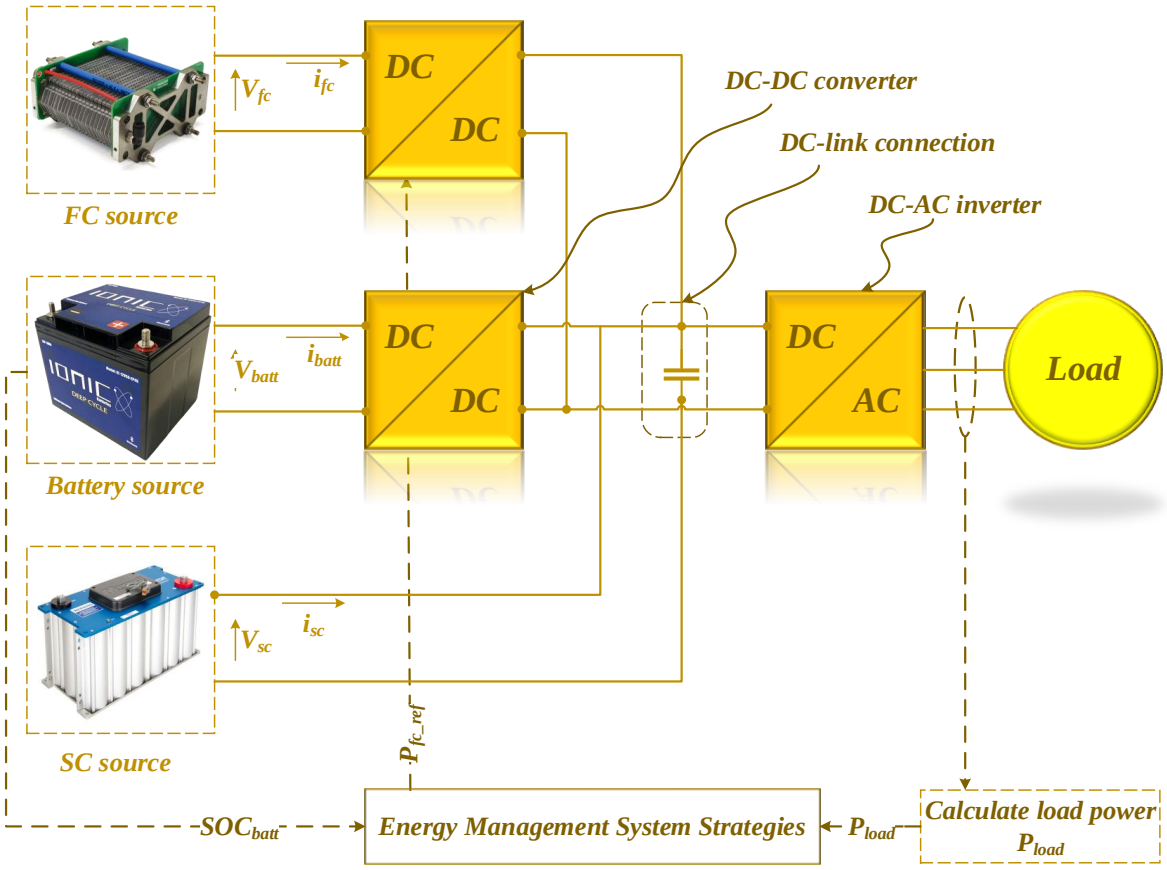

Figure 3.3: *Hybrid parallel system included FC, battery and supercapacitor.*

3.4.1 DC to AC inverter

The average value model for the DC-AC inverter is shown in Figure (3.4). It is an idealized model used for lengthy simulation studies, and it does not include power electronic switches and switching signals, according to the author of [34].

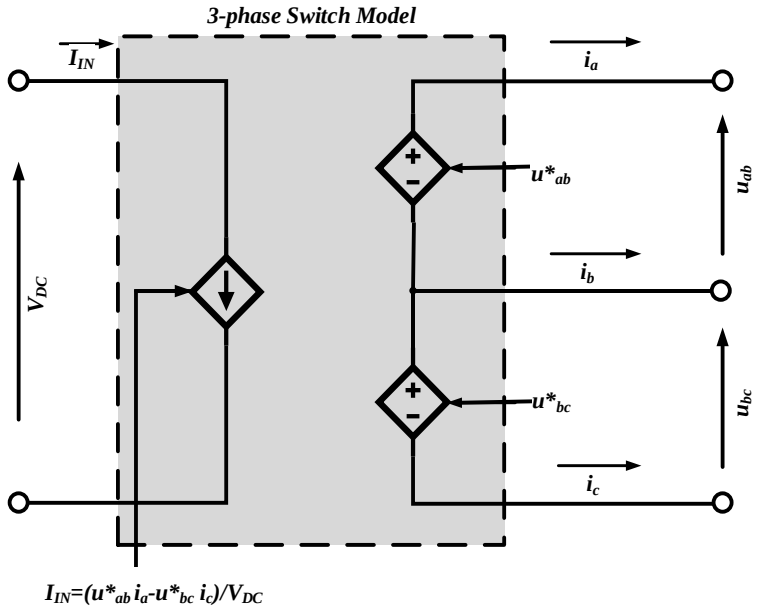

Figure 3.4: *DC-AC inverter average model.*

The two regulated voltage sources, which are the AC output voltages of the inverter model, are controlled by line-to-line reference voltages u_{ab}^{*} and u_{bc}^{*} .

The reference voltages $v_a^{*}, v_b^{*}, v_c^{*}$ defined by equation (3.1) and load currents i_a, i_b, i_c are used for computing the AC power according to the equation (3.2).

$$\begin{cases} v_a^{*} = \sqrt{2}\ V_{nom\_rms} \sin(2\pi ft) \\ v_b^{*} = \sqrt{2}\ V_{nom\_rms} \sin(2\pi ft - 120°) \\ v_c^{*} = \sqrt{2}\ V_{nom\_rms} \sin(2\pi ft + 120°) \end{cases} \tag{3.1}$$

Where V_{nom_rms} is the nominal rms phase voltage, and f is the frequency.

$$P_{AC} = v_a^{*} i_a + v_b^{*} i_b + v_c^{*} i_c \tag{3.2}$$

Knowing that:

$$i_a + i_b + i_c = 0 \tag{3.3}$$

Using equation (3.3), the equation (3.2) can be rewritten as follows:

$$P_{AC} = v_a^{*} i_a + v_b^{*}(-i_a - i_c) + v_c^{*} i_c \tag{3.4}$$

This equation can be put in the following form:

$$P_{AC} = (v_a^* - v_b^*)i_a - (v_b^* - v_c^*)i_c \tag{3.5}$$

In which:

$$u_{ab}^* = v_a^* - v_b^* \tag{3.6}$$

$$u_{bc}^* = v_b^* - v_c^* \tag{3.7}$$

Finally, the AC power P_{AC} is expressed as in equation (3.8).

$$P_{AC} = u_{ab}^* i_a - u_{bc}^* i_c \tag{3.8}$$

The equivalence between the power of the AC side and that of the DC side determines the DC current as given in equation (3.9).

$$I_{IN} = \frac{u_{ab}^* i_a - u_{bc}^* i_c}{V_{DC}} \tag{3.9}$$

3.4.2 AC Load

As stated by the author of [21], the load is shown as a three-phase controlled current source as appears in Figure (3.5), where the current flowing through the load is determined via the three-phase apparent power load profile S, the power factor $\cos(\varphi)$, and the nominal line voltage V_{nom_rms}. Therefore, the modeling of load is given as follows:.

Equation (3.10) computes the complex number of impedance module Z.

$$Z = \frac{V_{nom\_rms}^2}{P + jQ} \tag{3.10}$$

where the active power P and reactive power Q are given in equations (3.11) and (3.12), respectively.

$$P = \left(\frac{S}{3}\right) \cos(\varphi)$$

(3.11)

$$Q = \sqrt{\left(\frac{S}{3}\right)^2 - P^2} \tag{3.12}$$

Accordingly, to calculate the load voltage vector v_S in stationary frame, the load three-phase voltage v_a, v_b, v_c are transformed using the following equation:

$$v_S = T\left[v_a, v_b, v_c\right]' \tag{3.13}$$

$$T = \sqrt{\frac{2}{3}}\begin{bmatrix} 1 & -\frac{1}{2} & -\frac{1}{2} \\ 0 & \frac{\sqrt{3}}{2} & -\frac{\sqrt{3}}{2} \end{bmatrix} \tag{3.14}$$

Then, one may calculate the phase currents i_a, i_b, i_c based on the following inverse transformation:

$$\left[i_a, i_b, i_c\right]' = T^{-1}\frac{v_s}{Z} \tag{3.15}$$

$$T^{-1} = \sqrt{\frac{2}{3}}\begin{bmatrix} 1 & 0 \\ -\frac{1}{2} & \frac{\sqrt{3}}{2} \\ -\frac{1}{2} & -\frac{\sqrt{3}}{2} \end{bmatrix} \tag{3.16}$$

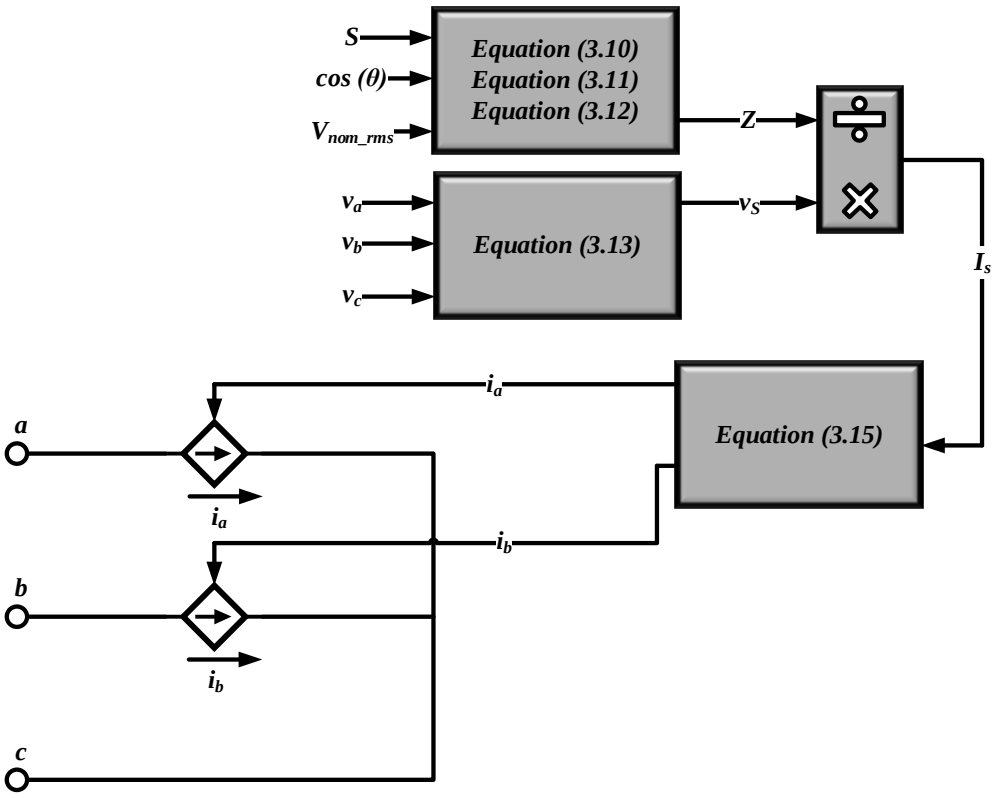

Figure 3.5: *AC load model.*

In this study, the value of V_{nom_rms} is set to $115\ V$ and the frequency f is $400\ Hz$ for aircraft application.

3.5 Suggested energy management strategies

There are several strategies used in management systems, we will study some of them, including SMC, PI-based EMS, ECMS, and EEMS strategies.

3.5.1 State machine control strategy

To determine the point of operation for each HPS' component, the author in [26] developed a SMC strategy according to eight states. This control approach seeks to avoid continuous changes in the FC reference power due to its slowly dynamic response [27]. Hence, when the HPS components hit their limits, the reference power changes; whereby, in this case, the following limits have been considered: maximum and minimum FC power values (P_{fc_min}, P_{fc_max}), and the nominal FC power (P_{fc_nom}); battery SOC (SOC_{min}, SOC_{max}); maximum charge battery power (P_{batt_char}).

The operational state here is determined by the SMC strategy, which is dependent on the demanded load and the battery SOC. For the battery SOC, three levels were evaluated, high SOC when $(SOC_{\max} < SOC)$, normal SOC when $(SOC_{\min} < SOC < SOC_{\max})$, and low SOC $(SOC < SOC_{\min})$, in which the SOC of battery in this case takes the following values $(SOC_{\min} = 60\%\ ,\ SOC_{\max} = 85\%)$.

A summary of the SMC strategy is displayed in Figure (3.6), in which, eight possible states are suggested.

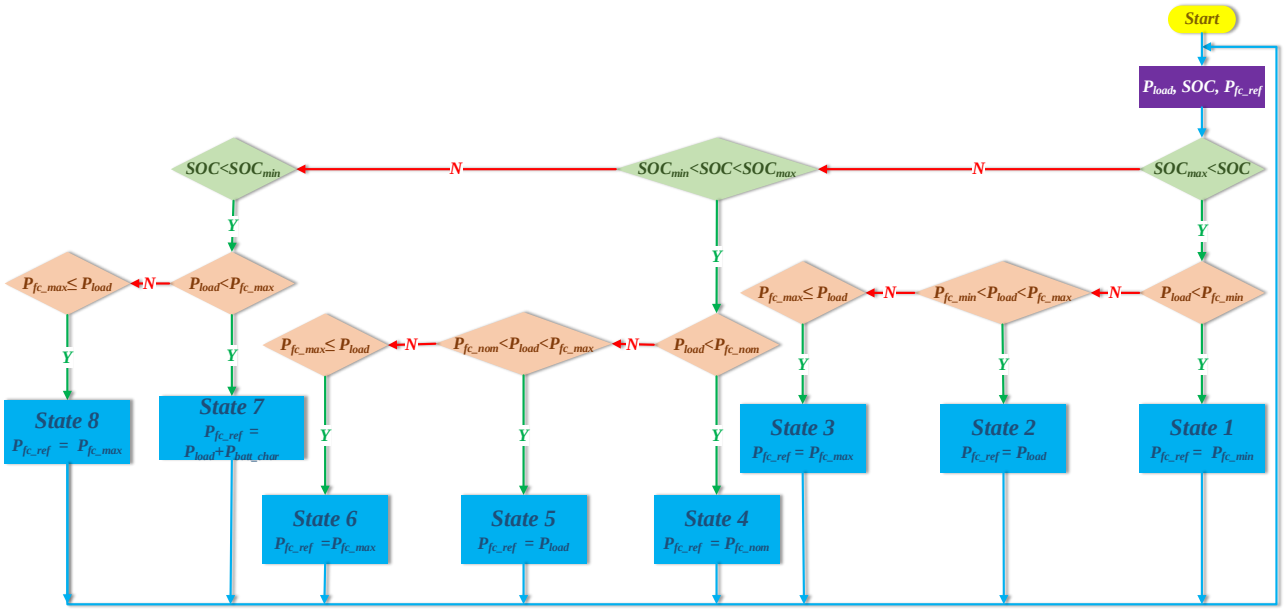

Figure 3.6: *Proposed state machine control strategy diagram.*

Below is a description of the operation states, and as known, in order to meet load power needs at all times, the HPS has been designed such that the FC and battery work together.

State 1: $\left(SOC_{max} < SOC \ \& \ P_{load} < P_{fc\_min}\right)$

When the battery SOC is high and the load's power (P_{load}) requirement is lower than the minimum FC power, the HPS embraces this mode. In this condition, the FC runs at minimum power. Consequently, the FC's reference power is given in equation (3.17).

$$P_{fc\_ref} = P_{fc\_min} \tag{3.17}$$

State 2: $\left(SOC_{max} < SOC \ \& \ P_{fc\_min} < P_{load} < P_{fc\_max}\right)$

In this state, the battery SOC is set to its maximum limit, while the power consumed by the load ranges between minimum and maximum of the FC power, thus, the FC feeds the load. Therefore, the FC's reference power is given in equation (3.18).

$$P_{fc\_ref} = P_{load} \tag{3.18}$$

State 3: $\left(SOC_{max} < SOC \ \& \ P_{fc\_max} \leq P_{load}\right)$

The FC works at maximum power when the battery's SOC reaches its upper limit and the power consumed by the load is more than or equal to the maximum FC power. In light of this, the reference power of FC is given in equation (3.19).

$$P_{fc\_ref} = P_{fc\_max} \tag{3.19}$$

State 4: $\left(SOC_{min} < SOC < SOC_{max} \ \& \ P_{load} < P_{fc\_nom}\right)$

The HPS functions just as it did in state one in this situation, but when it has normal SOC battery, and the FC operates at nominal power. This means that the FC's reference power is given in equation (3.20).

$$P_{fc\_ref} = P_{fc\_nom} \tag{3.20}$$

State 5: $\left(SOC_{min} < SOC < SOC_{max} \ \& \ P_{fc\_nom} < P_{load} < P_{fc\_max}\right)$

In this condition, when the SOC of the battery is limited in its scope, the HPS operates in the same manner as in-state two; therefore, the FC feeds the load. Thus, the FC's reference power is given in equation (3.21).

$$P_{fc\_ref} = P_{load} \tag{3.21}$$

State 6: $\left(SOC_{min} < SOC < SOC_{max} \ \& \ P_{fc\_max} \leq P_{load}\right)$

Similar to state three, while the battery SOC ranges between its minimum and maximum values, the FC functions at maximum power. As a result, the FC's reference power is given in equation (3.22).

$$P_{fc\_ref} = P_{fc\_max} \tag{3.22}$$

State 7: $\left(SOC < SOC_{min} \ \& \ P_{load} < P_{fc\_max}\right)$

The FC must provide the required load in addition to the maximum charge power of the battery if the battery SOC falls below a level and the power consumed by the load is less than the FC's maximum value power. As a consequence, the FC's reference power is given in equation (3.23).

$$P_{fc\_ref} = P_{load} + P_{batt\_char} \tag{3.23}$$

State 8: $\left(SOC < SOC_{min} \;\&\; P_{fc\_max} \leq P_{load}\right)$

In this low SOC condition, the FC operates at maximum power, just as it did in earlier states when the load's power consumption is more than or equal to the maximum FC power. The FC's reference power as an outcome is given in equation (3.24).

$$P_{fc\_ref} = P_{fc\_max} \tag{3.24}$$

❖ **Simulation results and interpretations**

The SMC is implemented in MATLAB-Simulink employing SPS. Figure (3.7) represents the results obtained.

The FC works as anticipated; it follows the load until the battery's SOC is at its minimum, at this point the FC charges the SC over their reference voltage $\left(270\ V\right)$, forcing the DC-bus voltage regulator to demand a negative current to attempt to recharge the battery again.

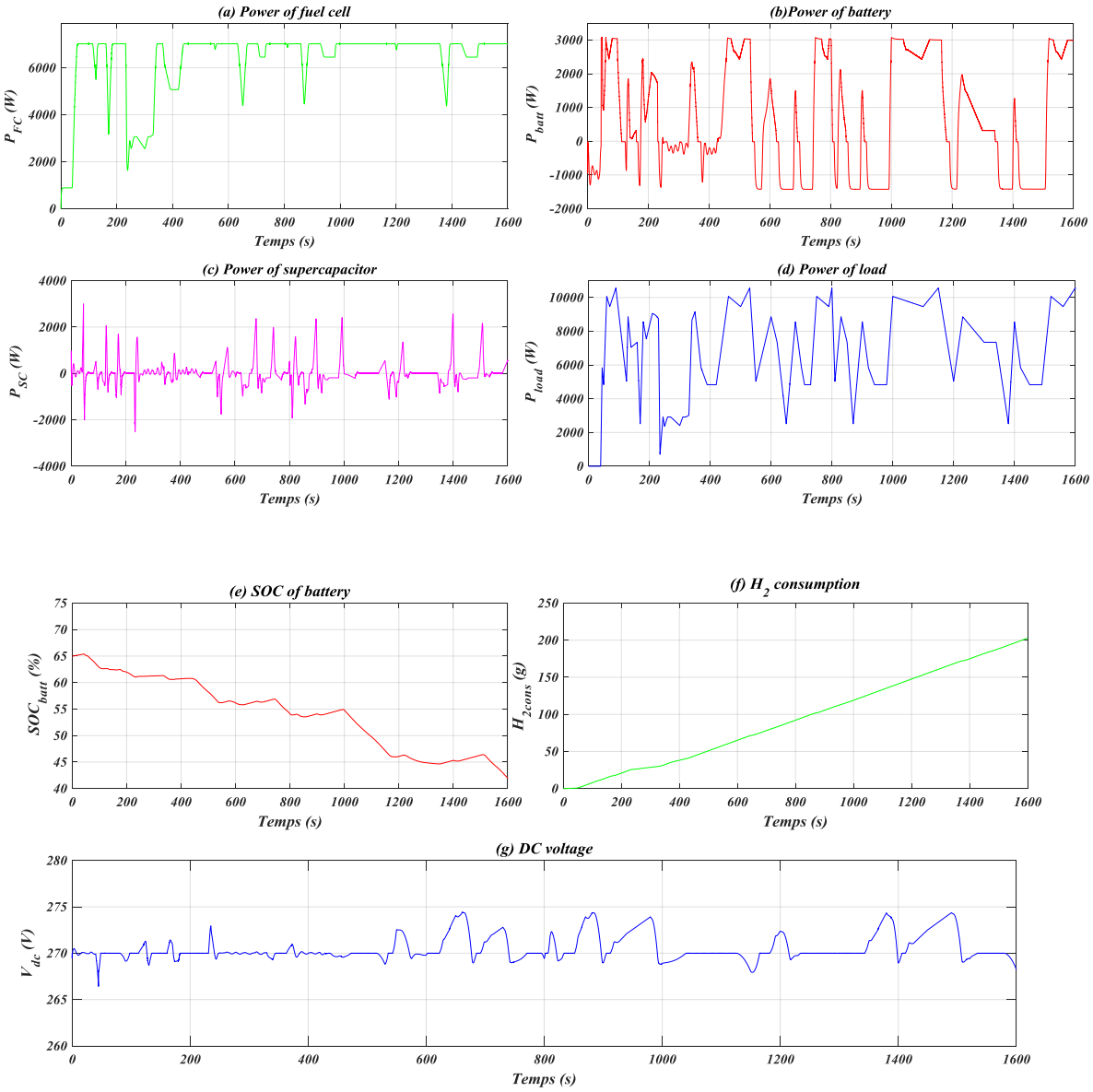

Figure 3 7: *Simulation results of state machine control strategy.*

3.5.2 PI-based energy management strategy

This approach control, known as passive control [6], employs a PI regulator to manage the battery's state of charge. Indeed, when the battery SOC is greater than the reference, the FC output is reduced and the battery supplies full power, and when the SOC is lower than the reference, the FC delivers nearly all of the load power [127]. Therefore, the PI regulator output is the battery power, which is then subtracted from the load power to get the FC reference power. Figure (3.8) depicts the algorithm of PI-based EMS.

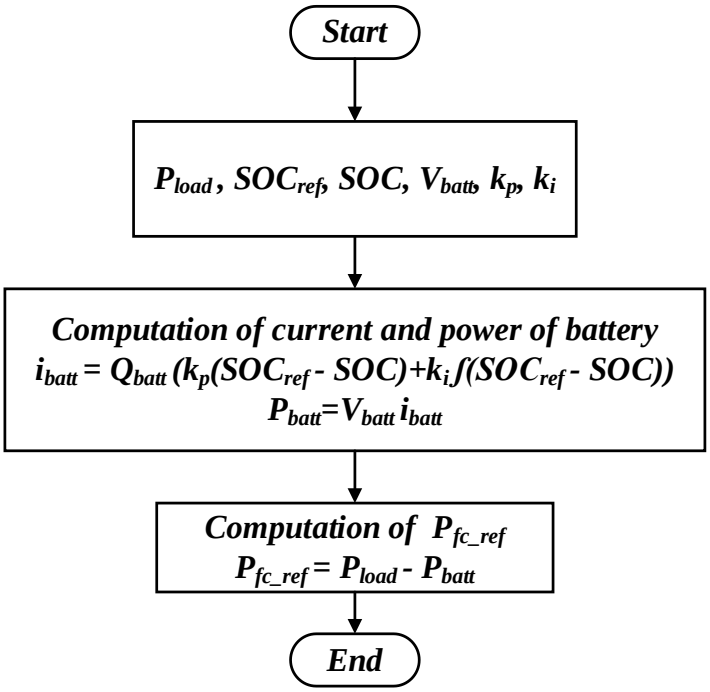

Figure 3.8: *Flowchart of the PI-based energy management strategy.*

- Q_{batt} is the battery capacity (Ah).
- V_{batt} is the battery voltage.
- i_{batt} is the battery current.
- k_p is the proportional gain.
- k_i is the integral gain.
- SOC_{ref} is the reference state of charge of battery.
- SOC is the state of charge of battery.

❖ Simulation results and interpretations

The PI-based EMS is implemented in MATLAB-Simulink employing SPS toolbox. Figure (3.9) represents the obtained results.

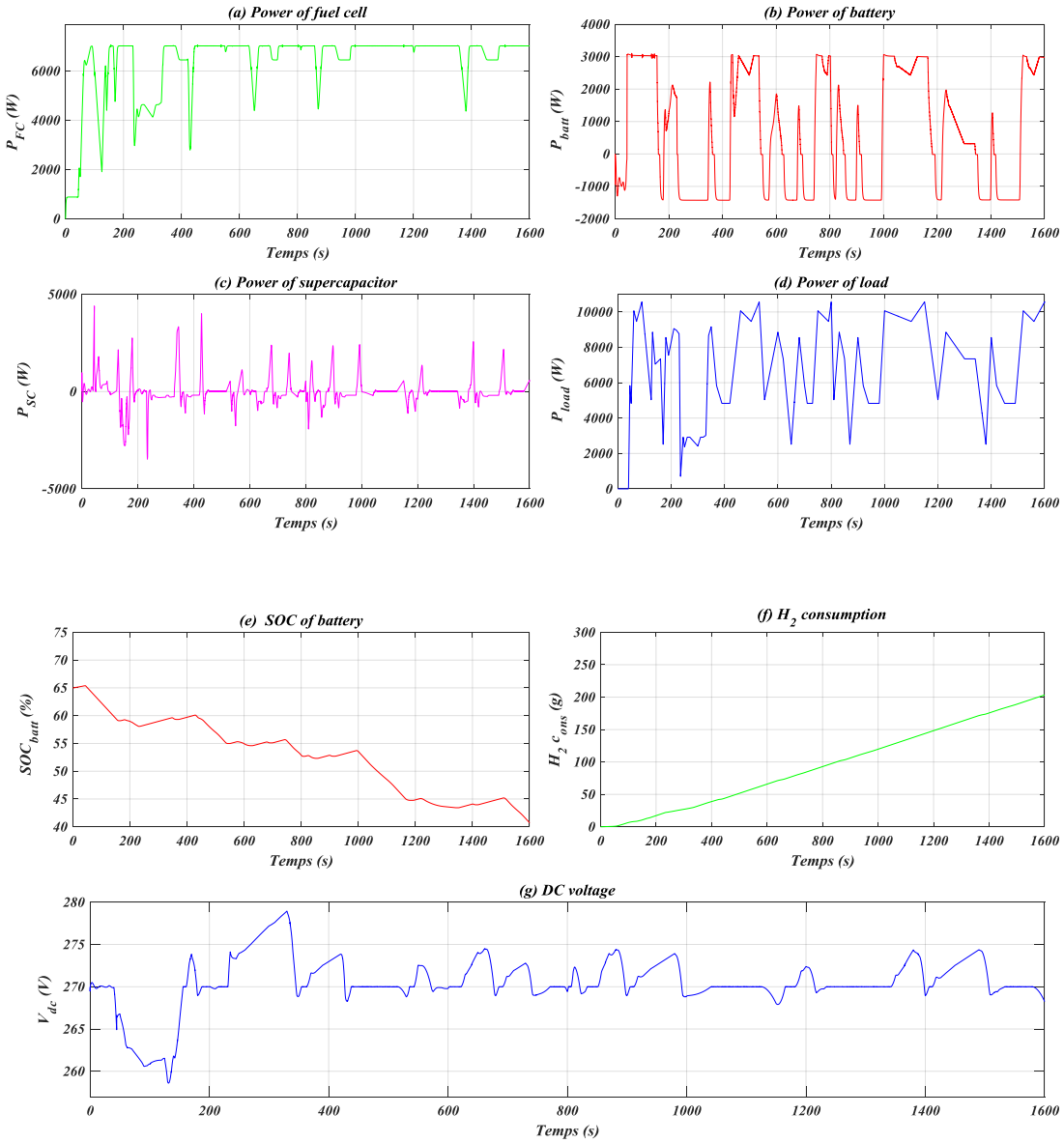

Figure 3.9: *Simulation results of PI-based energy management strategy.*

Because the battery empties fast to reach the reference SOC, the battery offers full power; similarly, the FC reference power is low, and the SC discharges to aid the battery; as a result, the DC-bus voltage falls below the reference voltage. Following that, the FC attempts to produce load power and recharge the battery, therefore providing the SC above their reference voltage and the FC follows the load as in the prior strategy.

3.5.3 Equivalent consumption minimization strategy

The ECMS is classified as a local optimization control strategy that is commonly utilized in instantaneous energy management, and its purpose is to reduce fuel consumption by limiting the fuel consumed by the FC and the equivalent fuel necessary to maintain the battery's

SOC [6]. Therefore, a number of authors [128] [129] suggested real-time OSs such as ECMS. For the studied HPS to meet the aims of the ECMS, this study employs the approach suggested by [21], and the equation (3.25) is defined to describe the minimization.

$$J = \min\ (P_{fc} + \alpha_p P_{batt})\,\Delta T \tag{3.25}$$

Under the equality constraints shown in the equation (3.26):

$$P_{load} = P_{fc} + P_{batt} \tag{3.26}$$

where $P_{fc}, P_{batt}, P_{load}$ are the FC power, battery power and load power, respectively, ΔT is the sampling time, and α_p is the penalty coefficient.

The definition of the penalty coefficient α_p [130] [131] is considered in the equation (3.27).

$$\alpha_p = 1 - 2\mu \frac{(SOC - 0.5\ (SOC_{\max} + SOC_{\min}))}{SOC_{\max} + SOC_{\min}} \tag{3.27}$$

where, the μ is balance coefficient, and SOC_{min}, SOC_{max} are the minimum and maximum battery *SOC*.

The balance coefficient μ is a variable equivalence factor that may be modified to reflect the battery's characteristics of charging and discharging [132]. This constant is chosen to balance the battery SOC during the entire cycle, and because it has different values, an optimum value is obtained (0.6 in this study) [131].

As a knowledge, there are a numerous of constraints on this optimization issue, including the battery SOC, battery power, and FC power limitations [131]:

$$Subject\ to \begin{cases} P_{fc\_\min} \le P_{fc} \le P_{fc\_\max} \\ P_{batt\_\min} \le P_{batt} \le P_{batt\_\max} \\ 0 \le \alpha_p \le 100 \end{cases} \tag{3.28}$$

where P_{fc_min}, P_{fc_max} are the minimum and maximum fuel cell power, $P_{batt\_min}, P_{batt\_max}$ are the minimum and maximum battery power.

The algorithm describing the ECMS is illustrated in Figure (3.10).

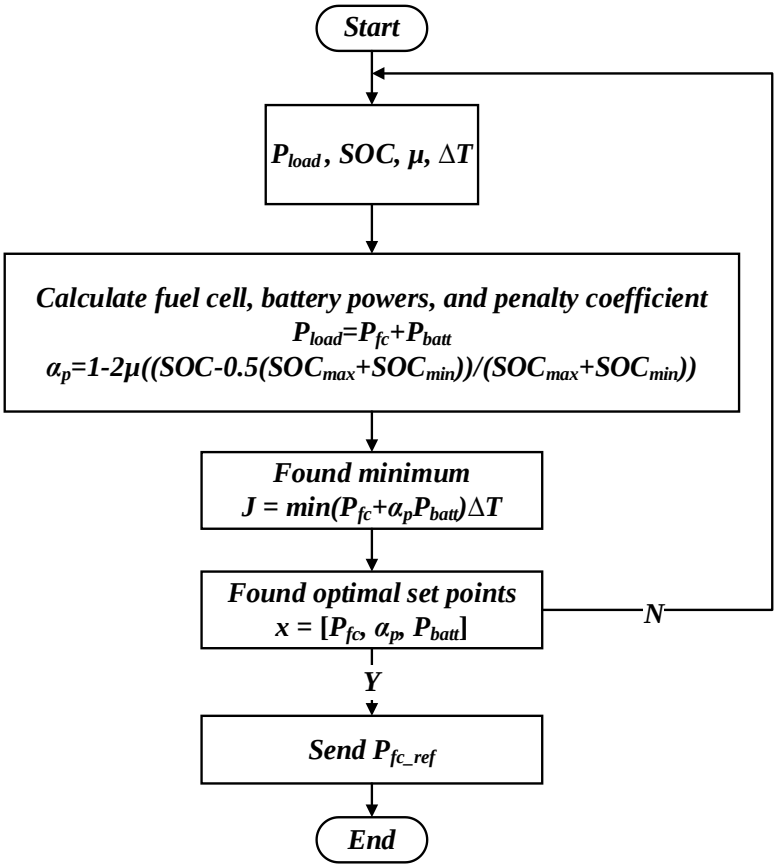

Figure 3.10: *Algorithm of the ECMS.*

❖ Simulation results and interpretations

Figure (3.11) represents the simulation results of the equivalent consumption minimization strategy.

Right after the FC is underpowered; it attempts to recharge the battery, even if the battery SOC is higher than the minimum. As a result, the FC charges the SC over their reference voltage more frequently to let the DC bus voltage regulator ask for a negative current to replenish the battery.

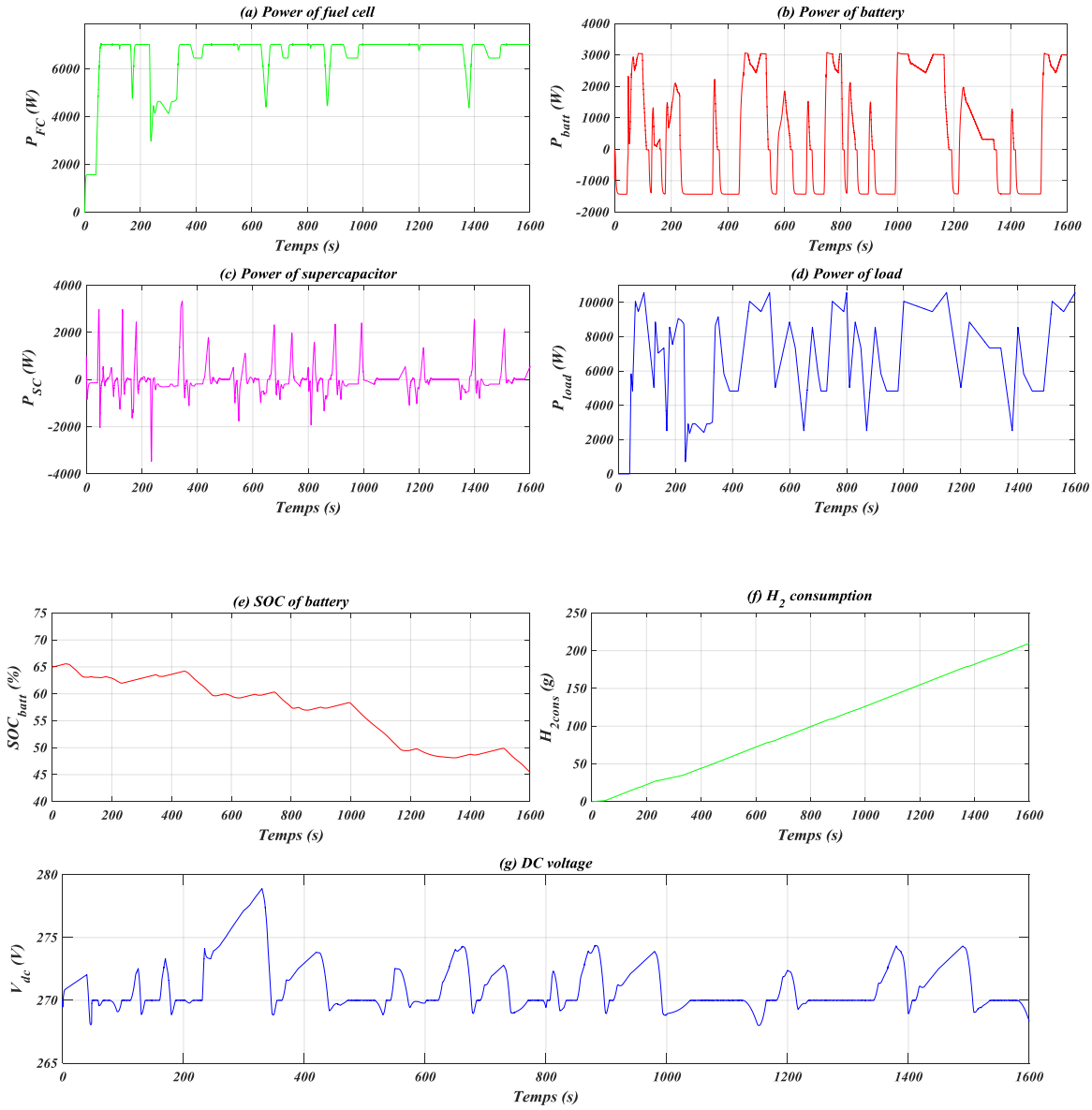

Figure 3.11: *Simulation results of ECMS.*

3.5.5 External energy maximization strategy

The EEMS, also known as equivalent hydrogen consumption, focuses on determining the optimal power distribution that reduces the hydrogen consumption of the HPS. It has two parts: the hydrogen consumption of the FC and the equivalent hydrogen consumption of the battery and the SC [101]. Figure (3.12) represents the ECMS.

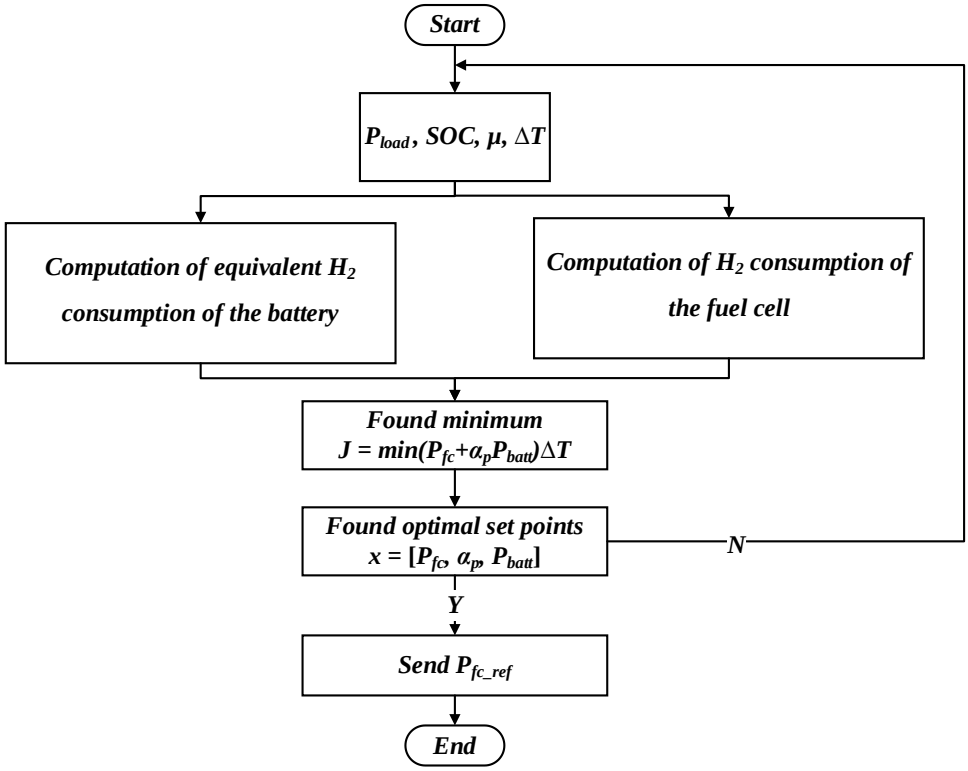

Figure 3.12: *Principle of ECMS algorithm based on EEMS.*

❖ H_2 consumption minimization strategy

This term is given to the equivalent hydrogen consumption of the storage system. A hydrogen consumption minimization algorithm similar to that in [21] is considered in this study, where the suggested strategy seeks to maximize the battery and supercapacitor energies at each given moment (external energy maximization strategy) while maintaining the battery SOC and DC bus voltage within their working boundaries. To find an optimal solution, P_{batt} and ΔV should be determined in order to minimize the following objective function.

$$J = -\left[P_{batt}\Delta T + \frac{1}{2}\, C_r . \Delta V^2\right] \tag{3.29}$$

Under the inequality constraint presented in the equation (3.30).

$$P_{batt}\ \Delta T \le (SOC - SOC_{\min})\ V_{batt}\ Q_{batt} \tag{3.30}$$

Within the boundary conditions presented in following equation.

$$Subject\ to\ \begin{cases} P_{batt\_\min} \le P_{batt} \le P_{batt\_\max} \\ V_{DC\_\min} - V_{DC} \le \Delta V \le V_{DC\_\max} - V_{DC} \end{cases} \tag{3.31}$$

where ΔV is the SC charge/discharge voltage and C_r is the rated capacitance of the SC, V_{DC_min}, V_{DC_max} are the minimum and maximum of the DC-bus voltage, and V_{batt} is the rated battery voltage.

The hydrogen consumption minimization strategy algorithm is illustrated in Figure (3.13).

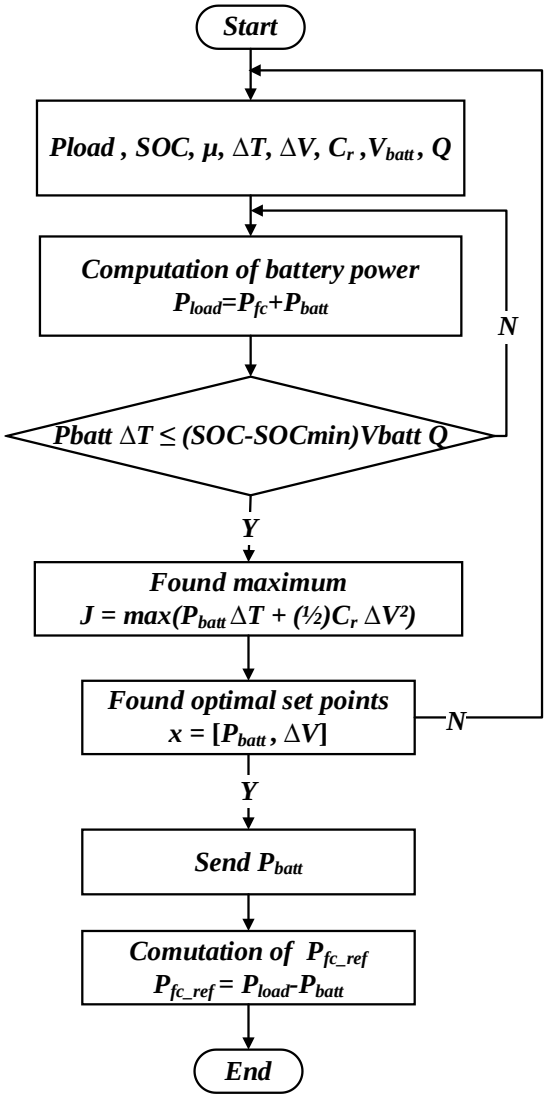

Figure 3.13: *Algorithm of H_2 consumption minimization.*

❖ Simulation results and interpretations

The simulation results of the H_2 consumption minimization strategy are illustrated in Figure (3.14).

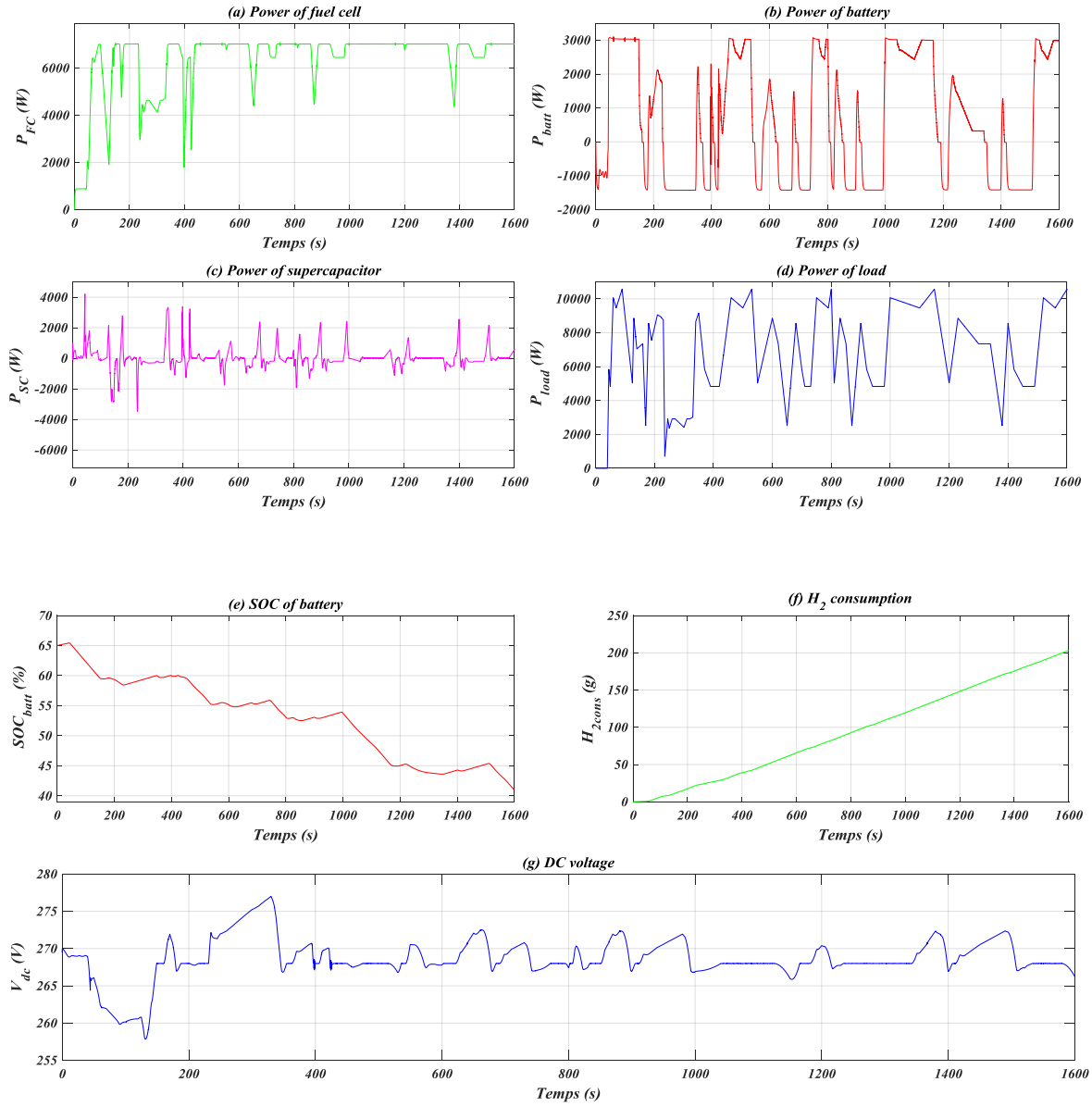

Figure 3 14: *Simulation results of H_2 consumption minimization strategy.*

The approach operates similarly to a traditional PI controller in that the battery declines quickly to reach its minimum SOC, and then the FC attempts to supply load power and recharge the battery. When the simulation starts, the FC reference power is low, and the SC discharge to assist the battery, causing the DC-bus voltage to fall below the reference voltage.

3.5.7 Comparison of the proposed strategies

In this section the SOC of the battery and fuel consumption are adopted as two criteria to perform a comparative study between the different strategies.

To figure out how much hydrogen is required to power a FC for a specific period, it is crucial to calculate the FC's hydrogen consumption. This can aid in ensuring that there is enough hydrogen to satisfy the HPS's energy requirements.

The hydrogen consumption is computed as considered in the equation (3.32) [23].

$$Cons\ H_2 = \frac{N_{fc}}{F}\int_0^t i_{fc}\,dt \tag{3.32}$$

where t is the time, and its value is $1600\ s$, F is the Faraday constant, N is the number of fuel cells.

Table (3.3) summarizes the hydrogen consumption for each strategy. From this table, the external energy maximization approach consumes the smallest quantity of fuel, followed by the PI-based energy management strategy. The state machine control requires higher quantity of fuel than each of them. Moreover, the fuel consumed with the equivalent consumption minimization method is greater than that needed for the other strategies.

Strategy	State machine control	PI-based energy management strategy	ECMS	EEMS
H_2 consumption	205	203	215	202

Table 3.2: *Strategies' hydrogen consumption.*

Table (3.3) recapitulates the battery SOC for all strategies. As observed from Table (3.3), the PI-based energy management strategy consumes more battery energy than the state machine control strategy. In comparison to the equivalent consumption minimization, greater battery energy is consumed by the external energy maximizing strategy.

Strategy	State machine control	PI-based energy management strategy	ECMS	EEMS
SOC battery	42 – 65%	41 – 65%	45 – 65%	41 – 65%

Table 3. 3: *Battery SOC of suggested strategies.*

In comparison to all strategies, the external energy maximizing strategy performed better in terms of fuel economy, while the equivalent consumption minimization strategy is better in terms of using battery energy. Besides, the DC-bus voltage was kept constant throughout all strategies.

3.6 Conclusion

This chapter presents the most prevalent hybrid power systems' energy management strategies. These strategies included the state machine control strategy, PI-based energy management strategy, equivalent consumption minimization strategy, and external energy maximization strategy. To experience them, a variable AC load was modeled and connected to an average model of a DC-DC converter and DC-AC inverter. As anticipated, the simulation results show that the HPS components work together in order to meet load power needs at all times. According to the simulation results, the EEMS consumes the least amount of fuel, and the ECMS consumes a small amount of battery energy. Besides, the DC-bus voltage was kept constant using all strategies.

General Conclusion

The work carried out in this thesis concerns the control and power management of a stand-alone hybrid power system. The considered HPS encompasses a fuel cell, battery, supercapacitor, and load. The overall control strategy of the HPS is based on a two-level structure, in which the top level is an energy management and the local one is a power control. To ensure that the HPS will be able to meet the load demand with variable profile, the energy management strategy must be properly designed to be effective. The appropriate strategy is chosen depending on fuel consumption and load conditions. The energy management and power regulation system also control the load scheduling operation during lack of fuel or slow FC response conditions with inadequate energy storage in order to avoid a system black-out. Based on the reference dynamic operating points of the individual subsystems, the local controllers control the FC and storage systems.

In chapter one, an overview of the suggested HPS was presented first. Then, comprehensive details were given to provide an understanding of the operating principle of the FC source and storage energy sources including Li-ion battery and SC.

In the next chapter each component of the HPS was modeled. The power converters were modeled using average value modeling approach, which greatly reduced the simulation time. The obtained models include the impact of the voltage and current dynamics to match as closely as possible with the real system. Using Sim Power System (SPS) library, a simulation model was developed. Simulations showed that the power of each source can be effectively controlled.

In the last chapter, a state of the-art of commonly used EMS schemes was presented; four of them were selected and implementation. These strategies included: the state machine control strategy, PI-based energy management strategy, equivalent consumption minimization strategy and external energy maximization strategy, which is based on maximizing the energy delivered by the battery and SC at any given instant while meeting their operating constraints. To ensure a fair comparison, the EMSs were designed following the same requirements. To conclude, each scheme is chosen based on a specific criterion to prioritize. As an example, depending on the operating life of each energy source, the EMS can be chosen to either minimize the stress on the FC system, the battery system or SC system, hence maximizing the life cycle of the HPS. Also, if the target is to reduce the fuel

consumption, the strategy based on the classical PI or EEMS could be selected. An alternative is to design a multi-objective optimization EMS to optimize all the performance criteria.

Last but not least, some suggestions for further work on the topic covered in this thesis are listed below:

- Simulation of the HPS in more realistic conditions using switching models for the DC-DC converters instead of average models.
- Application of artificial intelligent EMSs based on fuzzy logic systems and machine learning.
- Utilization of interleaved DC-DC converters as an alternative to conventional DC-DC converters to reduce the ripple of the input and output currents.
- Expansion of the HPS by adding other renewable sources like PV system.
- Experimental validation of the proposed HPS governed by the suggested EMSs.

References

[1] K. Talus and M. Martin, "A Guide to Hydrogen Legislation in the USA: A Renewed Effort," The Journal of World Energy Law & Business, vol. 15, no. 6, pp. 449-461, 2022.

[2] A. Martínez Lozano, "Technological Assessment of Hydrogen (Future Scenarios: Sociological, Environmental, Economic, and Energetic Aspects)", Master's Thesis, Freiburg University & University of Gothenburg, 2022.

[3] M. F. M. Sabri, K. A. Danapalasingam, and M. F. Rahmat, "A Review on Hybrid Electric Vehicles Architecture and Energy Management Strategies," Renewable and Sustainable Energy Reviews, vol. 53, pp. 1433-1442, 2016.

[4] H. A. Muqeet, H. M. Munir, H. Javed, M. Shahzad, M. Jamil, and J. M. Guerrero, "An Energy Management System of Campus Microgrids: State-of-the-Art and Future Challenges," Energies, vol. 14, no. 20, pp. 1-34 6525, 2021.

[5] D. W. Gao, Energy storage for sustainable microgrid, Academic Press, 2015.

[6] S. C. Erensoy, "Simulation and Energy Management Strategy Development for a Fuel Cell Hybrid Electric Powertrain of a Zero-Emission Boat", Master's Thesis, Instituto Superior Técnico, 2018.

[7] A. Panday and H. O. Bansal, "A Review of Optimal Energy Management Strategies for Hybrid Electric Vehicle," International Journal of Vehicular Technology, vol. 2014, 2014.

[8] C. Zhang, Y. Shen, and Y.-X. Wang, "Wavelet Transform-Based Energy Management Strategy for Fuel Cell/Variable-Structure Super-capacitor Hybrid Power System," in conference proceedings of 2020 Asia Energy and Electrical Engineering Symposium (AEEES): IEEE, pp. 732-736., Chengdu, China, 2020.

[9] Q. Xue, X. Zhang, T. Teng, J. Zhang, Z. Feng, and Q. Lv, "A Comprehensive Review on Classification, Energy Management Strategy, and Control Algorithm for Hybrid Electric Vehicles," Energies, vol. 13, no. 20, pp. 1-30 5355, 2020.

[10] F. Seydali, "Contribution à l'Optimisation de la Gestion de l'Energie d'un Micro-réseau Continu," Thèse de Doctorat, Université de M'sila, 2022.

[11] H. Khayyam and A. Bab-Hadiashar, "Adaptive Intelligent Energy Management System of Plug-In Hybrid Electric Vehicle," Energy, vol. 69, pp. 319-335, 2014.

[12] Z. Lei, D. Qin, L. Hou, J. Peng, Y. Liu, and Z. Chen, "An Adaptive Equivalent Consumption Minimization Strategy for Plug-In Hybrid Electric Vehicles Based on Traffic Information," Energy, vol. 190, pp. 1-26, 116409, 2020.

[13] M. Dhifli, S. Jawadi, A. Lashab, J. M. Guerrero, and A. Cherif, "An Efficient External Energy Maximization-Based Energy Management Strategy for a Battery/Supercapacitor of a Micro Grid System," International Journal of Computer Science and Network Security, vol. 20, no. 1, pp. 196-203, 2020.

[14] Y. Huang, H. Wang, A. Khajepour, H. He, and J. Ji, "Model Predictive Control Power Management Strategies for HEVS: A Review," Journal of Power Sources, vol. 341, pp. 91-106, 2017.

[15] M. Husein and I.-Y. Chung, "Day-Ahead Solar Irradiance Forecasting for Microgrids Using a Long Short-Term Memory Recurrent Neural Network: A Deep Learning Approach," Energies, vol. 12, no. 10, pp. 1-21 1856, 2019.

[16] S. Panda and N. K. Yegireddy, "Multi-Input Single Output SSSC Based Damping Controller Design by a Hybrid Improved Differential Evolution-Pattern Search Approach," ISA transactions, vol. 58, pp. 173-185, 2015.

[17] H. Peng, J. Li, L. Löwenstein, and K. Hameyer, "A Scalable, Causal, Adaptive Energy Management Strategy Based on Optimal Control Theory for a Fuel Cell Hybrid Railway Vehicle," Applied Energy, vol. 267, pp. 1-17 114987, 2020.

[18] Z. Chen, X. Zhang, and C. C. Mi, "Slide Mode and Fuzzy Logic Based Powertrain Controller for the Energy Management and Battery Lifetime Extension of Series Hybrid Electric Vehicles," Journal of Asian Electric Vehicles, vol. 8, no. 2, pp. 1425-1432, 2010.

[19] F. A. Alturki, H. MH Farh, A. A. Al-Shamma'a, and K. AlSharabi, "Techno-Economic Optimization of Small-Scale Hybrid Energy Systems Using Manta Ray Foraging Optimizer," Electronics, vol. 9, no. 12, p. 2045, 2020.

[20] D. Yousri, T. S. Babu, and A. Fathy, "Recent Methodology Based Harris Hawks Optimizer for Designing Load Frequency Control Incorporated in Multi-Interconnected Renewable Energy Plants," Sustainable Energy, Grids and Networks, vol. 22, pp. 1-15 100352, 2020.

[21] S. Njoya Motapon, "Design and Simulation of a Fuel Cell Hybrid Emergency Power System for a More Electric Aircraft: Evaluation of Energy Management Schemes," PHD Thesis, École de Technologie Supérieure. Université du Québec, 2013.

[22] Q. T. Tran, K. Davies, and S. Sepasi, "Isolation Microgrid Design for Remote Areas with the Integration of Renewable Energy: A Case Study of Con Dao Island in Vietnam," Clean Technologies, vol. 3, no. 4, pp. 804-820, 2021.

[23] R. E. Giachetti, C. J. Peterson, D. L. Van Bossuyt, and G. W. Parker, "Systems Engineering Issues in Microgrids for Military Installations," in conference proceedings of INCOSE International Symposium, 2020, vol. 30, no. 1, pp. 731-746, Naval Postgraduate School.

[24] S. Gronau, J. Hoelzen, T. Mueller, and R. Hanke-Rauschenbach, "Hydrogen-Powered Aviation in Germany: A Macroeconomic Perspective and Methodological Approach of Fuel Supply Chain Integration into an Economy-Wide Dataset," International Journal of Hydrogen Energy, vol. 48, no. 14, pp. 5347-5376, 2023.

[25] M. H. Akhoundzadeh, S. Panchal, E. Samadani, K. Raahemifar, M. Fowler, and R. Fraser, "Investigation and Simulation of Electric Train Utilizing Hydrogen Fuel Cell and Lithium-Ion Battery," Sustainable Energy Technologies and Assessments, vol. 46, pp. 1-13 101234, 2021.

[26] L. Fernandez, P. Garcia, C. Garcia, J. Torreglosa, and F. Jurado, "Comparison of Control Schemes for a Fuel Cell Hybrid Tramway Integrating Two DC/DC Converters," International Journal of Hydrogen Energy, vol. 35, no. 11, pp. 5731-5744, 2010.

[27] L. M. Fernandez, P. Garcia, C. A. Garcia, and F. Jurado, "Hybrid Electric System Based on Fuel Cell and Battery and Integrating a Single DC/DC Converter for a Tramway," Energy Conversion and Management, vol. 52, no. 5, pp. 2183-2192, 2011.

[28] T. Salameh, A. G. Olabi, M. A. Abdelkareem, M. S. Masdar, S. K. Kamarudin, and E. T. Sayed, "Integrated Energy System Powered a Building in Sharjah Emirates in the United Arab Emirates," Energies, vol. 16, no. 2, pp. 1-20, 769, 2023.

[29] P. Kundu and K. Dutta, "Hydrogen Fuel Cells for Portable Applications," in book section of Compendium of hydrogen energy, Elsevier, pp. 111-131, 2016.

[30] M. N. Boukoberine, M. F. Zia, M. Benbouzid, Z. Zhou, and T. Donateo, "Hybrid Fuel Cell Powered Drones Energy Management Strategy Improvement and Hydrogen Saving Using Real Flight Test Data," Energy Conversion and Management, vol. 236, pp. 1-11 113987, 2021.

[31] N. Khabazi Kenari, N. Feghhi Farahmand, and S. Iranzadeh, "A Comprehensive Model for Energy Management Strategies in Coordination with Manufacturing and Organization Strategies and its Effect on Energy Management Performance," Cogent Business & Management, vol. 5, no. 1, pp. 1-17 1463605, 2018.

[32] A. M. O. Haruni, "A Stand-Alone Hybrid Power System with Energy Storage," Phd Thesis, University of Tasmania, 2013.

[33] R. Lasseter et al., "Integration of Distributed Energy Resources. The CERTS Microgrid Concept," in report of Lawrence Berkeley National Lab (LBNL), Berkeley, CA (United States), 2002.

[34] C. Wang, "Modeling and Control of Hybrid Wind/Photovoltaic/Fuel Cell Distributed Generation Systems," Phd Thesis, Montana State University, 2006.

[35] C. Wang, M. H. Nehrir, and S. R. Shaw, "Dynamic Models and Model Validation for PEM Fuel Cells Using Electrical Circuits," IEEE Transactions on Energy Conversion, vol. 20, no. 2, pp. 442-451, 2005.

[36] P. Thounthong, "Control of Hybrid Renewable Energy Power Plant for Autonomous Systems," Phd Thesis, Université de Lorraine, 2020.

[37] K. W. Suh, Modeling, Analysis and Control of Fuel Cell Hybrid Power Systems. Phd Thesis, University of Michigan, 2006.

[38] A. El-Aal and A. E.-M. M. M. Aly, "Modelling and Simulation of a Photovoltaic Fuel Cell Hybrid System," Phd Thesis, University of Kassel, 2005.

[39] S. Carbonell Daura, "Energy Management of a Fuel Cell plus Battery Powertrain," Master Thesis, Universitat Politècnica de Catalunya, 2021.

[40] E. Effori, "Modélisation de l'Electrode à Oxygène pour Cellules à Oxyde Solide: Etude des Mécanismes Réactionnels et de l'Impact de la Dégradation," Thèse de doctorat, Université Grenoble Alpes, 2021.

[41] N. Karami, "Control of a Hybrid System Based PEMFC and Photovoltaic Panels," Phd Thesis, University Aix-Marseille, 2013.

[42] A. Hermann, T. Chaudhuri, and P. Spagnol, "Bipolar Plates for PEM Fuel Cells: A Review," International journal of hydrogen Energy, vol. 30, no. 12, pp. 1297-1302, 2005.

[43] V. Skákalová et al., "Chemical Oxidation of Graphite: Evolution of the Structure and Properties," The Journal of Physical Chemistry C, vol. 122, no. 1, pp. 929-935, 2018.

[44] L. Chen et al., "Microporous Layers with Different Decorative Patterns for Polymer Electrolyte Membrane Fuel Cells," ACS Applied Materials & Interfaces, vol. 12, no. 21, pp. 24048-24058, 2020.

[45] A. Navarro, M. Gómez, L. Daza, and J. Lopez-Cascales, "Production of Gas Diffusion Layers With Cotton Fibers for Their Use in Fuel Cells," Scientific Reports, vol. 12, no. 1, pp. 1-10, 2022.

[46] A. El Kharouf, N. Rees, and R. Steinberger Wilckens, "Gas Diffusion Layer Materials and Their Effect on Polymer Electrolyte Fuel Cell Performance–Ex Situ and in Situ Characterization," Fuel Cells, vol. 14, no. 5, pp. 735-741, 2014.

[47] S. Longo, M. Cellura, F. Guarino, M. Ferraro, V. Antonucci, and G. Squadrito, "Life Cycle Assessment of Solid Oxide Fuel Cells and Polymer Electrolyte Membrane Fuel Cells: A Review," Hydrogen Economy, pp. 139-169, 2017.

[48] H. Ito, T. Maeda, A. Nakano, and H. Takenaka, "Properties of Nafion Membranes Under PEM Water Electrolysis Conditions," International Journal of Hydrogen Energy, vol. 36, no. 17, pp. 10527-10540, 2011.

[49] Not-quite-lithium-ions-move-batteries-2017 Available online: https://www.electronicsweekly.com/news/research-news (accessed 30 Mai 2023).

[50] Somerset, NJ. NEI Corporation Extends Its Capabilities to Develop PEMs for Fuel Cells (PRWEB) March 31, 2016 ,Available online: https://www.prweb.com/releases/2016/04/prweb13304088.htm (accessed 20 Mai, 2023).

[51] R. Melendez, "Design of a Power Management Model for a Solar/fuel Cell Hybrid Energy System," Master Thesis, Florida Atlantic University, 2010.

[52] D. Linden and T. B. Reddy, Handbook of Batteries, 3 Ed. McGraw-Hills, 2002.

[53] J. Alzieu and J. Robert, "Accumulateurs au Lithium," Techniques de l'Ingénieur Accumulateurs d'Energie, 2005.

[54] K. Xu, "Nonaqueous Liquid Electrolytes for Lithium-Based Rechargeable Batteries," Chemical Reviews, vol. 104, no. 10, pp. 4303-4418, 2004.

[55] C. J. Orendorff, "The role of Separators in Lithium-ion Cell Safety," The Electrochemical society interface, vol. 21, no. 2, pp. 61-65, 2012.

[56] G. Fisher, "Pouch, Cylindrical or Prismatic: Which Battery Format Will Rule the Market," Addionics, London, UK, 14th April, 2021.

[57] D. Li, D. L. Danilov, H. J. Bergveld, R.-A. Eichel, and P. H. Notten, "Understanding Battery Aging Mechanisms," in book section of Future Lithium-Ion batteries, pp. 220-250, 2019.

[58] A. Salamani, "Synthèse et Caractérisation de Nouveaux Matériaux de Cathode pour Générateurs Electrochimiques," Thèse de Doctorat, Université de M'sila, 2018.

[59] M. Sellali, "Commande d'un Système Multi-Sources Dédié au Véhicule Électrique," Thèse de doctorat, Université Mohamed Khider, Biskra, 2020.

[60] K. Persson, V. A. Sethuraman, L. J. Hardwick, Y. Hinuma, Y. S. Meng, A. Van der Ven, V. Srinivasan, R. Kostecki and G. Ceder, J. Phys. Chem. "Graphite anode", 2010. Available online: https://www.chemtube3d.com/lib_graphite-2 (accessed 16 Mai, 2023).

[61] R. Yazami and P. Touzain, "A Reversible Graphite-Lithium Negative Electrode for Electrochemical Generators," Journal of Power Sources, vol. 9, no. 3, pp. 365-371, 1983.

[62] L. Qian et al., "Electrochemical Synthesis of Mesoporous FePO4 Nanoparticles for Fabricating High Performance LiFePO4/C Cathode Materials," Microporous and Mesoporous Materials, vol. 152, pp. 128-133, 2012.

[63] J. Asenbauer, T. Eisenmann, M. Kuenzel, A. Kazzazi, Z. Chen, and D. Bresser, "The Success Story of Graphite as a Lithium-Ion Anode Material–Fundamentals, Remaining

Challenges, and Recent Developments Including Silicon (Oxide) Composites," Sustainable Energy & Fuels, vol. 4, no. 11, pp. 5387-5416, 2020.

[64] A. Manthiram and J. B. Goodenough, "Layered Lithium Cobalt Oxide Cathodes," Nature Energy, vol. 6, no. 3, pp. 323-323, 2021.

[65] C. K. Dyer, P. T. Moseley, Z. Ogumi, D. A. Rand, and B. Scrosati, Encyclopedia of Electrochemical Power Sources, Elsevier Science & Technology, 2009.

[66] "Global and China Lithium Battery Electrolyte Industry Report", Available online: https://industry-research-reports.blogspot.com/2015/01/research-announces-global-and-china.html?spref=pi (accessed 31 Mai, 2023).

[67] H.-G. Steinrück et al., "The Nanoscale Structure of the Electrolyte–Metal Oxide Interface," Energy & Environmental Science, vol. 11, no. 3, pp. 594-602, 2018.

[68] R. Andersson, O. Borodin, and P. Johansson, "Dynamic Structure Discovery Applied to the Ion Transport in the Ubiquitous Lithium-ion Battery Electrolyte LP30," Journal of the Electrochemical Society, vol. 169, no. 10, pp. 1-10, 2022.

[69] S. S. Zhang, "A Review on the Separators of Liquid Electrolyte Li-Ion Batteries," Journal of Power Sources, vol. 164, no. 1, pp. 351-364, 2007.

[70] A. Lipschultz, "Batteries in a Portable World," Biomedical Instrumentation & Technology, vol. 49, no. 2, pp. 134-134, 2015.

[71] D. Rekioua and E. Matagne, Optimization of Photovoltaic Power Systems: Modelling, Simulation and Control, Springer Science & Business Media, 2012.

[72] P. C. Blaud, "Développement d'un Modèle de Simulation de Supercondensateur et Validation Expérimentale," Thèse de Doctorat, École de Technologie supérieure, 2012, Université du Québec.

[73] R. Niu and H. Yang, "Modeling and Identification of Electric Double-Layer Supercapacitors," in conference proceedings of 2011 IEEE International Conference on Robotics and Automation, pp. 1-4. Shanghai, China, 2011.

[74] B. Pal, S. Yang, S. Ramesh, V. Thangadurai, and R. Jose, "Electrolyte Selection for Supercapacitive Devices: A Critical Review," Nanoscale Advances, vol. 1, no. 10, pp. 3807-3835, 2019.

[75] N. I. Jalal, R. I. Ibrahim, and M. K. Oudah, "A Review on Supercapacitors: Types and Components," in conference proceedings of Journal of Physics: Conference Series, 2021, vol. 1973, no. 1, pp. 1-8, University of Babylon, Iraq.

[76] M. Vangari, T. Pryor, and L. Jiang, "Supercapacitors: Review of Materials and Fabrication Methods," Journal of Energy Engineering, vol. 139, no. 2, pp. 72-79, 2013.

[77] A. Arya, M. Iqbal, S. Tanwar, A. Sharma, A. Sharma, and V. Kumar, "Mesoporous Carbon/Titanium Dioxide Composite as an Electrode For Symmetric/Asymmetric Solid-State Supercapacitors," Materials Science and Engineering: B, vol. 285, p. 115972, 2022.

[78] A. González, E. Goikolea, J. A. Barrena, and R. Mysyk, "Review on Supercapacitors: Technologies and Materials," Renewable and Sustainable Energy Reviews, vol. 58, pp. 1189-1206, 2016.

[79] O. LeBlanc, "Mathematics of Ultracapacitors," ed: GE Global Research, Technical Report, 1993.

[80] M. S. Halper and J. C. Ellenbogen, "Supercapacitors: A Brief Overview," The MITRE Corporation, McLean, Virginia, USA, vol. 1, 2006.

[81] M. V. Kiamahalleh, S. H. S. Zein, G. Najafpour, S. A. SATA, and S. Buniran, "Multiwalled Carbon Nanotubes Based Nanocomposites for Supercapacitors: A Review of Electrode Materials," Nano, vol. 7, no. 02, pp. 1-27, 2012.

[82] B. E. Conway, V. Birss, and J. Wojtowicz, "The Role and Utilization of Pseudocapacitance for Energy Storage by Supercapacitors," Journal of Power Sources, vol. 66, no. 1-2, pp. 1-14, 1997.

[83] S.-M. Chen, R. Ramachandran, V. Mani, and R. Saraswathi, "Recent Advancements in Electrode Materials for the High-Performance Electrochemical Supercapacitors: A Review," Int. J. Electrochem. Sci, vol. 9, no. 8, pp. 4072-4085, 2014.

[84] E. Frackowiak and F. Beguin, "Electrochemical Storage of Energy in Carbon Nanotubes and Nanostructured Carbons," Carbon, vol. 40, no. 10, pp. 1775-1787, 2002.

[85] S. Pasricha and S. R. Shaw, "A Dynamic PEM Fuel Cell Model," IEEE Transactions on Energy Conversion, vol. 21, no. 2, pp. 484-490, 2006.

[86] E. U. Ezeodili, "Power Management of a Grid Forming Enabled Hybrid Energy System," Master Thesis, Auburn University, 2021.

[87] R. K. Sharma and S. Mishra, "Dynamic Power Management and Control of a PV PEM fuel-cell-based standalone ac/dc microgrid using hybrid energy storage," IEEE Transactions on Industry Applications, vol. 54, no. 1, pp. 526-538, 2017.

[88] J. Lee, T. Lalk, and A. Appleby, "Modeling Electrochemical Performance in Large Scale Proton Exchange Membrane Fuel Cell Stacks," Journal of Power Sources, vol. 70, no. 2, pp. 258-268, 1998.

[89] M. El-Sharkh, A. Rahman, M. Alam, P. Byrne, A. Sakla, and T. Thomas, "A Dynamic Model for a Stand-Alone PEM Fuel Cell Power Plant for Residential Applications," Journal of Power Sources, vol. 138, no. 1-2, pp. 199-204, 2004.

[90] J. Hirschenhofer, "Fuel Cell Handbook. /[JH Hirschenhofer, DB Stauffer, RR Engleman, and MG Klett]," US Department of Energy, Office of Fossil Energy. Federal Energy Technology Center, p. 198, 1998.

[91] C. Zhu, X. Li, L. Song, and L. Xiang, "Development of a Theoretically Based Thermal Model for Lithium Ion Battery Pack," Journal of Power Sources, vol. 223, pp. 155-164, 2013.

[92] V. Benamara, "Etude et Simulation d'un Panneau Solaire Raccorde au Réseau avec Peripherique de Stockage," Thèse de Doctorat, École de Technologie Supérieure, Université du Québec, 2012.

[93] N. Tudoroiu, Battery Management Systems of Electric and Hybrid Electric Vehicles, Batteries, 2021.

[94] J. Marcicki, S. Onori, and G. Rizzoni, "Nonlinear Fault Detection and Isolation for a Lithium-Ion Battery Management System," in Conference Proceedings of Dynamic Systems and Control Conference, vol. 44175, pp. 607-614, Cambridge, Massachusetts, USA, 2010.

[95] C. Wu, C. Zhu, Y. Ge, and Y. Zhao, "A Review on Fault Mechanism and Diagnosis Approach for Li-Ion Batteries," Journal of Nanomaterials, vol. 2015, pp. 8-8, 2015.

[96] H. Taheri Ledari, "Robust Adaptive Nonlinear Control of Microgrid Frequency and Voltage in the Presence of Renewable Energy Sources," Doctoral Thesis, École de Technologie Supérieure, Université du Québec, 2017.

[97] A. Zorig, "Commandes Non Linéaires d'une Source Décentralisée Photovoltaïque à Base de Convertisseurs de Puissance Entrelacés et Parallèles," Thèse de Doctorat, Université Amar Telidji, Laghouat, 2017.

[98] M. Rezkallah, "Design and Control of Standalone and Hybrid Standalone Power Generation Systems," Doctoral thesis, École de Technologie Supérieure, 2016.

[99] R. L. Gour, "Small Signal Modelling of a Buck Converter using State Space Averaging for Magnet Load," International Journal of Recent Research in Electrical and Electronics Engineering (IJRREEE), vol. 3, no. 3, pp. 11-17, 2016.

[100] M. Hassan and A. A. Elbaset, "Small-Signal Matlab/Simulink Model of DC-DC Buck Converter Using State-Space Averaging Method," 17th International Middle-East Power System Conferennce (MEPCON'15), 2015.

[101] Z. Zhang, C. Guan, and Z. Liu, "Real-Time Optimization Energy Management Strategy for Fuel Cell Hybrid Ships Considering Power Sources Degradation," IEEE Access, vol. 8, pp. 87046-87059, 2020.

[102] "What is Management System? Definition and meaning", Available online: https://www.management-square.com/what-is-management-system (accessed 08 Mai, 2023).

[103] J. Wu, X. Wang, L. Li, and Y. Du, "Hierarchical Control Strategy with Battery Aging Consideration for Hybrid Electric Vehicle Regenerative Braking Control," Energy, vol. 145, pp. 301-312, 2018.

[104] O. Erdinc and M. Uzunoglu, "Recent Trends in PEM Fuel Cell-Powered Hybrid Systems: Investigation of Application Areas, Design Architectures and Energy Management Approaches," Renewable and Sustainable Energy Reviews, vol. 14, no. 9, pp. 2874-2884, 2010.

[105] J. Corcau and L. Dinca, "Fuzzy Energy Management Scheme for a Hybrid Power Sources of High-Altitude Pseudo-satellite," Modelling and Simulation in Engineering, vol. 2020, pp. 1-13, 2020.

[106] A. Keshtkar and S. Arzanpour, "An Adaptive Fuzzy Logic System for Residential Energy Management in Smart Grid Environments," Applied Energy, vol. 186, pp. 68-81, 2017.

[107] M. Jafari, Z. Malekjamshidi, J. Zhu, M. Khooban, and N. P. F. L.-B. Energy, "A Novel Predictive Fuzzy Logic-Based Energy Management System for Grid-Connected and Off-Grid Operation of Residential Smart Micro-Grids," 2020.

[108] S. Cui, Y.-W. Wang, J.-W. Xiao, and N. Liu, "A Two-Stage Robust Energy Sharing Management for Prosumer Microgrid," IEEE Transactions on Industrial Informatics, vol. 15, no. 5, pp. 2741-2752, 2018.

[109] R. H. Byrne, T. A. Nguyen, D. A. Copp, B. R. Chalamala, and I. Gyuk, "Energy Management and Optimization Methods for Grid Energy Storage Systems," IEEE Access, vol. 6, pp. 13231-13260, 2017.

[110] A. M. Helmi, R. Carli, M. Dotoli, and H. S. Ramadan, "Efficient and Sustainable Reconfiguration of Distribution Networks Via Metaheuristic Optimization," IEEE Transactions on Automation Science and Engineering, vol. 19, no. 1, pp. 82-98, 2021.

[111] C. Baron, A. S. Al-Sumaiti, and S. Rivera, "Impact of Energy Storage Useful Life on Intelligent Microgrid Scheduling," Energies, vol. 13, no. 4, pp. 1-23, 2020.

[112] P. Pisu, E. Silani, G. Rizzoni, and S. M. Savaresi, "A LMI-Based Supervisory Robust Control for Hybrid Vehicles," in conference proceedings of the 2003 American Control Conference, vol. 6: IEEE, pp. 4681-4686. Denver, Colorado, 2003.

[113] S. B. Patra, J. Mitra, and S. J. Ranade, "Microgrid Architecture: A Reliability Constrained Approach," in conference proceedings of IEEE Power Engineering Society General Meeting: IEEE, pp. 2372-2377. San Francisco, CA, USA, 2005.

[114] Ker Than, Ashley P. Taylor, "Tom Garner Charles Darwin's Theory of Evolution is one of the most solid theories in science. But what exactly is it?, " Available online https://www.livescience.com/474-controversy-evolution-works.html (accessed 15 Mai, 2023).

[115] W. Shi, N. Li, C.-C. Chu, and R. Gadh, "Real-Time Energy Management in Microgrids," IEEE Transactions on Smart Grid, vol. 8, no. 1, pp. 228-238, 2015.

[116] G. Paganelli, M. Tateno, A. Brahma, G. Rizzoni, and Y. Guezennec, "Control Development for a Hybrid-Electric Sport-Utility Vehicle: Strategy, Implementation and Field Test Results," in conference proceedings of the 2001 American Control Conference, vol. 6: IEEE, pp. 5064-5069, The Ohio State University, 2001.

[117] Y. Parvini, A. Vahidi, and S. A. Fayazi, "Heuristic Versus Optimal Charging of Supercapacitors, Lithium-Ion, and Lead-Acid Batteries: An Efficiency Point of View," IEEE Transactions on Control Systems Technology, vol. 26, no. 1, pp. 167-180, 2017.

[118] J. Wu, Z. Wei, K. Liu, Z. Quan, and Y. Li, "Battery-Involved Energy Management for Hybrid Electric Bus Based on Expert-Assistance Deep Deterministic Policy Gradient Algorithm," IEEE Transactions on Vehicular Technology, vol. 69, no. 11, pp. 12786-12796, 2020.

[119] H. P. Geering, Optimal Control with Engineering Applications. Springer, 2007.

[120] X. Zhang, C. C. Mi, A. Masrur, and D. Daniszewski, "Wavelet-Transform-Based Power Management of Hybrid Vehicles with Multiple On-Board Energy Sources Including Fuel Cell, Battery and Ultracapacitor," Journal of Power Sources, vol. 185, no. 2, pp. 1533-1543, 2008.

[121] Q. Li, W. Chen, Y. Li, S. Liu, and J. Huang, "Energy Management Strategy for Fuel Cell/Battery/Ultracapacitor Hybrid Vehicle Based on Fuzzy Logic," International Journal of Electrical Power & Energy Systems, vol. 43, no. 1, pp. 514-525, 2012.

[122] Y. Wu, A. Ravey, D. Chrenko, and A. Miraoui, "Demand Side Energy Management of EV Charging Stations by Approximate Dynamic Programming," Energy Conversion and Management, vol. 196, pp. 878-890, 2019.

[123] R. Zaccone, E. Ottaviani, M. Figari, and M. Altosole, "Ship Voyage Optimization for Safe and Energy-Efficient Navigation: A Dynamic Programming Approach," Ocean engineering, vol. 153, pp. 215-224, 2018.

[124] F. Pallonetto, M. De Rosa, F. Milano, and D. P. Finn, "Demand Response Algorithms for Smart-Grid Ready Residential Buildings Using Machine Learning Models," Applied energy, vol. 239, pp. 1265-1282, 2019.

[125] P. Thounthong, V. Chunkag, P. Sethakul, S. Sikkabut, S. Pierfederici, and B. Davat, "Energy Management of Fuel Cell/Solar Cell/Supercapacitor Hybrid Power Source," Journal of power sources, vol. 196, no. 1, pp. 313-324, 2011.

[126] A. M. Bassam, A. B. Phillips, S. R. Turnock, and P. A. Wilson, "Development of a Multi-Scheme Energy Management Strategy for a Hybrid Fuel Cell Driven Passenger Ship," International Journal of Hydrogen Energy, vol. 42, no. 1, pp. 623-635, 2017.

[127] C. Zheng, N. Kim, and S. W. Cha, "Optimal Control in the Power Management of Fuel Cell Hybrid Vehicles," International Journal of Hydrogen Energy, vol. 37, no. 1, pp. 655-663, 2012.

[128] P. García, J. P. Torreglosa, L. M. Fernández, and F. Jurado, "Viability Study of a FC-Battery-SC Tramway Controlled by Equivalent Consumption Minimization Strategy," International journal of hydrogen energy, vol. 37, no. 11, pp. 9368-9382, 2012.

[129] J. P. Torreglosa, F. Jurado, P. García, and L. M. Fernández, "Hybrid Fuel Cell and Battery Tramway Control Based on an Equivalent Consumption Minimization Strategy," Control Engineering Practice, vol. 19, no. 10, pp. 1182-1194, 2011.

[130] B. He and M. Yang, "Optimisation-Based Energy Management of Series Hybrid Vehicles Considering Transient Behaviour," International Journal of Alternative Propulsion, vol. 1, no. 1, pp. 79-96, 2006.